μPLASMA SURFACE MODIFICATION OF THERMOPLASTIC COMPOSITES AND THEIR AGEING BEHAVIOUR

by

Chang Che

A thesis submitted to the University of Birmingham

for the degree of

DOCTOR OF PHILOSOPHY

School of Metallurgy and Materials

College of Engineering and Physical Sciences

University of Birmingham

April 2023

Abstract

This thesis presents work declared in the publications section. The abstracts have been collated below:

Thermoplastic polymers generally exhibit relatively low surface energies, and this often results in limited adhesion when bonded to other materials. Plasma surface modification offers the potential to overcome this challenge through functionalisation of the polymer surfaces, and thereby enhance the bond strength between dissimilar materials. In this study, glass fibre reinforced polyamide 6 (GFPA6), high-density polyethylene (HDPE), polyamide 12 (PA12) and polyamide 6 (PA6) was modified using a novel µPlasma surface treatment technique. The physical and chemical changes following µPlasma surface modification of the polymer surfaces were characterised using Atomic Force Microscopy (AFM), Fourier Transform Infrared Spectroscopy (FTIR), and Raman Spectroscopy. These techniques confirmed an increase in surface polarity, roughness, and surface energy following µPlasma treatment. Following single µPlasma treatment scan of GFPA6 samples, a substantial enhancement in wettability (with contact angles decreasing by 46.3°, 47.3°, 42.6°, and 50.1° for GFPA6, HDPE, PA12, and PA6 respectively) was observed. However, the effect of the µPlasma modification was subject to a rapid ageing phenomenon in 5 hours. The ageing process was slower when the GFPA6 material was pre-dried and stored in low humidity conditions, thereby demonstrating the importance of the presence of moisture on the rate of ageing. The ageing process of three polymers (HDPE, PA12, and PA6) with different hydrophilicity over five hours was modelled using a modified stretched exponential function Kohlrausch–Williams–Watts (KWW) model, and it was found to

be dependent on the hydrophilicity of the polymers, with higher hydrophilicities resulting in faster ageing. The effectiveness of the adhesive bond of GFPA6-epoxy-aluminium joint with GFPA6 being treated by μPlasma was evaluated. Significant increases in the tensile shear strength of the joint from 1kN to 2.3kN were observed, with no ageing phenomenon after 24 days. These observations, coupled with the atmospheric nature of the technique, points to great potential as a rapid, on-line, and effective, polymer surface treatment technique.

Acknowledgement

I would like to express my deepest gratitude to my supervisors, Dr Mike Jenkins and Prof Hanshan Dong, for their unwavering support and guidance throughout this study. Without our regular meaningful discussions, coped with their invaluable advice, this project would not have been possible. I would also like to thank Dr Xiaoying Li, who has acted more than my supervisor and given me continuous assistance and support.

I am grateful to all members from Surface Engineering group, special thanks go to Dr Behnam Dashtbozorg for his patient and valuable contribution to my project. I would also like to express my gratitude to other members in School of Metallurgy and Materials, especially Dr Dan Reed for his assistance in performing Raman tests.

I am thankful to everyone involved in the Innovative Metal Processing (IMPaCT) Centre for Doctoral Training, including staff and students. I would also like to send my appreciations to the Engineering and Physical Sciences Research Council (EPSRC), grant reference EP/L016206/1, and the ESIF/ERDF Smart Factory Hub (SmartFub) programme in West Midlands, for their financial support throughout this study.

Finally, I wish to express my sincere appreciation to my family, especially my parents and grandparents for their precious support, as well as my friends, especially Dr Gareth Sheppard, Yuean Ma and Huize Fan, for their patient help and encouragement throughout this project over the years.

Publications

Published: Chang Che, Behnam Dashtbozorg, Xiaoying Li, Hanshan Dong, and Mike Jenkins, "Effect of μPlasma Modification on the Wettability and the Ageing Behaviour of Glass Fibre Reinforced Polyamide 6 (GFPA6)," *Materials,* vol. 14, no. 24, p. 7721, 2021.

Author Contributions: Conceptualization, M.J. and H.D.; methodology, B.D. and C.C.; validation, C.C.; formal analysis, C.C.; investigation, C.C.; resources, M.J. and H.D.; data curation, C.C.; writing—original draft preparation, C.C.; writing—review and editing, C.C., B.D., M.J., H.D. and X.L.; visualization, C.C.; supervision, M.J.; project administration, M.J. and H.D.; funding acquisition, H.D. and X.L.

Submitted: Chang Che, Behnam Dashtbozorg, Sahojun Qi, Matt North, Xiaoying Li, Hanshan Dong, and Mike Jenkins, “The ageing of μPlasma modified polymers: the role of hydrophilicity.”

Author Contributions: Conceptualization, M.J. and H.D.; methodology, C.C., and M.J.; validation, C.C.; formal analysis, C.C.; investigation, C.C.; resources, M.J. and H.D.; data curation, C.C., S.J. and M.J.; writing—original draft preparation, C.C.; writing—review and editing, C.C., B.D., M.J. and S.J.; visualization, C.C.; supervision, M.J.; project administration, M.J. and H.D.; funding acquisition, H.D. and X.L.

Submitted: Chang Che, Xueqi Zhu, Behnam Dashtbozorg, Xiaoying Li, Hanshan Dong, and Mike Jenkins, “Enhancing the bond strength between glass fibre reinforced polyamide 6 and aluminium through μPlasma surface modification.”

Author Contributions: Conceptualization, M.J. and H.D.; methodology, C.C., and M.J.; validation, C.C. and X.Z.; formal analysis, C.C., X.Z. and B.D.; investigation, C.C., and X.Z.; resources, M.J. and H.D.; data curation, C.C. and X.Z.; writing—original draft preparation, C.C.; writing—review and editing, C.C., M.J., and B.D.; visualization, C.C. and X.Z.; supervision, M.J.; project administration, M.J. and H.D.; funding acquisition, H.D. and X.L.

Table of Contents

List of Figures

List of Tables

List of Abbreviations

AC	Alternating Current
AFM	Atomic Force Microscopy
APTMS	3-Aminopropyl Trimethoxysilane
CFRP	Carbon Fibre Reinforced Plastics
DBD	Dielectric-Barrier Discharges
DC	Direct Current
DSC	Differential Scanning Calorimeter
FTIR	Fourier Transform Infrared Spectroscopy
GFPA6	Glass Fibre Reinforced Polyamide 6
HDPE	High-Density Polyethylene
KWW	Kohlrausch–Williams–Watts
LDPE	Low-Density Polyethylene
LLDPE	Linear Low-Density Polyethylene
PA12	Polyamide 12
PA6	Polyamide 6
PC	Polycarbonate
PEEK	Polyetheretherketone
PEN	Polyethylene Naphthalate
PES	Polyethersulfone
PET	Poly (Ethylene Terephthalate)
PMMA	Polymethylmethacrylate
PP	Polypropylene
PS	Polystyrene
RMS	Root Mean Square
RO	Reverse Osmosis
SEM	Scanning Electron Microscopy
T_g	Glass Transition Temperature
T_m	Melting Temperature
TPC	Thermoplastic Composites
UHMWPE	Ultra-High Molecular Weight Poly (Ethylene)
UV	Ultraviolet
XPS	X-Ray Photoelectron Spectroscopy

1 Introduction

The use of lightweight materials such as thermoplastic composites (TPCs), which are composed of thermoplastics matrices with additional reinforced fibres, have attracted significant interest in the automotive industry due to their excellent combination of good mechanical properties, ease of manufacture, low density and their ease of recycling [1, 2]. Among them, glass fibre reinforced polyamide 6 (GFPA6) has also gained extensive attention in the automotive and aerospace areas, owing to its good thermal stability and high tensile strength [3, 4]. Thermoplastic composites are typically used in applications where they are required to be bonded or joined with metals or other composites, such as load bearing components in automotive applications [5]. This design provides an ideal combination of desirable properties of different materials, such as excellent strength, stiffness, and resistance to crack-induced physical damage, as well as weight reduction when joining with metals [6].

Various technologies have been developed for the joining of two components such as polymers and metals, including mechanical fastening, welding and adhesive joining [7]. Adhesive joining, in particular, has been found to offer better seals while forming a defect-free connection, and is suitable for joining dissimilar materials [6]. To achieve good structural bond, an epoxy adhesive which exhibits high strength and temperature resistance when compared to other adhesives was selected for this study. Furthermore, it was found to offer a substantial improvement on the bonding strength between polymer and metal surfaces [8].

Prior to the bonding process, surface modifications are typically required to improve the surface adhesive properties of the thermoplastic surface [9]. Thermoplastic

surfaces normally exhibit low surface free energy, resulting in poor adhesive properties [10]. A range of studies have established that plasma treatments can improve the wettability of polymer surfaces [11-14]. Additionally, it has been reported that plasma treated surfaces can enhance the bonding strength between polymers and metals [15, 16]. Unlike conventional plasma treatment systems, that require low-pressure conditions (typically 50-400 Pa) [17], new μPlasma surface modification can be performed under atmospheric pressure. Consequently, the need for vacuum systems can be eliminated, thereby significantly reducing the treatment costs and increasing the flexibility of the treatment. In addition, μPlasma modifications allows precise, localised, multi-axial modification of samples, resulting in enhanced energy efficiency. Conventional plasma surface treatment on different kinds of polymers has also been reported, including polyamide materials, such as polyamide 12, polyamide 6,6 and polyamide 6 [18-22]. However, to the best knowledge of the authors, no previous studies have explored the bonding between glass fibre reinforced polyamide 6 (GFPA6) and aluminium, especially following plasma surface modification of the GFPA6 material. Therefore, it is critical to explore the feasibility of plasma treatment, especially μPlasma modification on modifying and improving the properties on GFPA6, as well as the underlying mechanism.

Although plasma treatments are well-established to induce exceptional changes to the surface of polymers, they are not permanent modifications. Polymer surfaces following plasma treatment are often accompanied by ageing phenomenon, including hydrophobic recovery (with chain reorientation and diffusion towards to the bulk), chain scission, crosslinking, and oxidation [23, 24]. Studies have demonstrated that the aging of polymers have a negative influence on the properties introduced by plasma

treatment, particularly associated with surface wettability. However, aging data, which can be documented by contact angle measurements, are usually reported on a daily or weekly basis. The initial dynamic changes in the first minutes or hours after plasma treatment are rarely reported. Therefore, it is essential to systematically study the initial ageing behaviour following plasma treatment to enable better understanding of this phenomenon. Moreover, a modified stretched exponential Cowie and Ferguson model [25], was utilised in this study to aid in the comprehension of the wettability aging process of polymers after µPlasma modification.

In addition, while investigations have revealed a variety of factors that contribute to the impact of the ageing behaviour, such as temperature [26], storage conditions [27], crystallinity [28], none has decoupled the effect of crystallinity and hydrophilicity on the ageing process. Therefore, given that polymers such as polyamides are more prone to moisture absorption, while polyethylene (PE) is a hydrophobic material that does not absorb moisture, it is necessary to explore the influence of hydrophilicity (i.e., moisture absorbance ability) on the ageing behaviour of the polymers after µPlasma modification.

Aims and Objectives

The aim of this project is to investigate the role of µPlasma surface modification on thermoplastic composites surfaces to enhance the adhesive bonding between thermoplastic and metal surfaces. To achieve this goal, the study can be broken down into the following objectives:

The first part is to investigate the effect of µPlasma modification on the wettability of glass fibre reinforced polyamide 6 (GFPA6) surfaces, and their short-term (minutes to hours) and long-term (days to weeks) ageing behaviour. To optimise µPlasma surface modification parameters, including printing rate, working distance and accelerating voltage. To develop a more reliable systematic protocol for measuring the contact angle of plasma treated fibre reinforced polymers to better characterise their surface wettability and ageing behaviour. In addition, to develop an approach to hinder or prevent complete hydrophobic recovery of the treated surfaces.

The second part is to explore the effect of µPlasma treatment on the surface morphology, wettability and surface chemistry of three thermoplastic polymers, including high-density polyethylene (HDPE), polyamide 12 (PA12) and polyamide 6 (PA6) with different hydrophilicities. To explore the effect of the different polymer hydrophilicities on the ageing process after µPlasma surface modification using the Cowie and Ferguson model [25].

The third part is to investigate the bonding strength of GFPA6-epoxy-aluminium after µPlasma surface modification through tensile lap-shear testing and to analyse the failure modes of the bond. To characterise the physical and chemical changes following surface modification of the on GFPA6 surface, as well as the influence of increased treatment repetitions (1, 10 and 20 µPlasma treatment scans) on the sample surface. To explore the ageing behaviour of the bonding strength of the joined GFPA6-epoxy-aluminium component.

2 Literature Review

2.1 Polymers

A polymer is a long chain molecule (which can also be termed a macromolecule), consisting of a sequence of repeating units, or monomers. For example, the repeating unit of polyethylene is shown below in Figure 2-1.

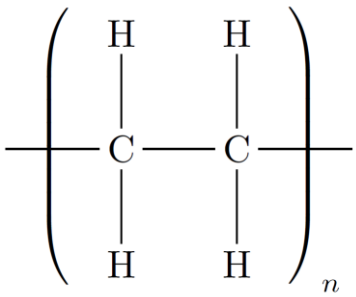

Figure 2-1. The repeat unit of polyethylene.

The backbone of a polymer is composed of covalently bonded carbon atoms, other constituent atoms may also be present, for example, nitrogen, oxygen, sulfur and chlorine among others. Depending on the chemical constituents of the polymer, secondary interactions may also be present, e.g., hydrogen bonds occur in polyamides [29].

Polymer chains can be linear, branched or cross-linked; schematic diagrams displaying these polymer structures are shown in Figure 2-2.

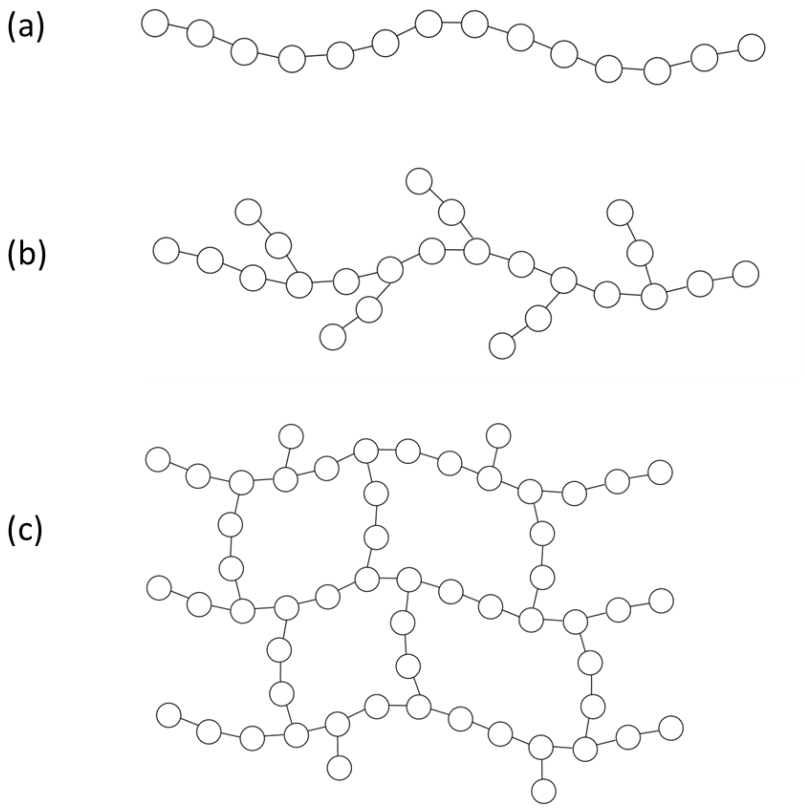

Figure 2-2. Schematic of linear, branched and cross-linked polymers (a) linear, (b) branched and (c) cross-linked.

Branched polymers have side chains attached to the main backbone. The chain architecture of cross-linked polymers is a three-dimensional network. Cross-links are usually composed of covalent bonds between two molecular chains that are formed during or after polymerisation, but ionic cross-links can be found e.g., Surlyn ionomer.

The properties of polymers such as thermal stability, tensile strength, viscosity and toughness are highly dependent on both the chain length and the chemistry of the repeat unit. Chain length is generally characterised in terms of a molecular weight and polymers exhibit a distribution of molecular weights [30]. Therefore, an average molecular weight is calculated.

2.1.1 Molecular Weight Distribution

Usually, as the molecular weight of a polymer increases, as do certain mechanical properties, such as tensile strength and stiffness [31]. Therefore, measuring the molecular weight is essential for understanding the behaviour of polymeric materials.

The two most common measures of the average molecular weight are number average molecular weight, M_n, and the weight average molecular weight (M_w).

The M_n average is an arithmetic mean and is defined as follows:

$$M_n = \frac{\sum_i N_i M_i}{\sum_i N_i} \tag{2-1}$$

Where, M_i is the molecular weight of a chain, N_i is the number of chains, and i is the number of polymer molecules [32].

The M_w average is a weighted mean and is defined as follows:

$$M_w = \frac{\sum_i N_i {M_i}^2}{\sum_i N_i M_i} \tag{2-2}$$

Where M_i is the molecular weight of a chain, N_i is the number of chains, and i is the number of polymer molecules [32].

Unlike M_n, M_w takes into account the mass of individual molecules. The larger the molecules, the greater contribution they make towards the average molecular weight.

2.1.2 Polymer Morphology

Polymer morphology is the overall form of the structure and arrangement of the molecules in a polymer. It plays an important role in determining the properties of polymers. There are amorphous and crystalline states in a polymer.

The amorphous state in a polymer has randomly distributed polymer chains without any order. The structure of the amorphous chains can be compared to spaghetti, and the term ‘spaghetti model’ is often used to describe amorphous polymers [33]. The unoccupied volume in an amorphous polymer is called free volume, which originates from poor packing of the polymer chains. On the contrary, the crystalline state has a highly ordered structure in which the chains are distributed in a repeating pattern. Unbranched linear polymers such as HDPE can potentially possess a crystallinity of up to 70%.

Polymers can be amorphous or semi-crystalline. Semi-crystalline polymers contain spherulites (shown in Figure 3), which are composed of repeating amorphous and crystalline phases. The crystalline phases within spherulites take the form of lamellae, which exhibit thicknesses of 10 nm to one centimetre [34]. The molecular chains, which are much longer than the thickness of the lamellae, can fold back and forward regularly on the surface of the lamella [35], but chain loops of various sizes also form. In addition, chains can link adjacent lamella, and these are known as tie-molecules.

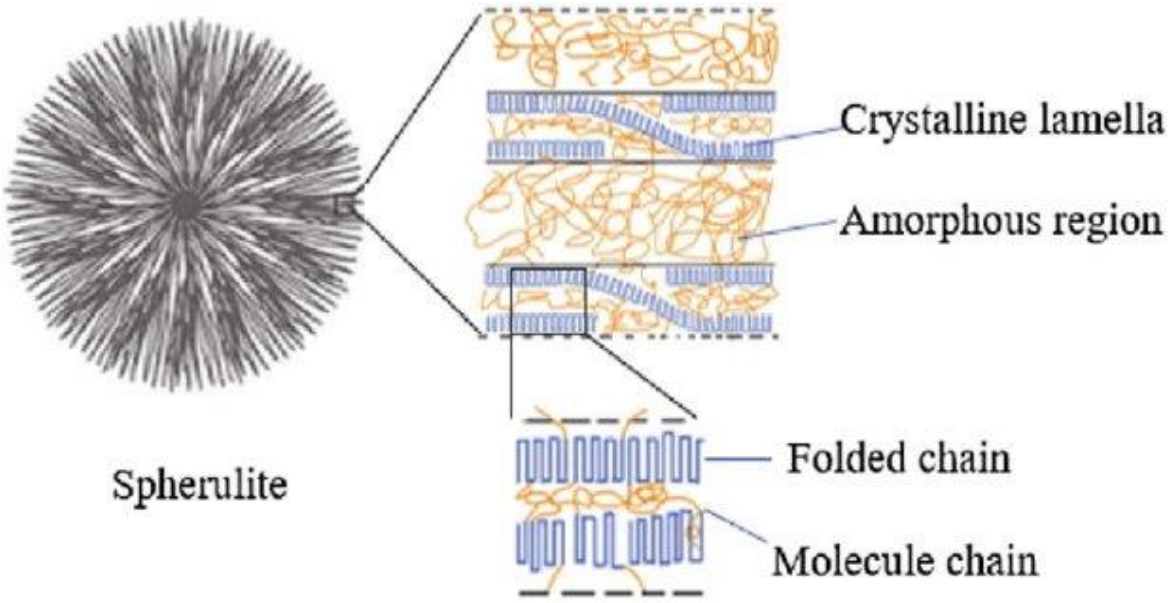

Figure 2-3. Schematic of spherulite that contains lamella and amorphous [36].

On heating, amorphous state in a polymer exhibit a glass transition temperature. Most of the amorphous chains exist in a rigid state at room temperature. Upon heating, the molecular chains absorb a certain amount of energy, providing them with increased mobility. At a certain temperature known as the glass transition temperature (Tg), the amorphous regions experience a transition from the rigid glassy state to a more flexible rubbery state, upon which the free volume of the system increases by approximately 2.5 times [30].

The glass transition temperature is present in both amorphous and semi-crystalline polymers, whereas only semi-crystalline polymers possess a melting temperature (T_m). Semi-crystalline polymers start to undergo softening above the T_g, and the crystalline regions begin to flow after the T_m is reached. The system exists in the rubbery state between the two temperatures T_g and T_m, in which the material present exhibits better elongation when a low load is applied. The transformations that occur between

different temperatures lead to changes in the morphologies of polymers, resulting in a change in physical properties. Therefore, it is important to identify and investigate the morphology of a polymer.

2.1.3 Thermoplastics

Polymers can be categorised into two groups: synthetic polymers and natural polymers. Synthetic polymers are produced via polymerisation, and can be further categorised into thermosets and thermoplastics. Thermosets polymers possess a three-dimensional crosslinking structure, which makes them highly resistant to deformation and heat. However, thermosets cannot be reshaped and remelted once processed, making recycling these polymers extremely difficult.

Typically, thermoplastics are a type of polymer that can be melted and reshaped multiple times without losing its original properties such as strength and flexibility, which makes them easier to recycle and therefore more environmentally friendly. Engineering thermoplastics are a group of thermoplastics that are characterised by high strength, stiffness, impact and chemical resistance, thermal stability, low weight, low cost, and ease of manufacture. This subset of thermoplastics are widely used in automotive and aerospace industries [37]. Some engineering thermoplastic examples are polyamide (PA), polyethylene (PE), polypropylene (PP) and polyetheretherketone (PEEK). The strength and stiffness performance of thermoplastics can be enhanced by the addition of reinforced fibres such as glass or carbon fibres [38]. Glass fibre reinforced polyamides are widely used in the automotive, construction, and electrical industries due to their high strength, stiffness, impact resistance and low cost [39].

Carbon fibre reinforced polyamides are used in automotive, aerospace, civil, and structural engineering due to their high strength, thermal stability and low weight [39].

One of the most versatile thermoplastics is polyethylene (PE). It is a semi-crystalline polymer with a relatively high crystallinity. PE possesses a simple molecular structure, which consists of long chains of repeating units of ethylene (C_2H_2). It is extensively used in flexible packaging applications due to its low cost, excellent electrical insulation, low coefficient of friction, chemical and fatigue resistance, and ease of processing [40, 41]. It is also often used in the automotive sector to produce laminates, membranes, and foams [40, 42]. However, PE is a hydrophobic thermoplastic polymer with low adhesion properties due to its nonpolar nature, which has limited its applications.

There are three main categories of polyethylene, which are low-density polyethylene (LDPE), linear low-density polyethylene (LLDPE) and high-density polyethylene (HDPE). HDPE is a polymer with highly regular packed chains, and a low degree of branching, typically less than 7 branch points per 1000 carbon atoms on the chains. The highly regular arrangement gives HDPE a high degree of crystallinity, which leads to high strength, low moisture absorption and high impact resistance. LDPE has an increased number of branched chains with approximately 60 branch points every 1000 carbon atoms, which imparts a lower degree of crystallinity compared to HDPE. Resultantly they are soft and flexible with good elongation, and this has led to their widespread use in packaging [43]. Additionally, the excellent chemical and corrosion resistance has led to their use as a protection coating [44]. LLDPE is a polymer that has been processed with a controlled number of short chain branches, and has properties such as tensile strength and density between HDPE and LDPE.

Another common thermoplastic is polyamide (nylon). Polyamide is a semi-crystalline linear thermoplastic polymer that consists of the amide (-CONH-) repeat linkage in the polymer backbone with a low glass transition temperature (T_g) [45]. When the temperature is below T_g, the material exhibits a relatively low strength and low toughness due to the lower mobility of the chains, whereas the material has increased toughness and reduced strength when the temperature is above T_g.

Polyamides were first invented in the 1930s, and first employed in industry in the 1950s [46]. They are widely utilised in the automotive area due to their excellent properties such as flexibility, toughness, resistance of abrasion and thermal stability [47]. They have been used as synthetic textile fibres, thermoplastic sheet composites, tapes, cable insulation and in medical applications such as orthopaedic implants and biosensors [48]. The most popular types of polyamides include polyamide 6, polyamide 6,6, and polyamide 12. Fibre reinforced polyamide composites are also used in engineering products in industry due to a combination of low cost and high performance [39].

Among polyamides, polyamide 12, which has a relatively lower melting temperature due to its longer aliphatic ($-CH_2$) chains, exhibits many exceptional properties. These includes low moisture absorption, high notched impact, high resistance to ultraviolet (UV), high chemical resistance (oils, solvents, alkalis), high resistance to pressure and abrasion, and high processability [49-51]. However, it is more expensive than polyamide 6 and polyamide 6,6.

Polyamide 6 is one of the few engineering polymers that can be used in the aerospace and automotive industries, due to its excellent abrasive wear resistance and

mechanical properties such as strength and toughness [52]. Polyamide 6 consists of 6 carbon atoms in its repeat unit. Among them, five of the carbon atoms belong to - (CH_2) - linkages, and the last one is part of a carbonyl C=O bond belonging to the (-CONH-) amide group. In the production process (polymerisation and crystallisation) of polyamide 6, hydrogen bonds form between amide hydrogen atoms and carbonyl oxygen atoms within the amide group as the chains open and extend. These hydrogen bonds can exist between adjacent chain units, or within a single chain, leading to the closely packed crystalline structure that gives polyamide 6 its outstanding properties [53].

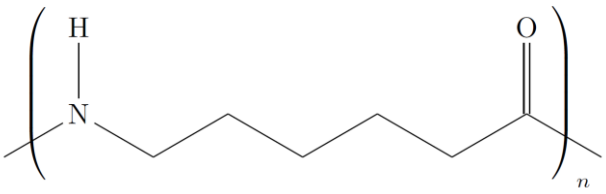

Figure 2-4. The repeat unit of polyamide 6.

To enhance the strength and stiffness of a material, it is common to add fibres such as glass and carbon fibres to a thermoplastic matrix, resulting in what are known as thermoplastic composites (TPCs). Glass fibres, for example, can improve the stiffness, strength, abrasion resistance, heat and chemical resistance of the composites [54]. Among glass fibre reinforced polymer composites, glass fibre reinforced polyamides exhibit excellent mechanical and thermal properties, which is attributed to the combination of properties from the glass fibres and polyamides. The remarkable performance of glass fibre reinforced polymers is highly dependent on suitable compositions, orientation, and interfacial strength of the matrix and fibres [55]. In terms

of applications, glass fibre reinforced polyamides are mainly used in the automotive industry (car bonnet, interior parts and under the hood) due to the weight reduction they provide.

2.1.4 Effect of Water in Polyamides and Polyethylene

Although polyamides possess excellent properties, they are also hygroscopic materials that absorb moisture from the air due to their large number of hydrophilic amide groups [56].

When the polyamide is exposed to a humid environment, the transport of water through the polyamide can affect the properties of the polymer. This is because water molecules can interact with the oxygen and hydrogen in the amide group in polymer chains and form hydrogen bonds, leading to an increase in the free volume of the polymer, thus causing swelling of the polyamide. The mobility of the chains can therefore be increased as the chains have more space to move. The increase in free volume can also weaken the hydrogen bonds between the polymer chains, as well as lower the glass transition temperature T_g, leading to a decrease in mechanical properties such as strength and stiffness [56]. This is also dependent on the different types of polyamides and the crystallinity. Studies have shown that the absorption of water has less effect on the polyamides with higher crystallinity [57, 58]. For example, Litvinov et al. [59] has pointed out that the water mainly diffuses into the amorphous phase in polyamide 6, which increases the chain mobility of the material.

Conversely, polyethylene is a hydrophobic material, which is resistant to hydrogen bonding due to its non-polar molecular structure [60]. This makes it difficult to interact with water, thus resulting in a low affinity for water [61].

2.2 Polymer Surfaces

The molecules in the polymer bulk are generally stable as they experience balancing forces from the molecules around them. However, the surface molecules only experience a force from the layer of molecules directly beneath them. Due to the uneven force, the free energy of the surface layer is higher than that of the bulk. The molecular chains tend to arrange randomly in the bulk. Conversely, the chains near to the surface have less freedom to move around compared to the chains in the bulk, and therefore tend to align parallel on the surface with separated chain ends to avoid reflection. Therefore, the free energy of the whole system is reduced. This is known as surface induced ordering [62]. The molecular chains in the bulk have a lower mobility than those on the surface due to the more ordered configuration of the bulk chains compared to the surface material. The glass transition temperature (T_g) of the polymer on the surface was determined to be lower than in the bulk [63]. This has been evidenced by measuring the Tg of polymer thin films by Forrest at al. [64], who found that Tg decreases linearly with film thickness.

The surface chains can also react with the environment when they are given sufficient mobility. Therefore, the surface functional groups are not permanently fixed. They can slowly diffuse and reorient from the outer surface to the bulk, even entire polymer chains with functional groups. This is called surface dynamic or hydrophobic recovery. Diffusion of the molecules from high concentration to lower concentration regions is

the driving force behind the recovery. The interaction between the surface functional groups and the polar or nonpolar environment is another driving force that can arrange the orientation of functional groups. For instance, the O-H groups change their orientation toward the surface and form hydrogen bonds if the air environment is replaced by water [65]. This is because the interaction of the energy of the polar groups with the polar environment compensates the dilution tendency [66]. The chain ends can enhance the surface mobility according to Kajiyama et al. who studied the surface mobility of Polystyrene (PS) [67].

Notable properties of polymer surfaces include surface energy and surface wettability, which influence the applications of the polymers. Therefore, the characterisation of the surface properties is essential.

2.2.1 Contact Angles

Contact angle measurement is one of the most important characterisation methods for determining the surface wettability. Contact angles are measured when the three-phase boundary is horizontally stable. When a drop of liquid is placed on a solid, the interaction between the solid and liquid can give information about the wettability of the solid material surface. If the contact angle of water on a solid surface is lower than 90 ^{o}, the solid material is considered hydrophilic. When the contact angle is higher than 90 ^{o}, the material is hydrophobic. The increase of the contact angles of the water with time is a good indication of hydrophobic recovery [68]. Generally, the contact angle depends on the roughness, chemical and topographical heterogeneity and arrangement of the surface [69].

2.2.2 Surface Free Energy

Since polymer surfaces experience an unbalanced force, they therefore always try to minimise the free energy in the whole system. The surface free energy is an evaluation of the interaction between the surface and the surroundings. It is the energy required to reach thermodynamic equilibrium, which can be used to describe wettability of the material. It is called surface tension on a liquid surface. The molecules within a liquid with a high surface tension attract to each other so they stick together on a solid surface with low energy, whereas the molecules with low surface tension tend to spread out on a solid surface with high energy. However, the value of surface free energy is not fixed, it depends on the liquids chosen for contact angle testing. Generally, the higher the surface free energy calculated with the same liquid, the higher the wettability of a solid material, therefore resulting in a lower contact angle on the surface.

The results of contact angles of two or more different liquids can be used to calculate the surface free energy using Fowkes theory [70]. The total surface free energy consists of dispersive surface energy and polar surface energy (as shown in Equation (2-3), where σ_S is the total solid surface energy, ${\sigma_S}^P$ is the polar components of solid surface energy, and ${\sigma_S}^D$ is the dispersive component of solid surface energy). The dispersive surface energy is the component of dispersion of the electrons in the molecules on the material surface, whereas the polar surface energy is the component of surface energy that results from the attraction of electrons in the molecules on the material surface.

$$\sigma_S = {\sigma_S}^P + {\sigma_S}^D \tag{2-3}$$

Similarly, the total surface tension of a liquid consists of the dispersive component of the surface tension and the polar component of the surface tension, as shown in Equation (2-4), where σ_L is the total surface tension of the wetting liquid, σ_L^D is the dispersive component of the surface tension of the wetting liquid, σ_L^P is the polar component of the surface tension of the wetting liquid.

$$\sigma_L = {\sigma_L}^P + {\sigma_L}^D \tag{2-4}$$

Mathematically, Fowkes theory is combined with two Equations, Young's Equation and Good's Equation.

Young's Equation is shown as below in Equation (2-5), where γ_{SL} is the interfacial tension between the solid and the liquid and θ is the contact angle of the solid-liquid interface.

$$\sigma_S = \gamma_{SL} + \sigma_L \cos\theta \tag{2-5}$$

Good's Equation is as below in Equation (2-6):

$$\gamma_{SL} = \sigma_S + \sigma_L - 2 \cdot \left(\sqrt{\sigma_S^D \cdot \sigma_L^D} + \sqrt{\sigma_S^P \cdot \sigma_L^P}\right) \tag{2-6}$$

Fowkes' surface energy theory is the combination of Young's Equation and Good's Equation above, as shown in Equation (2-7).

$$(\sigma_L^P)^{1/2} \cdot (\sigma_S^P)^{1/2} + (\sigma_L^D)^{1/2} \cdot (\sigma_S^D)^{1/2} = \frac{\sigma_L\ (\cos\theta + 1)}{2} \tag{2-7}$$

This Equation is mathematically the same as Owens/Wendt theory. However, Owens/Wendt theory often time-consuming, requiring the use of many probe liquids in

contact angle testing of the solid being analysed. In contrast, the Fowkes theory only requires two wetting liquids, one of which has a surface tension of only the dispersive component. This makes it easier due to the fact that when the polar component $\sigma_L^P = 0$, total surface tension $\sigma_L = \sigma_L^D$ according to Equation (2-4). This simplifies Equation (2-7) to Equation (2-8), allowing σ_S^D to be calculated directly from Equation (2-8), with the value of the liquid contact angle on a solid surface.

$$\sigma_S^D = \frac{\sigma_L\ (\cos\theta + 1)^2}{4} \tag{2-8}$$

Diiodomethane is usually recommended in Fowkes theory. This is because diiodomethane, due to its molecular symmetry, has only the dispersive component without the polar component. The total surface tension of the diiodomethane $\sigma_L = \sigma_L^D$ =50.8 mN/m.

After achieving the value of σ_S^D, the next step is to apply the value of the dispersive component σ_L^D to and the polar component σ_L^P of the surface tension of the liquid to the Fowkes theory Equation (2-7). The only unknown parameter σ_S^P can be calculated with the value of the liquid contact angle on the solid surface using Equation (2-7). The other commonly used test liquid is deionised water, which has a polar component of the surface tension σ_L^P = 46.6mN/m, and dispersive component of the surface tension σ_L^D = 26.4/m.

The total surface free energy can then be calculated through Equation (2-3) by adding σ_S^D and σ_S^P together.

2.2.3 Wetting Envelope

Wetting envelope is a graphical representation of the contact angle of a liquid droplet on a solid surface as a function of the surface energy of the solid. Liquids with surface energy of polar and dispersive components within the envelope exhibit a smaller contact angle than the set value. On the contrary, liquids with surface energy outside the envelope exhibit a bigger contact angle. The wetting envelope can be used to predict the wetting status of a liquid with certain polar and dispersive components on a solid surface, as the relationship between the contact angle and surface energy can be shown visually on the graph. The wetting envelope is a curve with dispersive component σ_L^D and polar component σ_L^P of liquid surface tension (an example is shown in Figure 2-5).

The derivation of wetting envelope Equation (2-12) is also based on the Young's Equation (2-5) and Fowkes theory (2-7). In this case, a complete wetting curve is generated, i.e., θ = 0°, therefore $\cos\theta$ =1. The next step is to simplify Fowkes theory by applying $\cos\theta$ =1 to the Equation (2-7).

Equation (2-9) shown below represents a cylindrical coordinate system. Any point in the coordinate system is determined by the values of the x and y axes, where they are the dispersive component σ_L^D and polar component σ_L^P of liquid surface tension respectively. R is the absolute value of the vector of the point to the origin of the coordinate. In the system, ϕ is the angle of the vector with respect to the x-axis, therefore $\sigma_L^D = R \cdot cos\phi$ and $\sigma_L^P = R \cdot sin\phi$, as shown in Equation (2-10) and (2-11).

$$R^2 = (\sigma_L^P)^2 + (\sigma_L^D)^2 \tag{2-9}$$

$$\sigma_L^D = R \cdot cos\phi \tag{2-10}$$

$$\sigma_L^P = R \cdot sin\phi \tag{2-11}$$

Through substituting Equation (2-9), (2-10) and (2-11) into Equation (2-7), it gives Equation (2-12). By plotting the value of R as a function of ϕ (change angles to radius), the wetting envelope can be achieved.

$$R = \left(\frac{\sqrt{\sigma_s^P} sin\phi + \sqrt{\sigma_s^D cos\phi}}{cos\phi + sin\phi} \right)^2 \quad for\ 0° \leq \phi \leq 90° \tag{2-12}$$

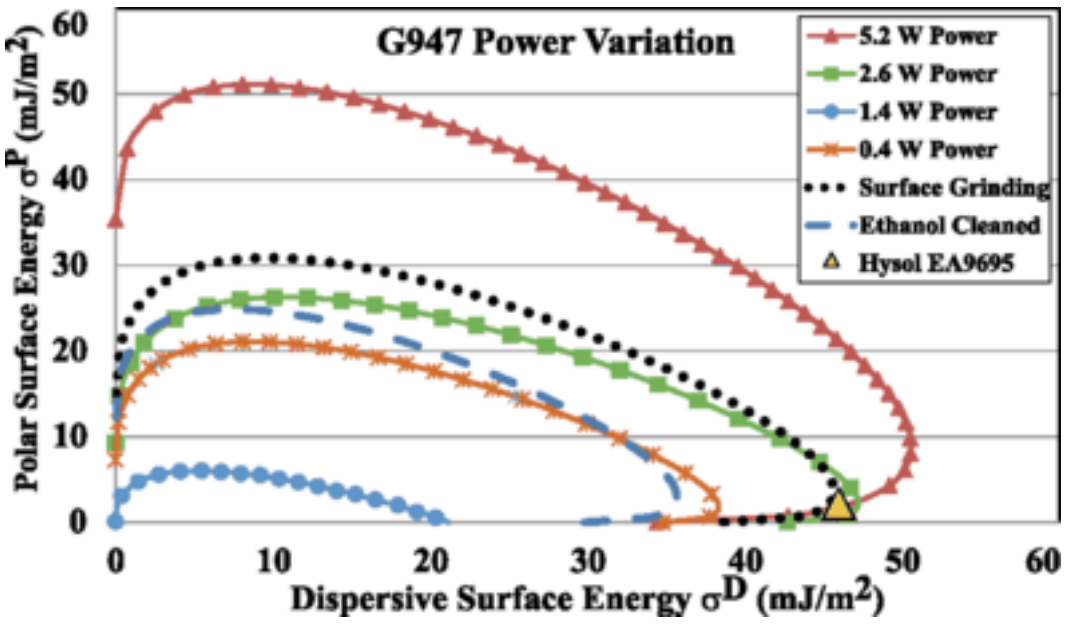

Figure 2-5. Example of wetting envelopes based on the Equations and experimentally obtained contact angles for the known liquids [71].

Each wetting envelope represents the wettability of a different solid surface. They can be used to predict the wetting effect of different liquids on the surface. Völkermeyer et al. [71] used this wetting envelope to show clearly and distinctly the variation in wettability of laser surface modified carbon fibre reinforced plastics (CFRP) at different powers of laser in Figure 2-5. Generally, the larger the wetting envelope, the better the wettability on the solid surface. If liquids with different polar and dispersive components are within the enclosed area, it implies that these liquids can completely wet the solid surface, while on the contrary, if the liquids are outside the enclosed area, these liquids cannot achieve complete wetting of the surface.

The analysis of contact angles, surface free energy and wetting envelope of the surface helps to provide a better understanding of the wettability of a material surface.

2.3 Surface Modifications

However, the poor adhesion properties of polymers have largely limited their applications due to their low surface energy. Numerous surface modifications have been introduced to modify the printability, adhesion and wettability of the polymer surface without affecting the bulk properties.

Surface modification can be used for a range of purposes, such as surface functionalisation, surface deposition, surface cleaning and surface deposition. There are various different kinds of surface modification methods including surface coating, laser treatment, mechanical treatment, wet chemical treatment, plasma treatment, ion beam, ion implantation, etc. However, some drawbacks have also been found in these treatments. The efficiency of the mechanical treatment has been found to be limited.

Wet chemical treatment is considered to display a lack of uniformity and reproducibility in the finished product, and there are also environmental and safety problems with this technique. Flame treatment is also environmentally unfriendly [72].

2.3.1 Wet Chemical Modification

Wet chemical treatment is treatment that involves the reaction between the chemicals in a solution and a surface. It can be used for improving polymer surface properties by spraying, dipping, or coating with chemicals. Through penetrating solvent into the polymer matrix, the contaminants can be removed from the surface and new functional groups can be introduced to modify the polymer surface. It is suitable for large scale treatment, low cost, and selective areas [73]. Regis et al. [74] investigated chemical treatment on polypropylene, and with the use of sodium hydroxide (NaOH), the cell attachment of biomolecules on polyethylene was improved. It was also found in the study of Marchand-Brynaert et al. [75] that carboxylic functional groups were introduced on poly(ethylene terephthalate) (PET) film after hydrolysis in aqueous acetonitrile followed by permanganate oxidation in sulfuric acid.

However, wet chemical treatment normally produces chemical waste which poses a risk to the environment, and has the potential to degrade the polymer surface, leading to lower mechanical strength and faster wearing [13].

2.3.2 Physical Modification

Physical surface modification is a simple, low cost, environmentally friendly treatment that can be performed to enhance polymer surfaces. Physical surface modification can only modify the surface wettability by physically increasing the surface roughness. It

does not change the inherent properties such as the chemistry of the polymers, and therefore does not cause ageing problems. A study by Encinas et al. [76] found that the roughness of polymeric materials such as polyethylene and polypropylene was increased by surface mechanical abrasion using grinding paper , leading to an increase in surface wettability. However, the change of surface wettability was limited compared to the result in the study of Moghadamzadeh et al., [77] who have found that mechanical abrasion with a further corona discharge treatment improved the adhesive property significantly. However, physical modification is almost impossible to apply on fibres and powders [73].

2.3.3 Ultraviolet (UV) Surface Modification

UV surface modification is a treatment that can be used to modify the surface of photo (light-sensitive) polymers using UV light. It is a low temperature, non-contact treatment that can be operated under atmospheric pressure. The UV light can penetrate the surface to induce crosslinks on the polymer surface by initiating a photochemical reaction, thus changing the properties of the polymer surface. UV surface modification can modify the polymer surface without affecting the bulk because UV light can only penetrate into the surface by tens of micro meters. It can also modify the polymer surface physically by hardening the surface, and chemically by introducing new functional groups on the surface. It is a high-speed chemical free process, which is efficient, simple to operate and environmentally friendly. For example, Breuer et al. [78] has improved adhesive bonding strength between polypropylene and epoxy adhesive using UV laser radiation.

However, the polymers that are suitable for the treatment are limited as they must be photo active to the UV light, and there is potential that the UV light can deteriorate the polymer surface [73]. Eve et al. [79] investigated the relationship between the UV light and degradation of PolyMethylMethAcrylate (PMMA), it was found that a decrease in strength and Young's modulus was related to the increase of the UV irradiation dose. It was also found in a study of Kaczmarek et al. [80] that the process of improving wettability by UV treatment is slower compared to plasma treatment.

2.3.4 Plasma Treatment (Low Pressure)

Among the surface modification techniques, plasma treatment has been proven to have many excellent advantages, as it is clean, fast, environmentally friendly, solvent free, and can be used to modify the surface area of heat-sensitive materials like polymers without affecting the bulk [81].

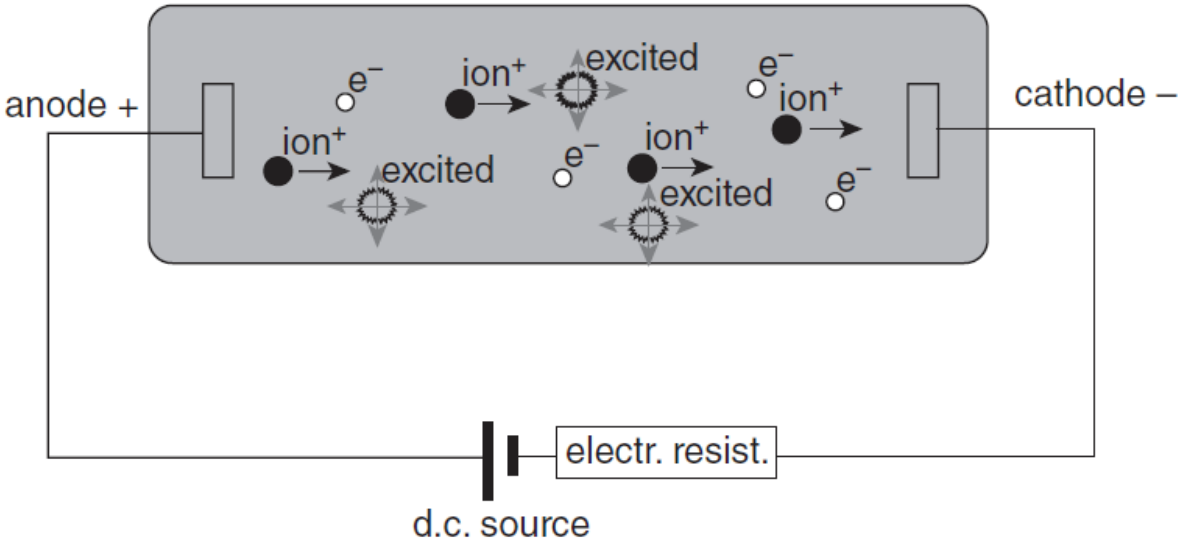

Figure 2-6. Schematic diagram of plasma formation, which consists of electrons, ions and energy-rich neutrals as excited states, by means of a direct current (DC) voltage power supply [82].

Plasma is the fourth state of matter in universe that possesses high energy. In plasma surface modification, the plasma is created by exposing gases such as oxygen and nitrogen to a high energy flow such as an electric field, therefore turning them into excited particles include electrons, ions, atoms, photons, radicals and other species (as shown in Figure 2-6) [73]. Generally, plasmas can be categorised as thermal (hot) and non-thermal (cold) plasmas. Thermal plasmas such as lightning and electrical arc generally possess a temperature of 10000K, while non-thermal plasmas such as low-pressure plasma generally possess temperatures in an order of 100K. In non-thermal plasmas, the electrons are at a high temperature (over 10,000 K). However, the density of electrons is very low and the majority of neutrons are at room temperature, resulting in the low temperature of the non-thermal plasma.

Low pressure plasma is a type of plasma that discharges under low pressure (≤ 1 Torr = 133 Pa) and high frequency (≥ 1 MHz). In this discharge, the electrons have enough energy to break the covalent bonds, while the ions and gas molecules remain at ambient temperatures. Therefore, the plasma reaction that occurs at ambient temperatures is suitable for thermally sensitive materials such as polymers [72].

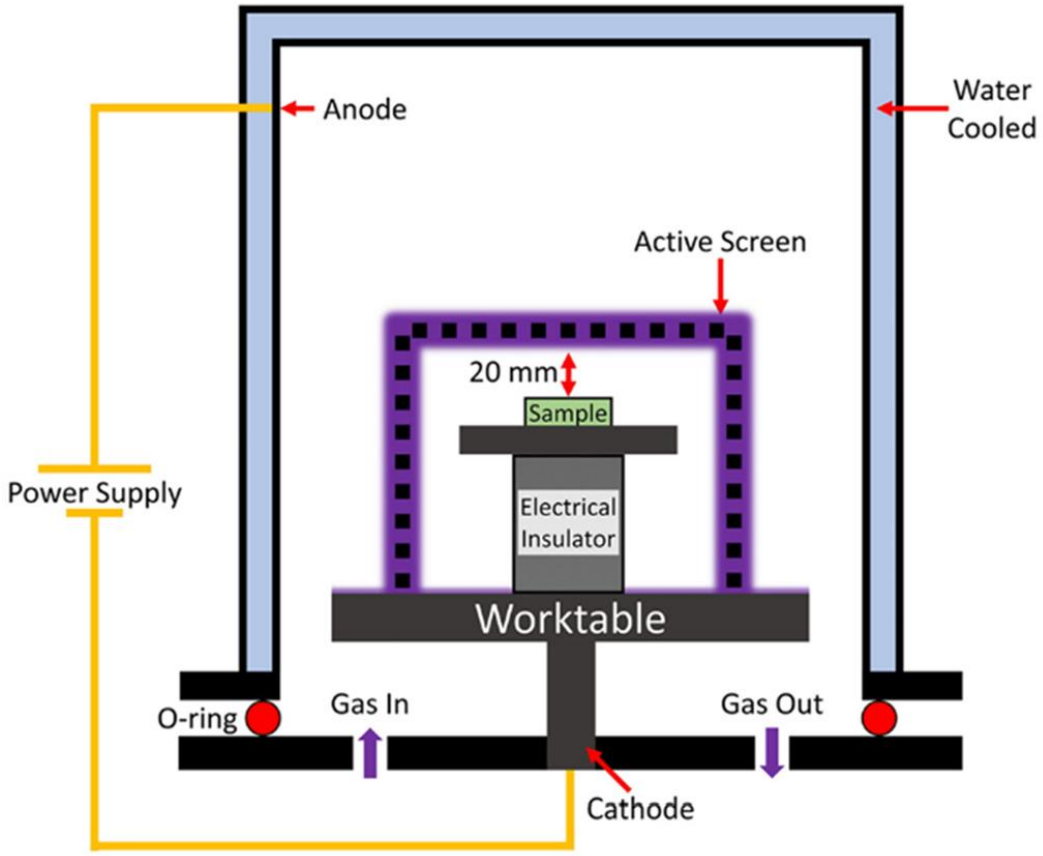

Figure 2-7. Schematic of samples in active screen chamber with sample on an electrical insulator [83].

Polymers cannot be treated using direct current (DC) plasma treatment, because the sample, as one of the electrodes in this technique, needs to be conductive to sustain the discharge. In addition, DC plasma treatment has the potential to cause damage to the material, through effects such as arcing, edge effects, and hollow cathode. To allow polymers to be treated by plasma without the risk of damage, active screen (AC) plasma treatment has been utilised [81]. Instead of directly applying the cathode potential to the samples like the DC plasma, the sample is designed to remain in a floating position surrounded by an active screen (as shown in Figure 2-7), which makes the plasma treatment of nonconductive polymers possible. During the AC process, a

perforated metal cage surrounds the sample, transferring the intense plasmas from the sample to the active screen system. Since the cathode is the mesh instead of the sample itself, the polymer samples can be treated more uniformly, and the damage to the samples is also avoided [83]. Fu et al. [81] has investigated the effects of active screen plasma treatment on polyurethane, the results of which showed that the surface roughness was increased, and new functional groups were introduced after the treatment, leading to the increase in wettability and cell attachment ability on the polyurethane surface. Kaklamani et al. [84] also found that active screen plasma nitriding improved the adhesive property of ultra-high molecular weight poly(ethylene) (UHMWPE).

2.3.5 Dielectric-barrier Discharges (DBD)

Dielectric-barrier Discharges (DBD) are a type of non-thermal plasma that is generated under atmospheric pressure. Shown in Figure 2-8 is a schematic diagram of one of the common configurations of the DBD system. Two dielectric materials are connected to electrodes with a high alternating current (AC) voltage (top electrode) and ground (bottom electrode). The dielectric barrier in the DBD structure is usually glass or silica glass. The dielectric materials act as barriers to prevent arcing and the generation of high temperatures. An alternating voltage is applied on the two dielectric materials and the discharge is created between them.

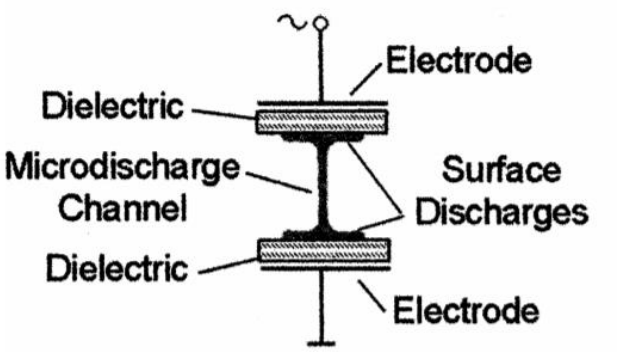

Figure 2-8. Schematic diagram of the configuration of the DBD system in a circuit [85].

In order to transmit an electric current, the electric field must be strong enough so as to breakdown the gas. The alternating current (AC) voltage is required to maintain a continuous discharge tunnel between the two dielectric materials [86]. During the positive half cycle of the applied voltage, the electric field between the two materials is strong enough to break the dielectric materials and form a discharge tunnel. At atmospheric pressure, the gases undergo electrical breakdown, leading to the formation of a large number of discharges. Each of these discharges has a nearly cylindrical plasma channel with a radius of about 100 μm and forms a large surface discharge on the surface of the dielectric. During the negative half cycle of the applied voltage the discharge tunnel collapses due to the switch of the voltage polarity. With the application of the alternating current, the process continues. When a direct current (DC) is applied rather than an AC voltage, the powerful electrical field is constantly present, which leads to a continuous high current discharge, causing damage to the electrodes and dielectric materials. Therefore, to avoid the damage to the configuration and to keep an appropriate discharge flow, an AC voltage is required in the DBD system. The discharge generated between the dielectric materials depends on the

thickness of the dielectric and the applied voltage. When the power is increased, more discharges per unit time and per unit area are added [87].

The DBD systems can be used to modify the surfaces of polymers. For example, Kostovthe et al. [88] found that the surface of polycarbonate became more hydrophilic due to the introduction of polar oxygen and nitrogen containing groups by DBD plasma treatment. Nastuta et al. [89] modified the surface wettability of polyethylene terephthalate (PET) by using different DBD configurations.

2.3.6 µPlasma Surface Modification (ambient pressure)

µPlasma is a plasma of small dimensions down to the micrometre scale containing reactive electrons, ions, photons and radicals. The design of the electrode configuration and dimensions of the discharge region can help with reducing the size of the discharge, and therefore can maintain stability of the plasma tunnel and operate under atmospheric pressures [90]. µPlasma surface modification can be operated under atmospheric pressure, and the non-thermal properties make it particularly suitable for thermally sensitive materials such as polymers. It is less expensive to operate as vacuum conditions are no longer required and energy and gas consumption is reduced compared to low pressure plasma treatment. µPlasma devices that operate under atmospheric pressure are more convenient and portable [91]. Another important advantage of µPlasma modification is that the technique allows for localised treatment of materials, thus reducing the energy waste. In addition, in many surface patterning processes, such as low-pressure plasma treatment and chemical vapour deposition, a physical mask is usually required, however in µPlasma patterning processes, a mask is not necessary. The µPlasma modification process is computer controlled and the

pattern of the treatment can be designed. However, this technique can not be applied on metals.

Figure 2-9. Shows the schematic of µPlasma modification setup. The µPlasmas can be generated between the needle electrode tips that are connected to a high voltage AC power supply and the grounded substrate. When the power supply is switched on with a suitable distance between the needles and the sample, the plasma is ignited. After activating the electrodes, the distance between the needle tips and the substrate is adjusted until the electric field becomes high enough that the charged particles in the air (or gas supplied) will be accelerated by the electric field. In this process, the accelerated particles can collide with atoms in the air, causing the ions and electrons to separate from each other. As a result, plasma streams are generated. The design of the needles in the configuration allows the plasma streams to be small and stable. The dielectric material silicon between the two electrodes is used for preventing the direct flash over. It is also worth noting that the distance between the needles and the substrate table needs to be controlled carefully to allow the plasma to ignite when the needle electrode is activated.

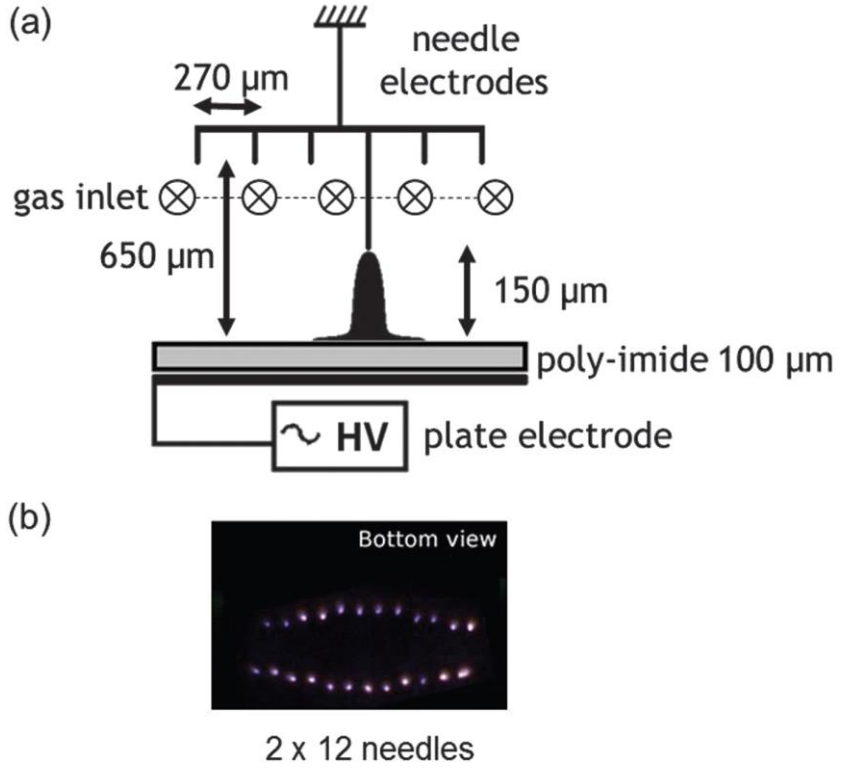

Figure 2-9. The schematic of the µPlasma modification setup that consists of 24 needle electrodes on the print head, a polymer sample and a substrate table [92].

It has been proven that plasma surface modification can improve the surface properties of polymers such as wettability and adhesive properties under different plasma treatment conditions [93-98]. However, despite all the advantages of µPlasma, limited publications studied the µPlasma treated polymers with this configuration [92, 99]. To the best knowledge of the author, only two papers mentioned µPlasma treated polymers. In the study of Schalken et al. [92], the plasma polymerisation of amine-containing films from 3-aminopropyl trimethoxysilane (APTMS) on fluorocarbon polymers was carried out by µPlasma, and with the needle configuration, dot-wise patterning and area selective functionalisation were achieved. Verkuijlen et al. [99] compared the effect of µPlasma treatment and UV-ozone on polycarbonate (PC) and polyethylene naphthalate (PEN). The results showed that more wettable surfaces with

higher oxygen containing groups were produced by microplasma treatment. Therefore, an investigation into the effects of μPlasma treatment on polymers is valuable.

There are also studies on the plasma treatment of engineering thermoplastics [100-107], such as the plasma treatment of carbon fibre reinforced polymers in PEEK, PP and PA6 composites [108-111]. However, there has been no study on the plasma modification of glass fibre reinforced polyamide 6. Therefore, the surface modifications caused by μPlasma on glass fibre filled PA6 is worth investigating.

2.4 Interaction Between Plasma and Polymers

Plasma can modify polymer surface properties physically and chemically, by removing the surface contaminants, increasing surface roughness, breaking chemical bonds and introducing new functional groups on the polymer surfaces [112].

Firstly, plasma treatment can clean the polymer surface by removing organic contaminants to prevent potential adhesion problems. Usually, the contaminants on the polymer surface are extremely difficult to remove, which could reduce the strength of the bond between the substrate and adhesive when joining dissimilar materials. The existence of the contamination layer might react and bond to the adhesives, providing loose bonding, leading to a negative effect on the polymer surface and subsequent experimental results. Therefore, it is necessary to remove the contaminants on the polymer surface. Plasma can remove the contaminants and the impurities on the surface layer by sputtering, ablation of the plasma particles and etching, and produce a clean surface for further surface modification.

Other than this, the plasma treatment process of the sputtering, ablation and etching on the surface can also change the roughness of a polymer surface. This is because amorphous materials are usually easier to remove than crystalline and filled materials due to their weakly ordered structure, thus producing surface textures and roughening the surface [113] . For example, a study by Pal et al. showed that plasma increased the roughness of polyethersulfone (PES) [114]. The increase in surface roughness provides a higher specific surface area and higher surface energy, which means bonding properties are improved. When joined with another material such as a metal through adhesive bonding, this can result in improved mechanical anchoring and mechanical interlocking stabilities [115].

Furthermore, plasma treatment can break chemical bonds and introduce new functional groups on the polymer surfaces. For instance, plasma treatment can introduce polar functional groups such as hydroxyl (-OH), carbonyl (C=O) and carboxyl (COOH) groups that contain oxygen on the surface [116], which contribute to the increase of surface energy. The change in chemical composition on the surface plays an important role on improving the hydrophilicity of the polymer. As a result of the physical and chemical modifications on the polymer surface, the surface energy and surface wettability can be improved, and therefore as can the adhesive properties.

There are some issues with plasma treatment such as ageing, degradation, oxidation and over etching, which can occur when the polymer is exposed to plasma for too long. During the etching process, the degraded fragments can be vaporized to form carbon dioxide, CO, H_2O, etc [117]. Although the etched structure of the surface is usually rougher than the original structure, leading to a surface with higher energy, over

etching can result in excessive removal of the material. For example, when fibre reinforced polymers are exposed to plasma for too long, over-etching exposes the fibre to the surface of the matrix, thus separating the fibres from the substrate and causing a reduction in mechanical properties include strength and stiffness.

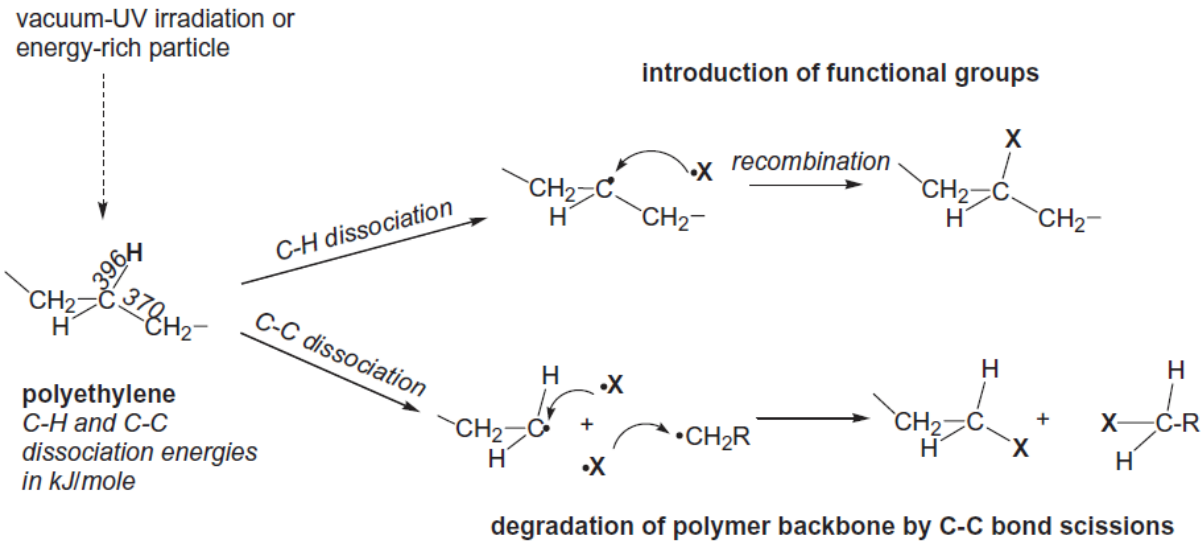

Figure 2-10. Schematic diagram of the response of polyethylene to plasma with vacuum-UV irradiation or energy rich particles (new introduced functional groups are represented by X) [117].

It is not only the collision of the plasma on the polymer that causes the reaction and etching, but also the plasma vacuum ultraviolet (UV) irradiation with extremely short wavelengths [118]. As shown in Figure 2-10, plasma with energetic particles and UV radiation can break the C-H bond and introduce new functional groups, as well as breaking the C-C backbone in polyethylene, which is known as chain scission. When the two C radicals formed after C-C bond scission cannot be immediately recombined, this leads to degradation of the polymer, as the bond strengths between C-C and C-H are similar.

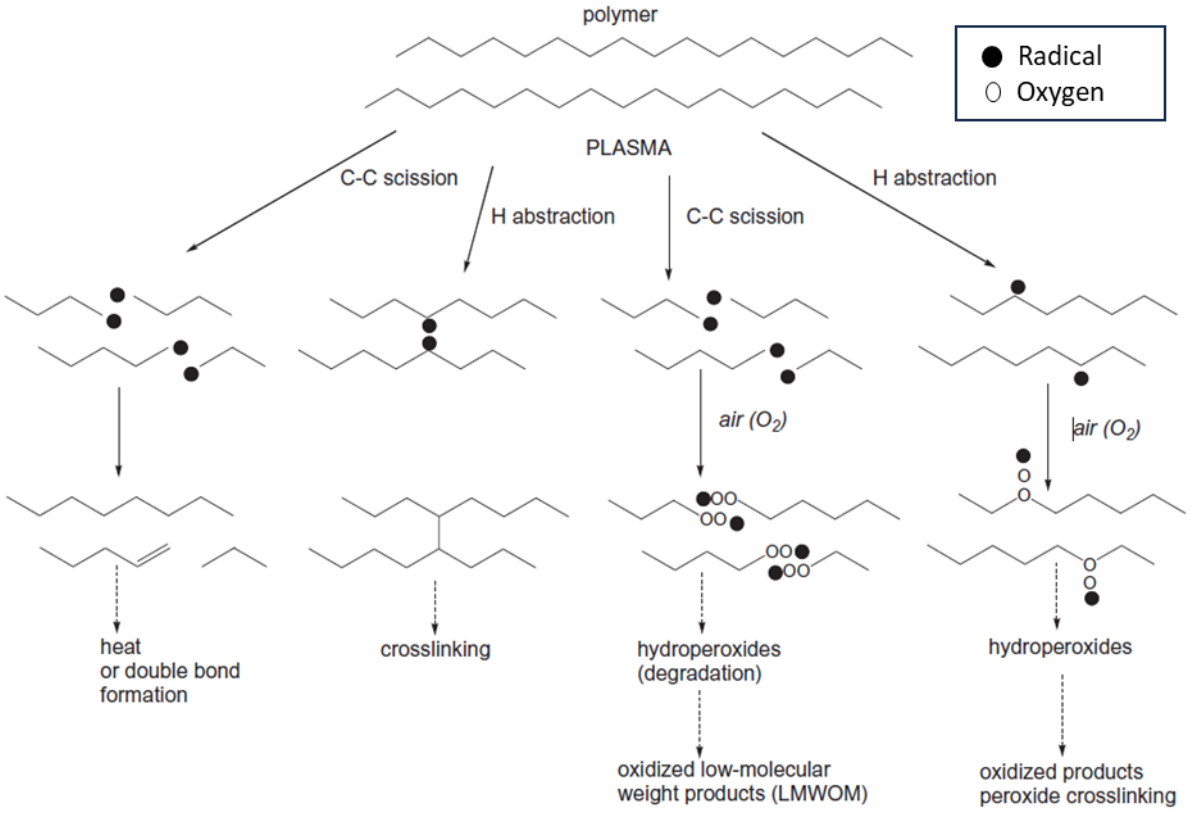

Figure 2-11. Schematic diagram of C-C scission, and the formation of C=C, crosslinking, degradation and oxidation [117].

Plasma treatment of polymers is also associated with crosslinking. The collisions of plasma can break the molecules on a polymer surface into numerous active species such as ions, electrons, photons, and free radicals. The formation of free radicals on the surface and near-surface layers can occur, undergoing radical to radical or radical to molecule reactions. The interaction between these free radicals can cause restructuring (as illustrated in Figure 2-11), leading to the generation of heat within the polymer, the formation of C=C bonds, cross-linking and degradation. The crosslinking traps the radicals in the near surface layers, and therefore oxidation can occur in the presence of oxygen. However, the formation of crosslinking can also create a very cohesive surface, which improves the heat resistance and bond strength of the

polymer [72]. Therefore, it is important to control the exposure time of polymers to plasma.

2.5 Permanence of the Effect of Plasma Treatment

Although plasma treatment can modify polymer surface wettability significantly, the changes tend not to be permanent. The polymer surface experiences an ageing behaviour that results in a decrease in wettability as a function of time. The ageing behaviour can be explained in several ways:

2.5.1 Non-degradative Process – Hydrophobic Recovery

Plasma treatment of polymer surfaces can introduce polar functional groups and thereby increase the surface energy of the material. To minimise the free energy of the system, the polar functional groups tend to reorientate or diffuse towards the bulk of the material, leading to a decrease in the hydrophilicity of the polymer surface when the modified polymer surface is exposed to non-polar environments such as air. This phenomenon is referred to as hydrophobic recovery, which is a non-degradable (a process does not cause degradation) process. The smaller molecules or species with lower molecular weight can diffuse into the near surface or bulk region, which is driven by the energy difference and the concentration of polar groups between the modified surface layer and the bulk material. The larger polymer chains that cannot easily diffuse instead undergo a reorientation process. As illustrated in Figure 2-12, the X functional groups rotate around the C-C bond towards the bulk, and the segments diffuse towards to the bulk.

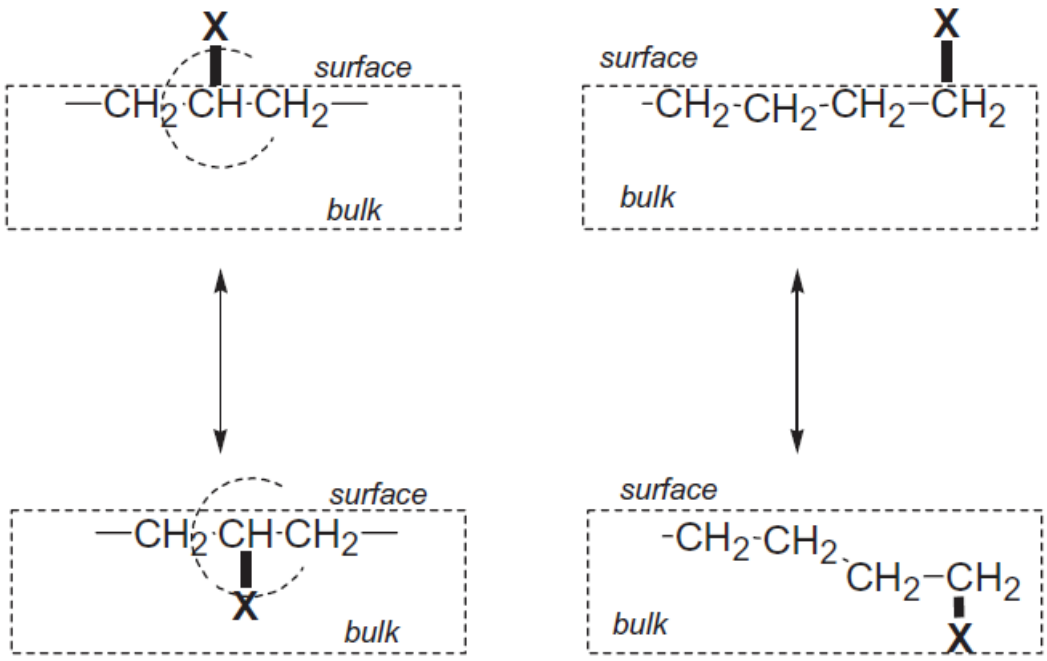

Figure 2-12. Schematic of hydrophobic recovery of chain rotation and diffusion back into the bulk [117].

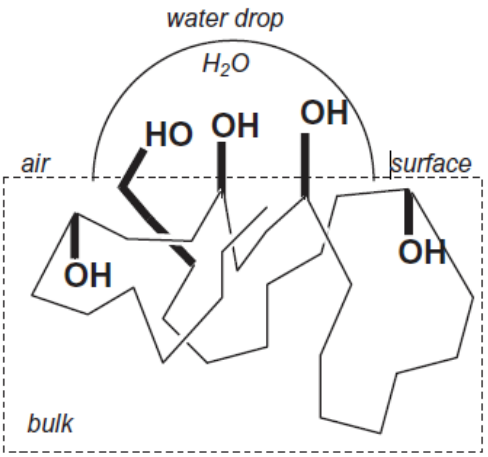

Figure 2-13. Schematic of O-H surface functional groups interacting with water [117].

If the air environment is replaced by a polar environment such as water, the polar functional groups remain on the surface. This is because the polar groups interact with

water and form chemical bonds such as hydrogen bonds with water molecules, which lock the polar functional groups onto the surface [119]. As shown in Figure 2-13, rather than rotating or diffusing back into the bulk, the polar O-H functional groups remain on the surface within the water droplet, forming hydrogen bonds with the water molecules.

2.5.2 Degradative Processes – Oxidation, Chain Scission and Crosslinking

In addition to hydrophobic recovery, a number of degradative processes such as oxidation, chain scission and crosslinking can also be attributed to the ageing of the polymer after plasma treatment. For example, Borcia et al, [120] has found during dielectric barrier discharge (DBD) plasma treatment, there were plasma-induced oxidation, chain scission and crosslinking happened on polymers with aromatic and non-aromatic structures, causing material degradation from surface to the bulk.

As mentioned above in section 2.4, plasma can break the C-H bond and introduce new functional groups, as well as breaking the C-C backbone and causing chain scission. Additionally, plasma can introduce free radicals into the surface and near-surface regions. The recombination of the two C radicals after chain scission can thereby lead to the crosslinking of the polymer. The free radicals are then trapped between the cross-linked lattices, undergoing a slow reaction with oxygen, thus allowing the polymer surface to degrade and age over time after plasma treatment. The higher the crosslink density, the higher the concentration of free radicals trapped near the surface.

2.6 The Factors Affecting the Permanence of Plasma Treatment

Studies have also shown that the wettability of polymer surfaces after plasma treatment is strongly dependent on the storage temperature and humidity, and the crystallinity of the material.

2.6.1 The Effect of Crystallinity on the Permanence of Plasma Treatment

The polymer ageing process after plasma treatment can be affected by the crystallinity of the polymer. The surfaces of polymers are highly mobile compared to those of metals and ceramics. This means that polymer solids can adapt to different environments with different surface configurations, thus minimising the total free energy of the system. However, after entering a new environment, the reorientation and change in equilibrium through the relaxation of the polymer surface will largely depend on its physical properties, such as surface crystallinity and density [121].

Within the amorphous region, molecular chains have high mobilities. Conversely, within the crystalline region the movement of chains is hindered due to the close packing of crystalline lamellae structure. In highly crystalline polymers, the rotating and penetrating motions of the molecular chains on the surface after plasma treatment are limited, therefore the hydrophobic recovery process is reduced. As a result, more polar functional groups remain on the polymer surface for a period after the plasma treatment, thus keeping surface wettability consistent.

As shown in the work of Kim [12], the crystallinity of LDPE is increased by annealing, and the change in surface hydrophilicity and functional groups present were investigated by contact angle measurement and X-ray photoelectron spectroscopy

(XPS). It was found that the quenched LDPE with lower crystallinity aged faster than the annealed LDPE with higher crystallinity, and it was suggested that the high crystallinity reduced the diffusion rate of the polar groups during ageing. In the study carried out by Hyun [121] different crystallinities of polymers were achieved by annealing for different time periods. It was found that the hydrophobic recovery time was also longer for samples with longer annealing times after plasma treatment, therefore indicating that higher crystallinities impeded the ageing process. The authors also proposed that the difference in the contact angle between the untreated and hydrophobic recovered surface represents the remaining polar functional groups on the surface, which is proportional to the crystallinity of the polymer.

Different crystallinities not only affect aging, but also lead to different interactions between polymer surfaces and plasmas. As shown in the study of Junkar et al. [122], the amorphous regions on a polymer surface are preferentially degraded and uniformly etched and melted by plasma, Therefore, amorphous materials can only withstand shorter plasma treatment times. Semi-crystalline polymers can withstand plasma treatment for much longer, resulting in an increase in surface roughness compared to amorphous polymers, leading to a better surface wettability.

2.6.2 The effect of humidity and temperature of the environment on the permanence of plasma treatment

Polymer ageing is also highly dependent on the storage conditions such as humidity and temperature of the environment.

The treated polymer surface is in a non-equilibrium state, and the chain segments tend to rearrange and recover to an equilibrium state with a minimal surface energy. The higher the temperature in the environment, the higher the energy the chains have, leading to an increase in their mobility. As a result, the surface of the polymer becomes less wettable when aged at higher temperature, as the increased mobility of the chains causes a more rapid decrease in wettability. Occhiello et al. [123] investigated the aging behaviour of polypropylene surfaces at different temperatures (77, 293, 333, 363, 393, 413, and 428K in air) after plasma treatment. The results show that the wettability of the polymers is time-dependent and decreases more rapidly at higher temperatures.

The relative humidity if the storage environment can also play a critical role in accelerating the ageing process. When the humidity of the surroundings increases, the polymer absorbs more water, leading to an expansion in the free volume between the polymer chains, therefore increasing the mobility of the polymer chains. As a result, the movement of the polar functional groups can be facilitated and they can reorientate or diffuse back to the bulk material easily [124]. Geyter et al. [124]studied the influence of relative humidity on the ageing of plasma treated polyethylene terephthalate (PET) films. The results showed that as the relative humidity increased, the water contact angle increased at a faster rate, demonstrating a faster ageing process.

In conclusion, an environment with a high temperature and humidity can accelerate the ageing behaviour of plasma treated polymers.

2.7 Modelling the Ageing Process

The energy that is distributed on the polymer surface experiences a fluctuation when exposed to a chemical or physical reaction by plasma treatment. Plasma treatment can disturb the polymer surface by introducing new functional groups and changing the surface morphology. Such disturbances can lead to non-degradative and degradative ageing behaviour including hydrophobic recovery, chain scission, crosslinking, and oxidation. In order to minimise the total free energy of the system, the chains, side chains, and functional groups undergo rearrangement, leading to a continuous slow relaxation from the non-equilibrium state to the final thermodynamic equilibrium state.

The investigation of the ageing behaviour of plasma treated polymers can be enhanced through the use of modelling techniques, which can provide a quantitative and predictive understanding of the process. By employing such modelling methods, it is possible to optimise plasma treatment parameters, thereby achieving a desired performance outcome. Mortazavi et al. [125] developed a combined model, including diffusion and molecular reorientation, along with the Cassie Equation, in order to describe the hydrophobic recovery process of plasma-treated polymers. The authors utilised curve fitting to derive $cos\theta$ as a function of time by curve fitting, which enables changes in the water contact angle during the recovery process to be calculated. The model was able to effectively fit experimental data obtained from a range of polymers, including (polyethylene) PE, (polypropylene) PP, (polystyrene) PS, (polyethylene terephthalate) PET and (Polymethyl methacrylate) PMMA. Furthermore, the model was used to quantify the impact of various parameters, such as temperature and treatment time on the hydrophobic recovery process.

$$cos\theta = C_0 \left(C_1 erf \frac{h}{2\sqrt{Dt}} + C_2 e^{\frac{-t}{\tau}}\right)(1 - cos\theta_U) + cos\theta_U \qquad (2\text{-}13)$$

The model Equation in question is shown in Equation (2-13), where C_0 is the initial concentration of modified molecules in the modified layer, h is the thickness of the modified layer, C_1 and C_2 are the contribution of the diffusion and the reorientation term, t is the recovery time, τ is the relaxation time, D is the self-diffusion coefficient of modified chains, θ is the contact angle, θ_U is the contact angle of the untreated surface.

2.8 Failure Modes

The adhesive bonding strength is normally determined by tensile lap-shear test. The failure modes after tensile lap-shear test are dependent on bonding strength and quality; therefore, it is necessary to analyse the bonding failure. According to ASTM D5573 – 99 (2019) standard [126], failure modes include adhesive failure, cohesive failure, thin-layer cohesive failure, fibre-tear failure, light-tear failure, and stock-break failure, as shown in Figure 2-14.

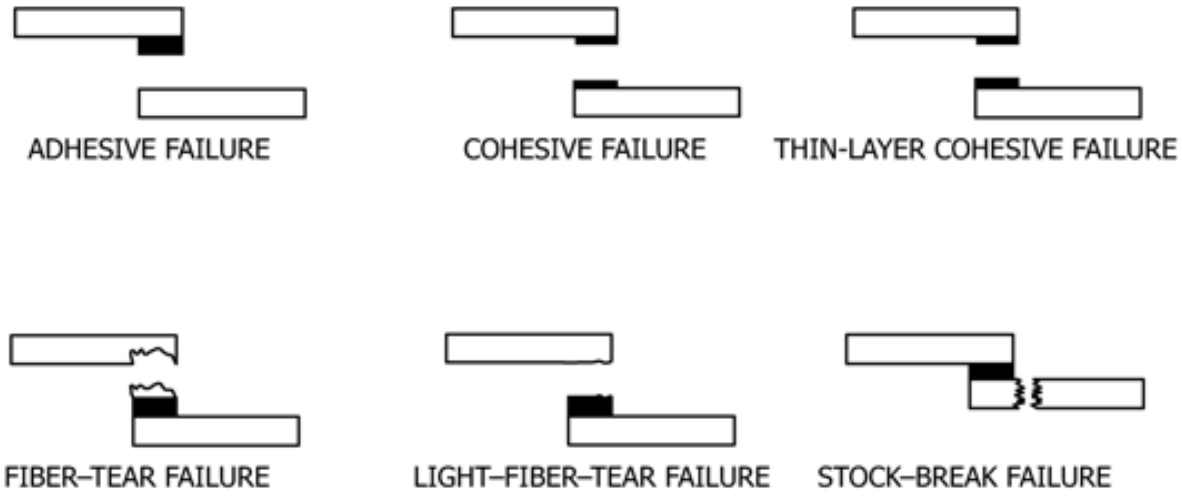

Figure 2-14. Schematic of failure modes for joining materials [126].

As illustrated, the adhesive failure is a failure that happens at the interface of the adhesive and the substrate material, it usually occurs when the adhesive bonding between the substrate material and adhesive is very weak, which is usually caused by insufficient or no surface preparation. The cohesive failure is a failure of the adhesive when the tensile lap-shear strength is not high enough. Substrate failure that occurs at the substrate instead of the adhesive can happen when the adhesive bonding between the substrate material and adhesive is stronger. The substrate failure includes fibre-tear failure, light tear failure and stock-break failure. A mixed failure can also happen when high tensile strength increases and cracks propagate in the adhesive [8].

The failure modes of bonded metal-composites and composites-composites by Araldite adhesive after tensile lap shear test failure was studied by Seyyed et al. [127]. In metal-composites failure, a mixed failure of cohesive failure and bond line failure (adhesive failure) were observed, while adherend failure (substrate failure) mode was only observed for composites-composites joints.

3 Effect of µPlasma Modification on the Wettability and the Ageing Behaviour of Glass Fibre Reinforced Polyamide 6 (GFPA6)

This work is presented in "Effect of µPlasma Modification on the Wettability and the Ageing Behaviour of Glass Fibre Reinforced Polyamide 6 (GFPA6)," *Materials,* vol. 14, no. 24, p. 7721, 2021. The authors contributiona are defined as: Conceptualization, M.J. and H.D.; methodology, B.D. and C.C.; validation, C.C.; formal analysis, C.C.; investigation, C.C.; resources, M.J. and H.D.; data curation, C.C.; writing—original draft preparation, C.C.; writing—review and editing, C.C., B.D., M.J., H.D. and X.L.; visualization, C.C.; supervision, M.J.; project administration, M.J. and H.D.; funding acquisition, H.D. and X.L.

Abstract

Glass fibre reinforced polyamide 6 (GFPA6) thermoplastic composites (TPCs) are promising materials with excellent properties, but due to their low surface free energy they are usually difficult to wet, and therefore, possesses poor adhesion properties. µPlasma modification offers potential solutions to this problem through functionalisation of the GFPA6 surface. In this study, the effect of µPlasma on the wetting behaviour of GFPA6 surfaces was investigated. Following single µPlasma treatment scans of GFPA6 samples, a substantial enhancement in wettability was observed. However, the effect of the µPlasma modification was subject to an ageing phenomenon, although the enhancement was still partially maintained after 4 weeks. The ageing process was slower when the GFPA6 material was pre-dried and stored in low humidity conditions, thereby demonstrating the importance of the storage environment to the rate of ageing. Orientation of the fibres to the observed contact angle was found to be crucial for obtaining reproducible measurements with lower

deviation. The influence of testing liquid, droplet volume and surface texture on the repeatability of the measured contact angle were also investigated.

Keywords: microplasma; thermoplastic composites; polyamide 6; wettability; ageing; contact angles

3.1 Introduction

Thermoplastic composites (TPCs) are a class of polymers that have attracted much attention due to the desirable combination of good mechanical properties, ease of manufacture, low density and their ease of recycling [1, 128]. In recent years, the industrial demand for glass fibre reinforced polyamides has increased, especially in the automotive sector, due to their excellent thermal stability, high toughness and stiffness [4, 129-132]. For example, Polyamide 6 with glass fibre reinforcement offers good thermal stability, and higher tensile strength [1, 133], which makes it an attractive material for the automotive industry. Often there is a requirement that the TPC is bonded to other structural materials, such as metals or other composites. However, due to the typically low surface free energy, poor chemical reactivity, polymers and TPCs are usually difficult to wet, and therefore, possess poor adhesion properties [134, 135]. A potential solution to this problem is through surface modification of the polymers or TPCs to improve their surface properties, while still retaining their desirable bulk properties.

A number of studies have demonstrated that surface treatments, such as laser treatment, chemical treatment, plasma treatment, ion beam and ion implantation [136-141], can enhance the wettability of different materials. In particular, plasma treatment of polymer materials has been shown to modify the surface by removing contaminants, introducing functional groups, and improving the surface free energy without affecting the substrate material [72]. Consequently, plasma surface modification of polymers has become an attractive solution to overcome the challenges associated with the poor wetting and adhesion of these materials. However, plasma-based techniques, such as

active screen plasma nitriding, are usually operated at low pressures, and therefore, require costly treatment chambers capable of achieving low pressures coupled with sufficiently powerful vacuum systems necessary to reach the desired pressures [72, 81, 142]. In addition, it is difficult, if not impossible, to achieve continuous treatment using the active screen plasma technique. To overcome these limitations, atmospheric plasma treatments have been explored, an example is a µPlasma modification. These plasma treatment techniques offer the ability to perform localised treatments under atmospheric conditions and thus demonstrate great promise for future industrial uptake [99, 143, 144].

Numerous studies have demonstrated that plasma surface treatment can modify the wettability of polymer surfaces significantly [93-98], however, despite its great potential, only two publications reported µPlasma modification on polymers [92, 99]. Plasma surface treatment on different kinds of polymers has also been reported, including polyamide materials, such as polyamide 12, polyamide 6,6 and polyamide 6 [18-22], however, there are no studies that report on the plasma treatment of glass-fibre reinforced polyamide 6.

While plasma treatments are effective in improving polymer surface wettability, it is well established that these enhancements are not permanent [145, 146]. A pronounced increase in wettability is typically observed immediately following plasma treatment, with a gradual decrease over time, to the point where the wettability of the surface almost matches the untreated polymer [135, 147]. This decay of the wettability over time is known as the hydrophobic recovery or ageing of the surface [119], and studies have reported these phenomena with different forms of plasma treatments, including

low-pressure plasma treatment of polyamide 6 rods [135] and polyamide 6 sheets [148], NH_3 plasma treatment of polyamide 6 foil [47], and atmospheric pressure plasma treatment of polyamide 6 fibres [149]. However, the ageing data was typically reported on a daily or weekly basis, with minimal focus on the initial changes within the first few minutes or hours after the treatment. Therefore, given the dynamic nature of the surface following plasma treatment, it is critical to investigate and characterise the initial wettability fluctuations and ageing behaviour following plasma treatment to enable a better understanding of this phenomenon, as well as approaches to prevent or slow this ageing behaviour.

To characterise the change in surface wettability after plasma treatments, many studies rely on the measurement of the contact angle. However, the reliability and validity of these measurements on hydrophilic, and potentially roughsurfaces have proven to be challenging. The measurement of contact angle is affected by numerous factors including the liquid used, the volume of the drop, ambient humidity and surface flatness. Studies by Baek et al. [150] and Li et al. [151] considered the effect of the external conditions on the measured contact angle in reverse osmosis (RO) membrane surfaces. It was established that using different droplet sizes, measuring times, liquid type and humidity can affect the contact angles of the material. However, there are no comparable studies involving polyamides (either filled or unfilled). In the case of polyamide 6, the measurement will be complicated because of the hygroscopic nature of the material [1], which can influence the accuracy of the contact angle measurement when using water. Moreover, the existence of fibres in fibre-reinforced polymer composites significantly increases the roughness of the material surface, which can also affect the contact angles. Therefore, it is clear that there is a need for systematic

investigation of the contact angle measurement procedure on GFPA6 materials, including characterisation of the effect of variables, such as the liquids used, orientation used to measure the angle, the location on the sample surface and the volume of the droplets.

Hence, the aims of this study were two-fold. The primary aim was to investigate the effect of μPlasma modification on the wettability of GFPA6 surfaces, and their short-term (minutes to hours) and long-term (days to weeks) hydrophobic recovery. The secondary aim was to develop a more reliable systematic protocol for measuring contact angles on GFPA6 to better characterise the surface wettability and ageing behaviour after the treatment. Finally, approaches that will hinder or prevent complete hydrophobic recovery of the treated surfaces are briefly explored.

3.2 Materials and Methods

3.2.1 Material

Celstran® CFR-TP PA6 GF60-03 tape (GFPA6, Celanese Corporation, Dallas, USA), which is a polyamide-6 matrix (40 wt%) reinforced with continuous unidirectional glass fibre (60% by weight), was used for all testing within this study. The sample was processed by injection molding into sheets, witha thickness of 0.3 mm, and a each sheet was cut to a size of 10cm×10cm. Thermal analysis was carried out using a differential scanning calorimeter (PerkinElmer DSC-7, PerkinElmer Inc., Waltham, USA), and the melting temperature (T_m) and glass transition temperature (T_g) were found to be 222.0 °C and 49.8 °C, respectively. The measured heat of fusion and calculated degree of crystallinity was found to be 43.88 Jg^{-1} and 19.08%, respectively.

3.2.2 µPlasma Modification

The untreated GFPA6 was initially cleaned using ethanol to remove any contaminants on the surface, and then the surface was dried in air. The cleaned sample was then µPlasma treated using a Roth & Rau Pixdro LP50 plasma inkjet printer (InnoPhysics, Eindhoven, Netherlands) (Figure 3-1) fitted with an InnoPhysics POD24 print-head (as illustrated in Figure 3-2a). There are 24 needles placed in two rows on a movable print head (as shown in Figure 3-2), which is connected to a high voltage alternating current power supply. The plasma within this study was ignited using a single row of 12 needles. The different combinations of parameters, including accelerating voltage, printing rate, and working distance were tested systematically by changing one of them at a timecoupled with results of material wettability (i.e., contact angle measurements) to optimise the treatment parameters. The optimal settings were determined as follows: an accelerating voltage of 7 kV, a printing rate of 20 mm/s, and a working distance from the sample surface to the tips of the printing needles of 100 µm. Patterns were designed as 20 × 20 mm^2 squares, where the plasma spots overlap with each other (shown in Figure 3-3), to produce uniform treatment coverage.

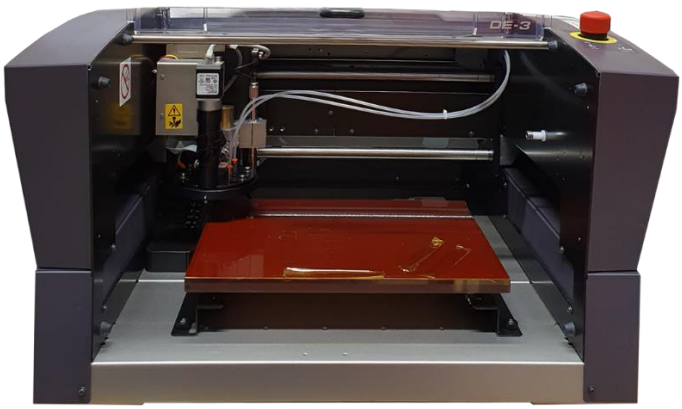

Figure 3-1. Image of µPlasma system.

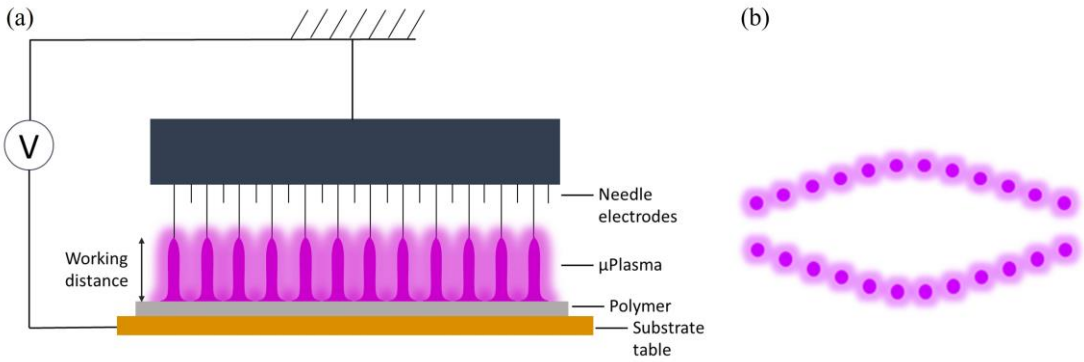

Figure 3-2. (a) Schematic of µPlasma modification setup. (b) µPlasma discharges pattern generated by 24 needle electrons from top view.

Figure 3-3. µPlasma modification pattern.

3.2.3 Scanning Electron Microscopy (SEM)

A JEOL 7000F SEM (JEOL, Japan, Tokyo manufacturer) with an ac-celerating voltage of 5 kV was used to characterise changes in the surface morphology following treatment of the GFPA6 material. Before SEM imaging, samples were gold sputter-coated using an EMITECH K550 set (EMITECH, Kent, UK) at a current of 25 mA and for a duration of 2 min.

3.2.4 Contact Angle Testing

Contact angle measurements were carried out using the sessile drop method with an experimental apparatus that complied with the ISO 19403-2:2020 standard [152]. Samples were placed on a height (*z*-axis) adjustable laboratory jack, while a light

source and a camera connected to a monitor were used to obtain a clear image of the droplet. The light source, sample surface and camera were placed in a straight line and at the same horizontal plane (i.e., same height/*z*-axis) to ensure contact angle measurements were obtained from the same viewpoint across different samples. Three repeats were performed on each sample to allow for average and standard deviation calculations of the measured contact angles. The measurements were carried out under ambient temperature and humidity conditions, where deionised water, diiodomethane, and glycerol were used as the liquids for the tests. To limit the potential influence of gravity, droplets were carefully deposited on the sample surface using a calibrated pipette. The average of the left and right contact angles was obtained for each individual droplet. The samples were oven dried at 80°C for 3h prior to the contact angle measurements during the optimisations.

The initial ageing process was tested every ten minutes for five hours, and was represented by measuring the wettability, i.e., the contact angles. The data was curve fitted using Cowie and Ferguson model [25]. For both wettability and ageing testing of sample surfaces, the overall average contact angle was calculated from the three repeat droplets on the same sample. The captured images were analysed using the contact angle plugin on ImageJ to obtain contact angle values.

3.2.5 Wetting Envelope and Surface Free Energy

To better understand the wettability changes following the µPlasma modification, surface free energy values were calculated, producing wetting envelopes to evaluate the changes in the surface free energy and predict the wetting capabilities against different liquids. Surface free energies of the surfaces were calculated based on

Young's Equation (3-1), which describes the relationship between the surface energy of a solid (σ_s), the surface tension of a liquid (σ_l), the solid-liquid interface tension (γ_{sl}), and the contact angle formed at the solid-liquid interface (θ), as well as Fowkes theory of splitting the total surface energies (both solid surfaces and liquids) into a combination of a dispersive, σ^D, and a polar, σ^P, component. Equation (3-3), which was used to calculate the surface energies, forms from the combination of Equations (3-1) and (3-2).

$$\sigma_S = \gamma_{SL} + \sigma_L \cos\theta \tag{3-1}$$

$$\gamma_{SL} = \sigma_S + \sigma_L - 2 \cdot \left(\sqrt{\sigma_S^D \cdot \sigma_L^D} + \sqrt{\sigma_S^P \cdot \sigma_L^P} \right) \tag{3-2}$$

$$(\sigma_L^P)^{1/2} \cdot (\sigma_S^P)^{1/2} + (\sigma_L^D)^{1/2} \cdot (\sigma_S^D)^{1/2} = \frac{\sigma_L \ (\cos\theta + 1)}{2} \tag{3-3}$$

Where σ_L^P is a polar component of the liquid surface tension, σ_S^P is the polar component of solid surface energy, σ_L^D is a dispersive component of the liquid surface tension, σ_S^D is the dispersive component of solid surface energy, and σ_L is the total liquid surface tension. The dispersive and polar components of solid surface energy, σ_S^P, were calculated by applying two different liquids, diiodomethane (σ_L^D = 50.8 mN/m, σ_L^P = 0) and deionised water (σ_L^D = 46.4 mN/m, σ_L^P = 26.4 mN/m) to Equation (3-3). Therefore, the total surface energy of the solid, σ_S, was calculated as $\sigma_S = \sigma_S^P + \sigma_S^D$.

When the polar and dispersive components of a standard liquid are brought into a coordinate system as a function, a wetting parameter *R* can be obtained using Equation (3-4), with polar ($R.cos\phi$) and dispersive ($R.sin\phi$) component contributions to the total magnitude of the surface energy being calculated using the formed angle (ϕ).

$$R^2 = (\sigma_L^P)^2 + (\sigma_L^D)^2 \quad (3\text{-}4)$$

$$\sigma_L^D = R \cdot cos\phi \quad (3\text{-}5)$$

$$\sigma_L^P = R \cdot sin\phi \quad (3\text{-}6)$$

Substituting these Equations (3-4)–(3-6) into Equation (3-7), which describes the surface energy contributions for a solid and liquid under complete wetting (i.e., cosθ = 1 or contact angle = 0), forms Equation (3-7). In this Equation, R, which is the absolute vector, can be calculated for different ϕ angles between 0 and 90°, to form a wetting envelope that describes the polar and dispersive surface tension limits for theoretical complete wetting of the surface. Comparisons of the area within the produced wetting envelope can give information related to the wetting capabilities of a surface, with larger wetting envelopes indicating greater surface wettability (i.e., more liquids are expected to be capable of fully wetting the surface).

$$R = \left(\frac{\sqrt{\sigma_s^P} sin\phi + \sqrt{\sigma_s^D cos\phi}}{cos\phi + sin\phi} \right)^2 \; for\; 0° \leq \phi \leq 90° \quad (3\text{-}7)$$

3.3 Results and Discussion

3.3.1 µPlasma Modification Process Optimisation

To optimise the µPlasma modification settings, the contact angles of untreated and µPlasma treated samples under different settings, including printing rate, the working distance (from the sample surface to the tips of the printing needles) and accelerating voltage, were measured (as shown in Figure 3-4). When keeping the voltage and

working distance constant, but changing the printing rate, the contact angles do not demonstrate substantial change. Although not significantly different, the biggest reduction in contact angle was found under 20 mm/s printing rate, and therefore, this was chosen for the following optimisation tests. When the voltage and printing rate were kept constant and the working distance was adjusted, the biggest reduction of contact angle was observed with a working distance of 100 μm. Therefore, a working distance of 100 μm (and printing rate of 20 mm/s) was chosen for the final process optimisation test (influence of accelerating voltage). A trend of continuously reducing contact angles was observed with increasing accelerating voltage, with an accelerating voltage of 7 kV demonstrating the largest reduction. This reduction in water contact angles was measured to be significant, going from 78.8 ± 3.1° (untreated) to 32.5 ± 4.7° following μPlasma modification at 7 kV. This indicates that the accelerating voltage is the dominating parameter of the μPlasma modification process for controlling final sample surface wettability. A higher accelerating voltage of 8 kV was also attempted; however, issues with the stability of the plasma prevented the further use of this setting (plasma remained active in between treatment scan lines).

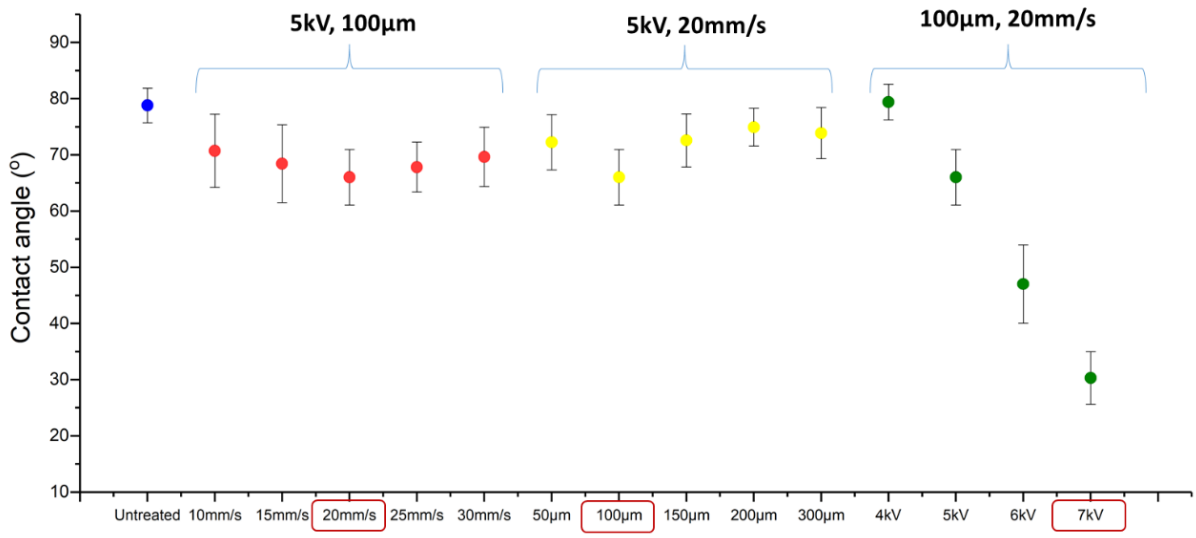

Figure 3-4. Contact angles of an untreated sample and µPlasma treated samples with different processing parameters (printing rate, working distance and accelerating voltage).

The increase in wettability can be attributed to the increase of the total surface energy and the formation of new polar groups following µPlasma modification (a more detailed explanation can be found in Section 3.2.5). The contact angles of untreated and µPlasma treated samples (1–10 treatment scans) are displayed in Figure 3-5. It was observed that no discernible enhancement or synergetic improvement could be observed in the surface wettability with increasing treatment numbers, i.e., it was found that a single treatment scan on the sample surface was sufficient to modify the wettability to the same degree as multiple scans. Similar results have been previously reported by Károly et al. [153], whereby no significant further enhancement in wettability of unfilled polyamide 6 surfaces was found with increasing plasma treatment time. Therefore, since increasing treatment numbers did not significantly enhance the wettability of the surfaces when compared to single treatment scans, all other tests performed within this study were carried out with surfaces subjected to a single

treatment scan. In summary, one treatment was found to induce enough modification of the surface to approximately reduce the contact angle by 50°.

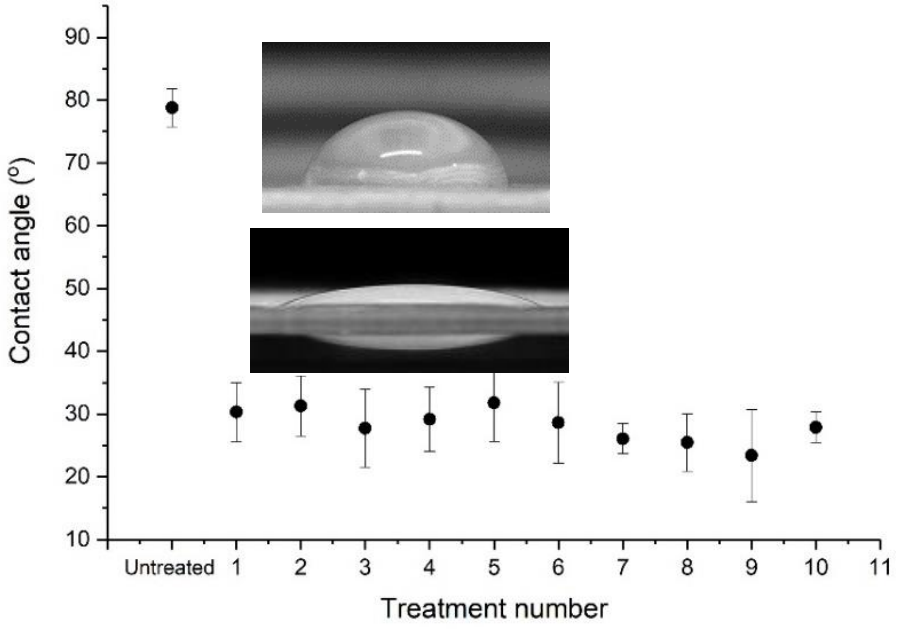

Figure 3-5. Contact angles of untreated and treated (with accelerating voltage of 7 kV, printing rate of 20 mm/s, and working distance of 100 µm) GFPA6 from 1–10 treatments.

3.3.2 Ageing of GFPA6 Surface after µPlasma Modification

Although µPlasma modification can significantly improve the wettability of GFPA6 surfaces, the effect was found to not be permanent when the sample surface was exposed to air. A sharp increase in the measured contact angles was observed immediately following µPlasma modification (0–80 min), revealing a fast-ageing mechanism. Figure 3-6a shows the increase in surface contact angle of µPlasma treated GFPA6 samples left to age in the air for 5 h. The value of the measured contact angle rose from 32.5° to 40.6° within the first 10 min, with a further increase to 53.7° after 80 min. This decrease in hydrophilicity is known as hydrophobic recovery, which is typically attributed to the reorientation and diffusion of the polar functional groups

that are produced, and introduced onto the surface of the samples, during the μPlasma modification. The increase in contact angles is much less significant between 80 min and 3 h, with gradual plateauing of the measured contact angles. Despite the ageing process, the measured contact angle did not return to values comparable to untreated (78.8 ± 3.1°) samples; the wettability modification of the sample surface partially remained, even up to 4 weeks of ageing (as shown in Figure 3-6b). This may develop due to the interaction between the polar groups formed on the GFPA6 surface and the water molecules on the top surface, with the absorption of moisture from the air acting to provide a polar environment that protects the decay of the polar groups. In summary, the μPlasma treated sample age and loses much of the wettability introduced onto their surfaces within the first two hours following treatment, and then levelled off in the next 4 weeks.

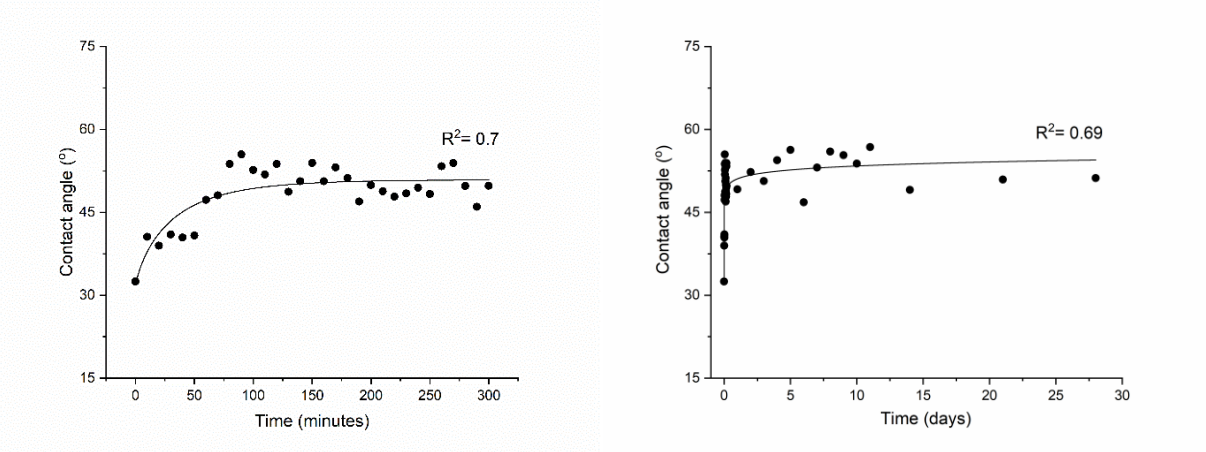

(a) (b)

Figure 3-6. Change of contact angles with ageing following μPlasma modification for: (a) 5 h, (b) 4 weeks (The curves were fitted using Python).

3.3.3 Optimisation of the Contact Angle Measurement Procedure

3.3.3.1 *Optimisation of the Contact Angle Measurement Protocol*

The glass fibre reinforcement was clearly visible in the composite samples, and this is illustrated in Figure 3-7a. To ensure that a sufficiently large and representative surface area was covered by the water droplet, the contact angle was recorded as a function of droplet size in the range of 2 to 20 µL. The number of fibres covered by each droplet was measured using ImageJ from SEM images, as shown in Figure 3-7a. Figure 3-8 shows the calculated number of fibres covered by each droplet size. The number of the fibres covered by the droplet increases with the droplet size. A 2 µL droplet has been calculated to cover approximately 103 fibres, which is assumed to be sufficient to reduce the contact angle error associated with the deviations introduced due to the fibre protrusions on the surface. Since all tested droplet sizes were found to be sufficient, 6 µL droplets were used within this study as they also correspond to the ISO standard (ISO 19403-2:2020), which enables clearer and more accurate droplet contours to be mapped during software angle measurements.

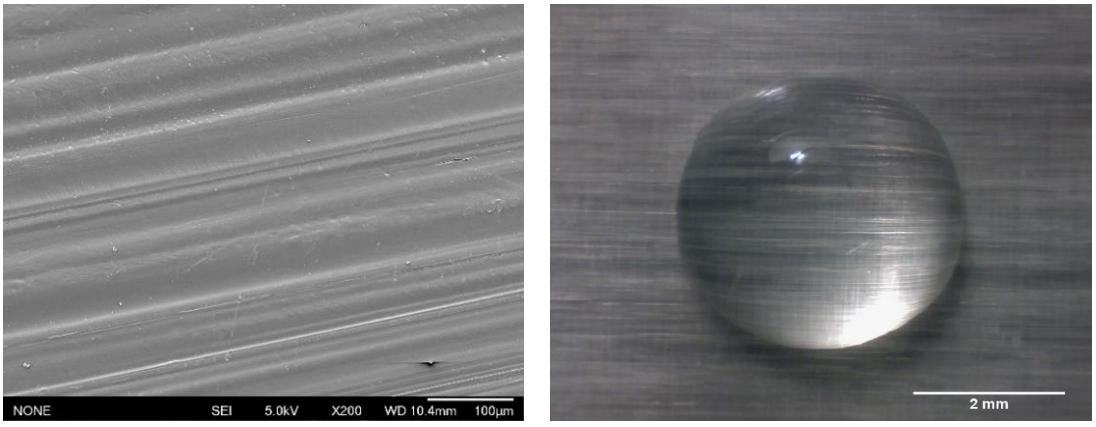

Figure 3-7. (a) SEM image of GFPA6 surface morphology, and (b) image of GFPA6 surface covered with a 6 µL water droplet.

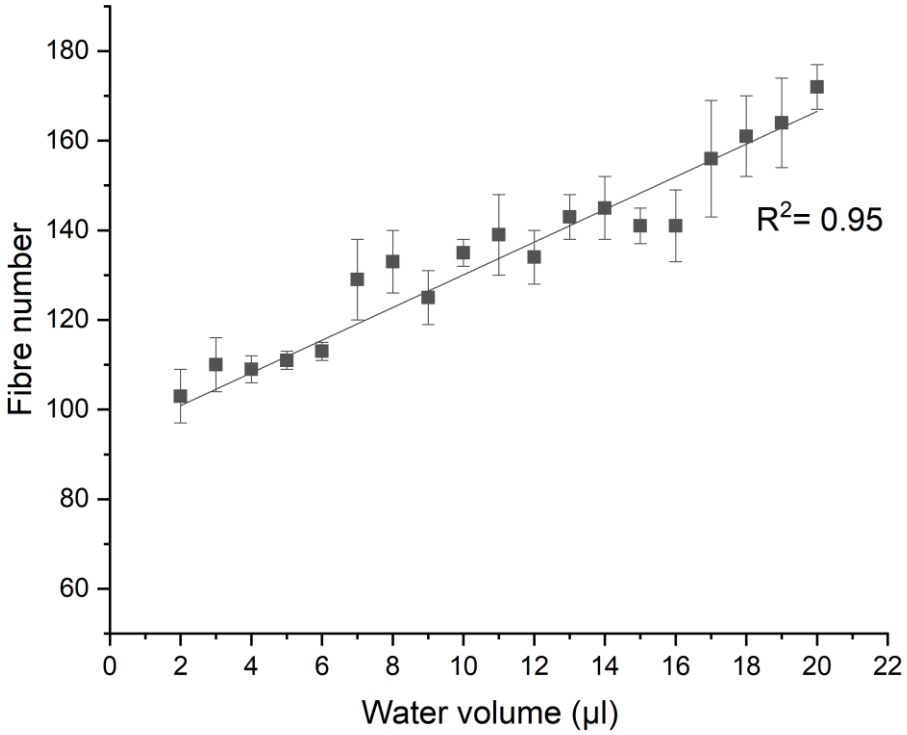

Figure 3-8. Graph displaying the effect of water droplet volume on the number of fibres covered on the untreated sample surface.

As shown in Figure 3-9a, two observer directions are possible when measuring contact angles, either parallel or perpendicular to the fibres, with the alignment of the fibres potentially influencing the measured value of the contact angles (as illustrated schematically in Figure 3-9). Therefore, contact angle mapping of the surfaces was performed using 50 deionised water droplets produced on a 5 × 10 cm^2 untreated sample surface, with measurements being recorded from both a parallel (a) and perpendicular (b) perspective to the fibres. The distribution of the contact angles of the 50 droplets are represented using colour heat mapping in Figure 3-10. The result demonstrates that the standard deviation is larger when the contact angles are measured perpendicular (±4.3°), rather than parallel (±3.1°), to the fibres. It can be

seen that the colour distribution is more uniform when measuring parallel to the fibres, this difference may arise due to the superficial fibres present in the perpendicular direction acting as walls to impede the spread of the droplet. This can, therefore, promote increased cohesion of the water molecules, thereby forming larger angles against the surface, or alternatively, when the force of water droplet is great enough to break beyond the wall, the angle returns to normal, or even smaller. Ultimately, this results in the incorrect measurement of contact angles, and increased variation in measured data, in comparison with measurements parallel to the fibres. Hence, all other contact angles measurements in this experiment were recorded parallel to the fibres, to enable accurate and reliable data to be recorded for the fibre reinforced polymer surface.

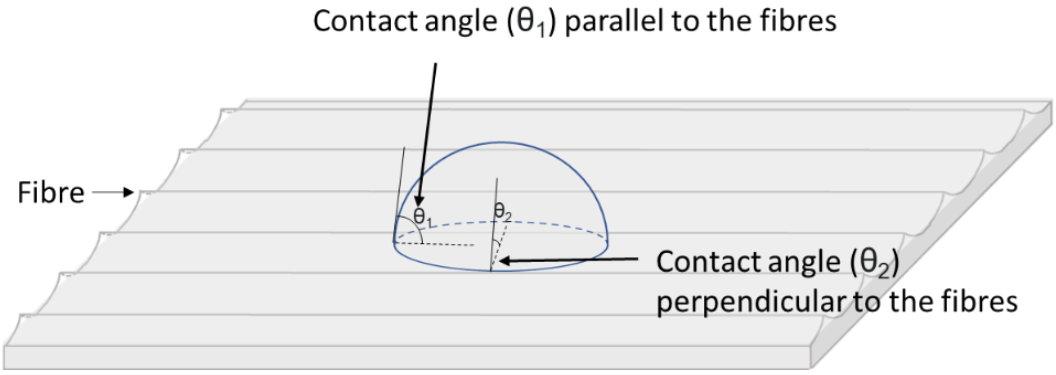

Figure 3-9. Schematic diagram of water contact angles measured parallel or perpendicular to the orientation of the fibres.

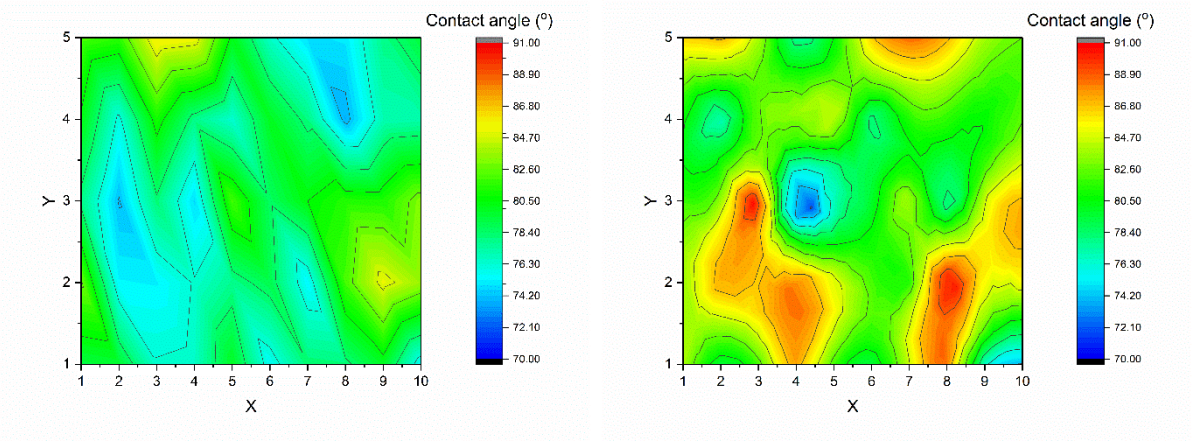

(a) (b)

Figure 3-10. Contact angles distribution represented by different colours on the untreated sample (5 × 10 cm^2) when measured at different fibre orientations: (a) parallel, (b) perpendicular to the fibres.

3.3.3.2 Optimisation of the Wettability Ageing of GFPA6 Samples

Given that polyamide 6 is hydrophilic, the water content in the sample may influence the ageing behaviour. To investigate this, the post-treatment time-dependence of the contact angles of untreated material was determined. Samples were either stored in the air prior to treatment or had been oven dried at 80°C for 3 h, contact angles were then recorded every 10 min for 5 h following µPlasma modification. It was observed that when the sample was dried before the treatment, the ageing process was impeded (Figure 3-11). The measured contact angle was found to plateau at 59.3° after 5 h of ageing, while the undried sample reached a plateau at 71.2°, with signs of further ageing still in progress. This suggests that the pre-existing moisture in the untreated material plays a significant role in facilitating the ageing process. This can potentially be attributed to the hydrated material providing a polar environment for the polar groups generated by the µPlasma modification, therefore, facilitating the reorientation

process of the polar groups and diffusion back into the bulk, which results in a less polar surface. Additionally, the moisture is mostly absorbed in the amorphous phase of the polymer, which can induce a reorganisation of the hydrogen bond structure of the material, leading to an expansion of the free volume and increased mobility of surface chains. Therefore, drying of the samples prior to µPlasma modification is necessary to slow down the ageing process.

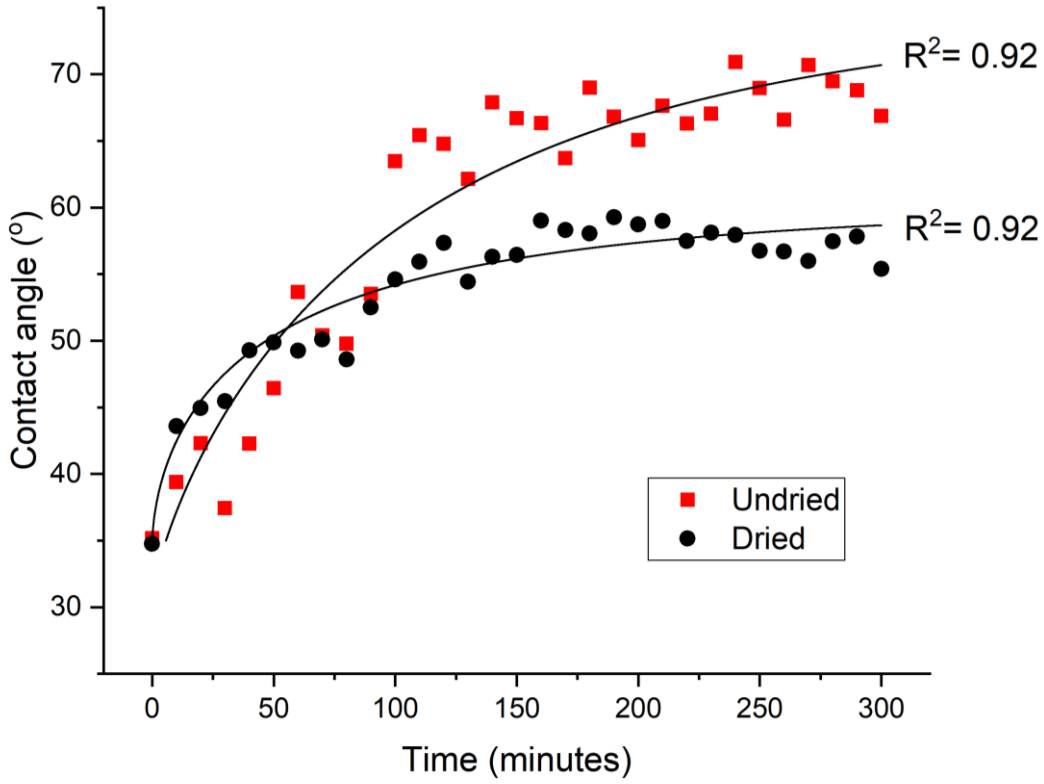

Figure 3-11. Ageing of dried and undried GFPA6 surface represented by contact angles after µPlasma modification.

As the µPlasma modification is highly sensitive to the working distance (distance between needle tips to sample surface), the roughness caused by the fibres in the surface of the material can affect the uniformity of the µPlasma modification, and

therefore, the resulting contact angle tests are prone to fluctuations. To optimise the measurement, and eliminate the inconsistencies, measurements of the contact angles on the same location are potentially more reliable. However, since the material is hydrophilic, it can absorb water during the measurements process, and this will influence the spreading of subsequent droplets on the surface (and also promote the ageing process as described above). Therefore, a different liquid diiodomethane, which is not absorbed by the material and vaporises quickly in the air, was used for contact angle tests on the same locations. It can be seen in Figure 3-12 that although the contact angles measured using diiodomethane show a similar trend to those made using water, large fluctuations compared to water measurements are observed and this masks the early stages of the ageing process. Therefore, it is not feasible to test contact angles on the same sample location using either water or diiodomethane, and different sample locations must be used for subsequent contact angle measurements. Results of contact angles of different liquids including water, diiodomethane and glycerol are shown in Figure 3-13. Among them, deionised water was found to give relatively lower fluctuations.

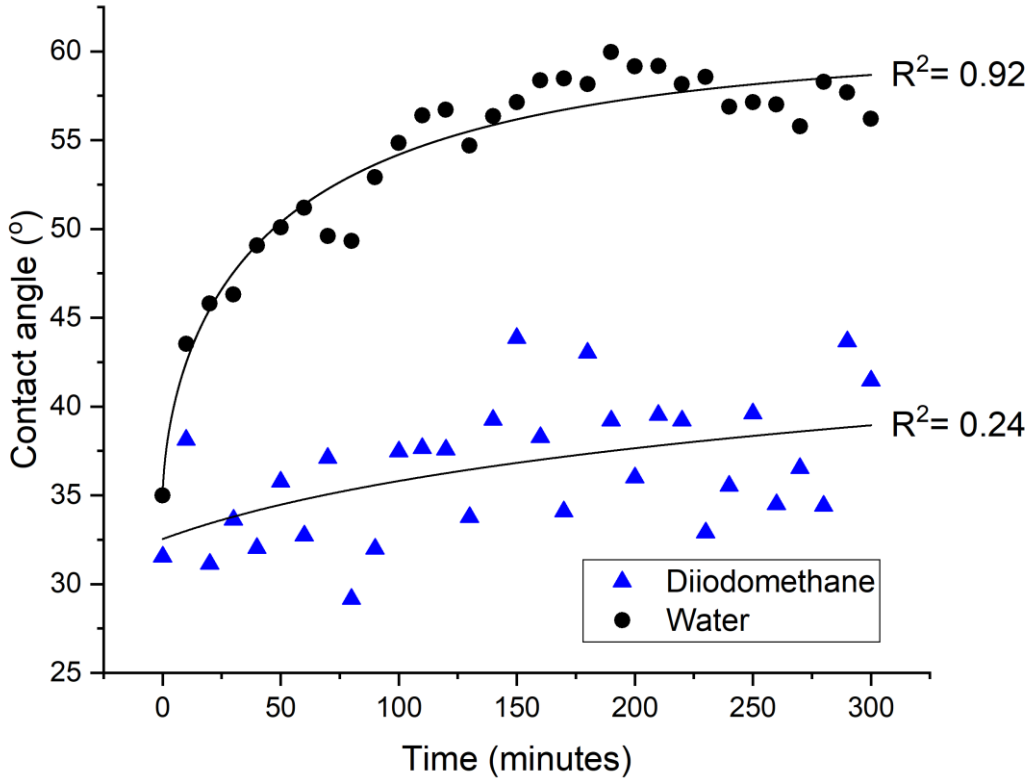

Figure 3-12. Ageing of GFPA6 surface represented by water and diiodomethane contact angles on the same locations after µPlasma modification.

In summary, there are two features of the GFPA6 material that need to be considered during the contact angle measurements for GFPA6, the absorbance of water into the matrix and the roughness caused by fibres on the surface. Using water droplets as small as 2 µL is sufficient to cover enough fibres to reduce errors. In this study, we used 6 µL, as recommended in the ISO standard, for increased consistency during the testing. The water can facilitate the ageing process; therefore, the samples need to be dried before the treatment, and testing on the same locations should be avoided. For a hydrophilic material, diiodomethane is more suitable for testing on the same locations; however, there is far more variability in comparison to water.

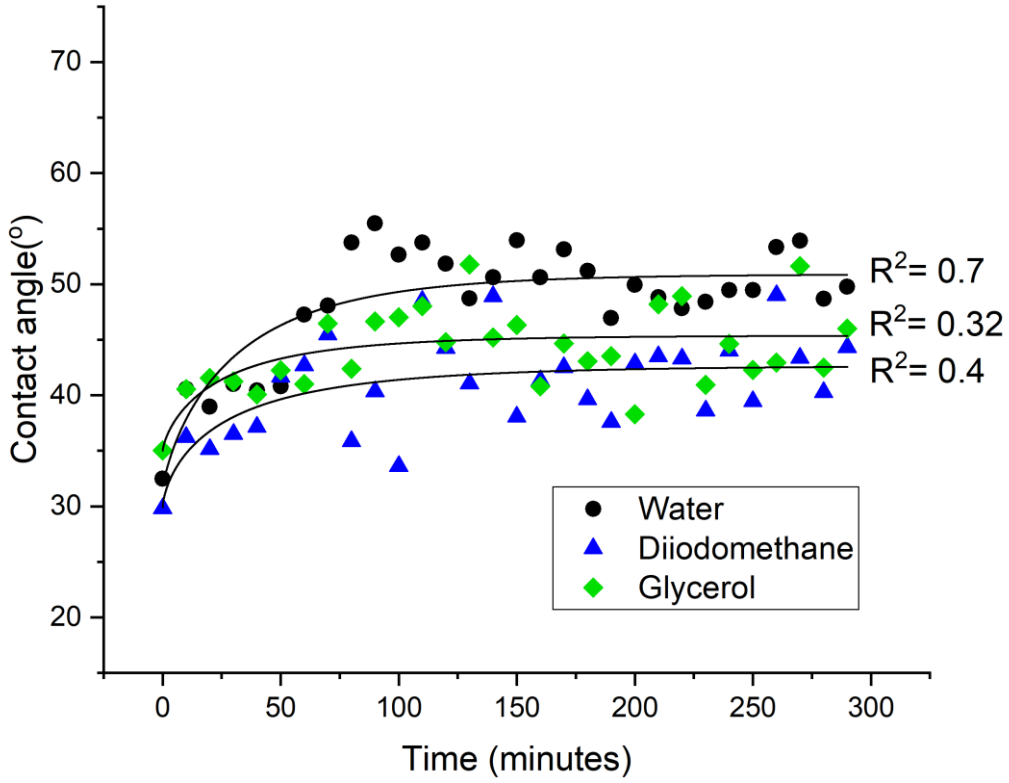

Figure 3-13. Ageing of GFPA6 surface represented by water, glycerol and diiodomethane contact angles on different locations after µPlasma modification.

3.3.4 Wetting Envelope and Surface Energy

The wetting envelope (shown in Figure 3-14) can be used to extrapolate the wettability of the untreated and treated surfaces, to hypothetical liquids with varying surface free energies, using the calculated surface free energies obtained with the Fowkes Equation. When the polar (σ^s) and dispersive components (σ^D) of a liquid are within the enclosed area of the produced wetting envelope, complete wetting (i.e., Cosθ = 1 or contact angle = 0 °) of the surface can be expected. As shown in Figure 3-14, the total area of the wetting envelope was the smallest for the untreated sample, before significantly increasing following the µPlasma modification (at 0 h). This indicates a

significant enhancement of the overall surface wettability of the GFPA6 following the initial treatment of the surface. The total area of the wetting envelope was then found to have a sharp, but smaller, decrease after one hour of ageing, with minimal changes over the following 2–5 h, therefore, indicating relatively stable surface wettability. However, it should be noted that, in all cases, the surface wettability of the treated surfaces was found to increase in comparison to the untreated surfaces.

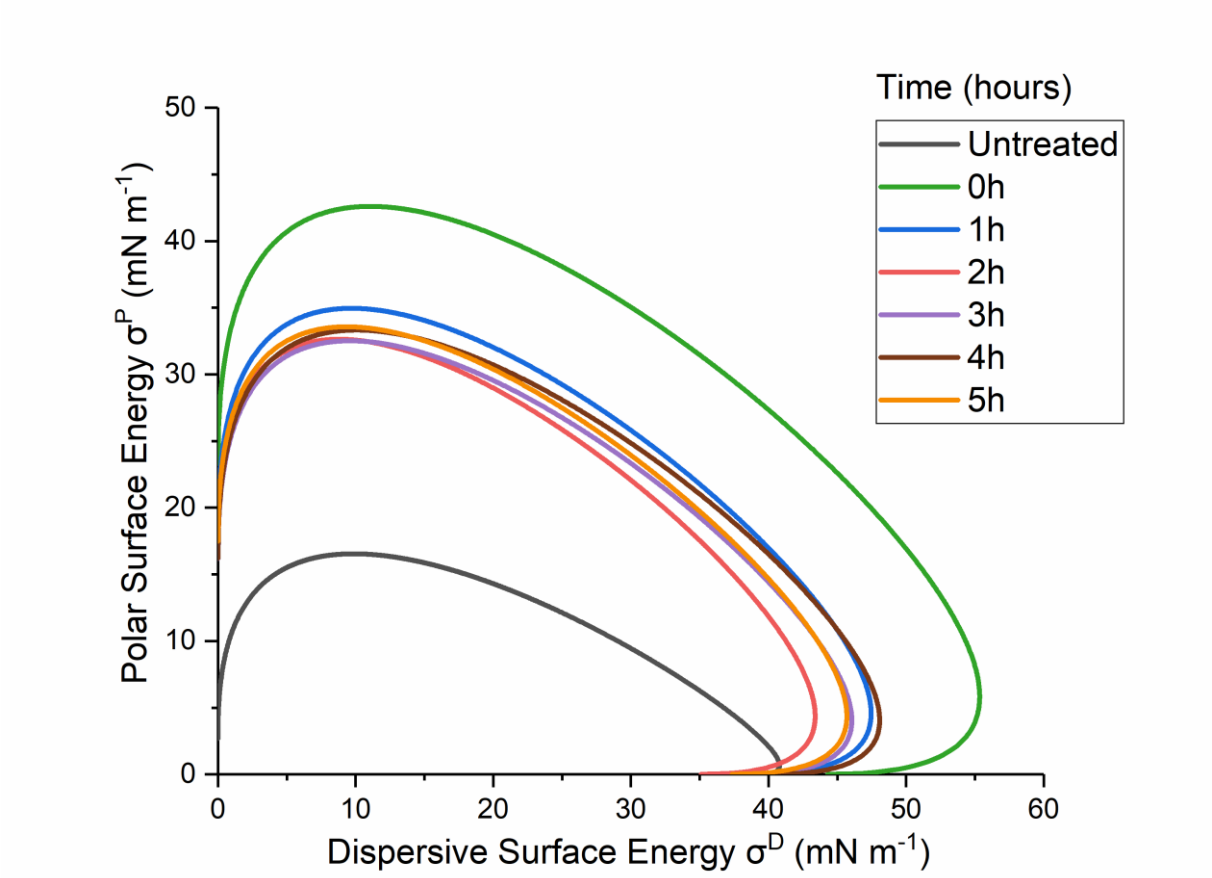

Figure 3-14. Wetting envelopes of untreated GFPA6 surface and µPlasma treated as a function of time (0–5 h after the treatment).

To better understand the wettability, the surface energy of untreated GFPA6 and treated GFPA6 aged for 5 h were measured using two different liquids (deionised water and diiodomethane). It can be seen from Figure 3-15 that the total surface free energy

increased from 42.2 mN/m to 67.6 mN/m. This increase can be attributed to the change in the polar component of the surface free energy, which significantly increased from 6.4 mN/m to 34.5 mN/m, and the decrease of the dispersive component of the surface free energy, from 93.6 mN/m to 65.5 mN/m. The total surface free energy decreased by 10.6 mN/m one hour after the treatment, with the polar and dispersive components decreasing and increasing by 2.5 mN/m each, respectively, therefore, indicating a slight reduction in surface wettability. All three surface free energies values (total, dispersive component, polar component) plateaued in the following three hours, remaining significantly higher than the total surface free energy of the untreated surfaces. This demonstrates that the μPlasma modification can both, significantly enhance the surface wettability, and retain elevated wettability following 5 h of ageing.

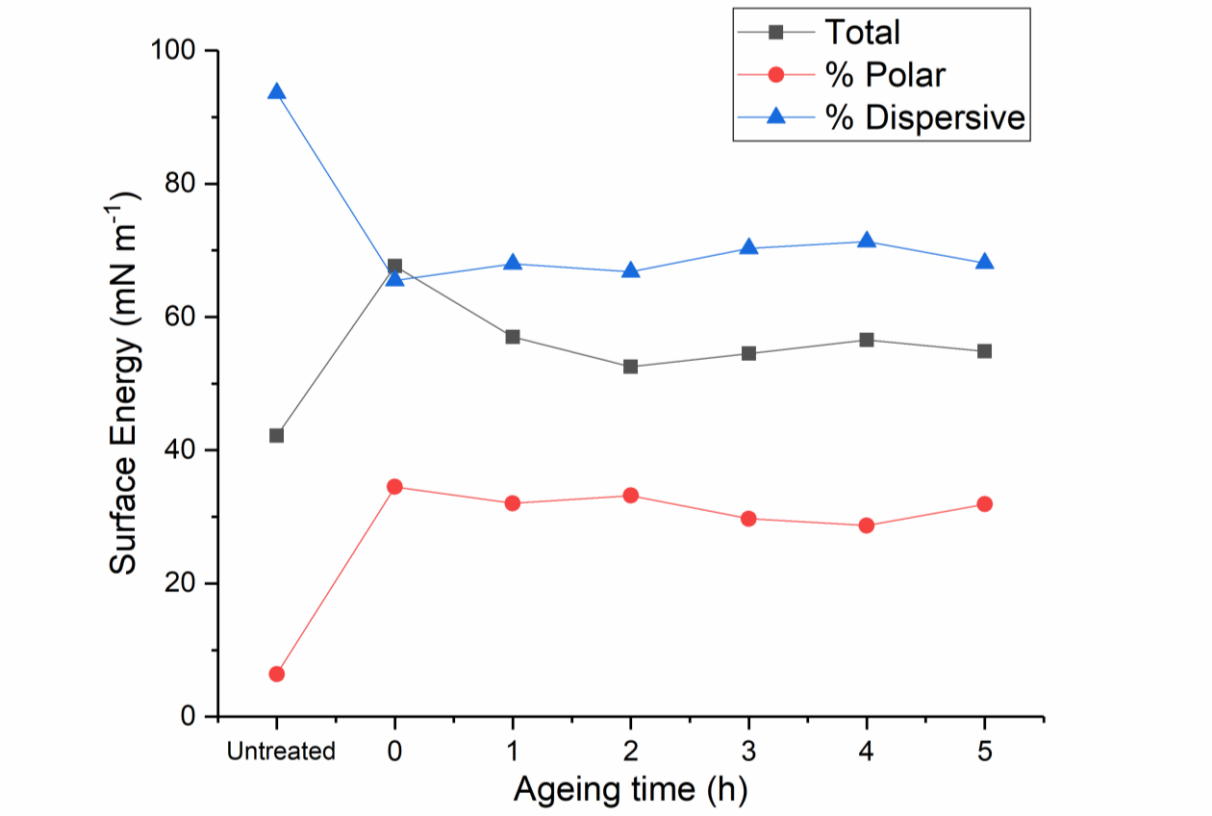

Figure 3-15. Total, polar and dispersive surface energy of untreated and treated GFPA6 ageing.

The results of the surface energy were consistent with the wetting envelope. The increase of wetting property of the GFPA6 right after the μPlasma modification was due to the increase of polar groups produced by the plasma. Although the treated sample recovered its property fast even in the first one hour, the wetting property was still partially remained when the surface energy levelled off over the next three hours.

3.3.5 Storage of Treated GFPA6

Figure 3-16 shows the variation of the water contact angle of μPlasma treated GFPA6 surfaces stored under different conditions in the air (with a humidity of 50–60%), in a desiccator (with humidity of 10–20%), and under vacuum for 4 weeks (with assumed humidity of 0%). It can be seen that all samples experienced hydrophobic recovery, but to varying degrees under different conditions. The ageing process was faster when the samples were stored in higher humidity environments. This could be due to the higher humidity causing plasticisation of the polymer, thus decreasing the glass transition temperature [154] and leading to an increased free volume on the surface, and higher mobility of the polymer chains at, or near, the surface, which accelerated hydrophobic recovery [124]. Furthermore, the hydrophilic groups generated by plasma may have been partially dissolved by water that was absorbed into the material from the environment. It was observed that the ageing process was slowed down significantly when the sample was stored in the vacuum, which suggests water was not the only variable facilitating ageing, but also the air. This could be due to the radicals that are produced by plasma treatment being trapped on or near to the material surface, which can then continuously react with the oxygen in the air after the treatment

[47]. Therefore, storing the μPlasma treated samples appropriately can largely inhibit the ageing process after μPlasma modification.

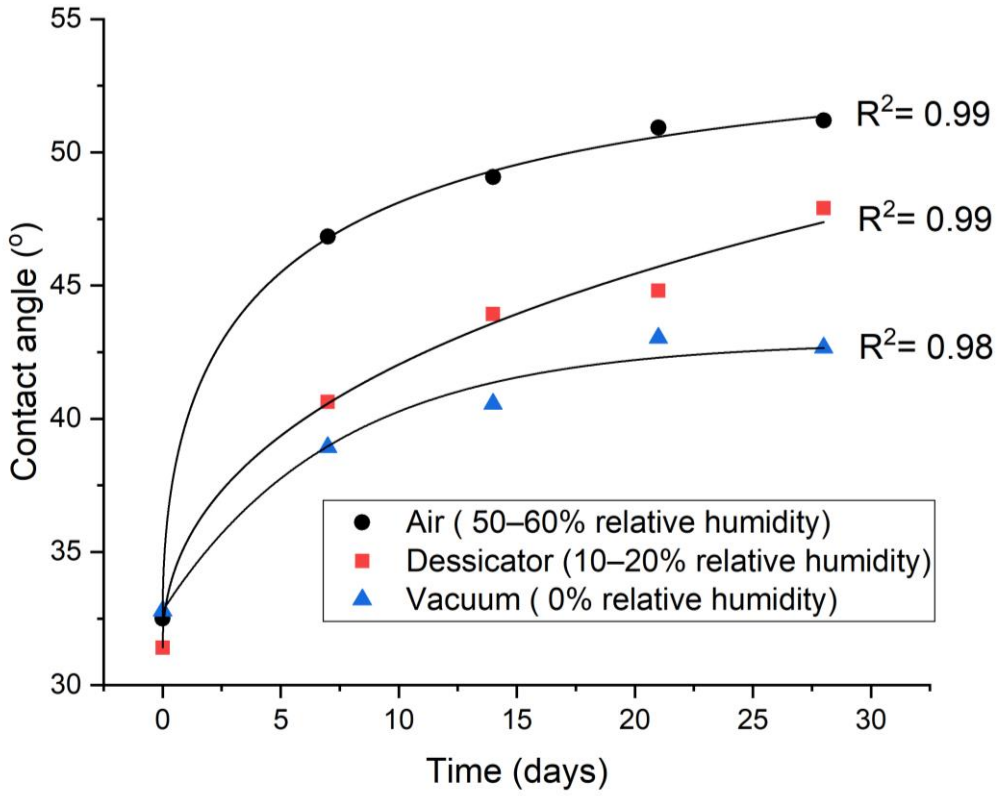

Figure 3-16. Ageing when store the μPlasma treated GFPA6 at different conditions.

3.4 Conclusions

This study has shown that the novel technology of μPlasma modification can effectively improve the wettability of the GFPA6 surfaces and benefits are achieved after only a single treatment scan (water contact angles decreased from 78.8° to 32.5°). However, hydrophobic recovery is observed (contact angle recovered to 53.7° after 80 min) and there is a lack of permanence in these benefits. It was apparent that the sample environment strongly influenced the timescale and extent to which hydrophobic

recovery could take place with dry atmospheres and dried samples clearly hindering the recovery process. The study has also shown that it is more reliable to measure contact angles on different locations of the surface due to the hydrophilic nature of the material.

The contact angle measurements were optimised for the untreated GFPA6 surfaces and for representing the ageing behaviour after the µPlasma modification. Regarding the increase of roughness on the surface caused by the fibres, even with 2 µL it was found to sufficiently minimise the error caused by the varying fibre coverage. The orientation of the fibres was found to affect the accuracy of the contact angle measurements, with measurements parallel to the fibres demonstrating higher consistency compared to measurements perpendicular to the fibres. High surface roughness influences the uniformity of the µPlasma modification due to the high sensitivity of the device to the working distance between the needles and the specimen surface. As it is not absorbed by the material, evaporates quickly in air, and does not facilitate the accelerated ageing of the surface, diiodomethane was used to test on the same location of the sample surface to reduce the inconsistency of the contact angle measurements. However, the result demonstrated that the diiodomethane contact angles fluctuated greatly, making it difficult to see clear trends of the ageing behaviour. Consequently, contact angle testing on the different locations was found to give relatively more accurate results. Different liquids were used to test ageing on the treated surface of different locations. All three liquids tested (deionised water, diiodomethane and glycerol) showed similar trends of ageing. Among them, deionised water was found to give relatively lower fluctuations. Therefore, deionised water on different locations on the µPlasma treated GFPA6 surface was deemed the most

appropriate approach. The results of contact angles of deionised water and diiodomethane were used to calculate the surface free energies of the samples and to plot their wetting envelopes. The change of surface free energy was consistent with the wetting envelope. The increase of wettability of the GFPA6 was attributed to the relative increase in the polar component content following μPlasma modification. Although the treated samples initially recovered their total surface free energy within the first hour, the wetting properties were still partially retained over the next 4 weeks.

4 The Ageing of µPlasma Modified Polymers: the Role of Hydrophilicity.

Abstract

Thermoplastic polymers exhibit relatively limited surface energies and this results in poor adhesion when bonded to other materials. Plasma surface modification offers the potential to overcome this challenge through the functionalisation of the polymer surfaces. In this study, three polymers of differing hydrophobicity (HDPE, PA12 and PA6) were subjected to a novel, atmospheric µPlasma surface treatment technique and its effectiveness at increasing the surface energies was evaluated via measurement of the contact angle. To characterise the physical and chemical changes following µPlasma surface modification, the surface morphology was observed using atomic force microscopy (AFM) and the functionalisation of the surface was evaluated using infrared spectroscopy. Immediately after treatment, the contact angle decreased by 47.3° (HDPE), 42.6° (PA12) and 50.1° (PA6), but the effect was not permanent in that there was a pronounced relaxation or ageing phenomenon in operation. The ageing process over five hours was modelled using a modified stretched exponential function Kohlrausch–Williams–Watts (KWW) model and it was found that the ageing rate was dependent on the hydrophilicity of polymers, with polyamides ageing more rapidly than polyethylene.

Key words: µPlasma; thermoplastics; polymers; wettability; ageing; contact angles; modelling

4.1 Introduction

Thermoplastic polymers are deployed in a multitude of applications ranging from single-use packaging to their use in the automotive and aerospace industries. Engineering polymers such as polyamides (PAs) have gained widespread use in the automotive sector due to their desirable physical properties, such as high toughness, good thermal stability, mechanical strength, and impact resistance [45, 47]. However, some polyamides are more prone to moisture absorption which can cause degradation during processing [1]. Commodity polymers such as polyethylene (PE) are extensively used as a flexible packaging material due to adequate flexibility and strength coupled with low cost [40]. Unlike polyamides, it is a well-established that PE is a hydrophobic material with non-polar characteristics, thus making it a challenging polymer to wet or print on [41]. In general, polymeric surfaces are often characterised by poor wettability [155], which limits their potential in certain applications such as joining dissimilar materials using adhesives.

To overcome this challenge and improve the versatility of polymeric materials in applications that require adhesive bonding, various surface modification techniques are commonly employed. Numerous studies have shown that plasma treatments are some of the most promising surface modification methods. These techniques are capable of altering the physical and chemical properties of a material surface, thereby significantly enhancing the surface wettability and adhesion properties without influencing the bulk properties of the material [83, 93, 94, 156]. Among the plasma treatments currently available, µPlasma surface modification is particularly interesting, because unlike traditional plasma treatments that require low-pressure conditions

(typically 50-400 Pa) [17], μPlasma modifications can be performed under atmospheric conditions, thus significantly reducing the processing costs [157]. Given these advantages over conventional plasma treatment methods, μPlasma technology may enable future integration with robotic systems, thereby enabling precise, localised, and multi-axially adjustable μPlasma modification of geometrically complex industrial components.

Although it is well established that plasma surface treatment can change the surface morphology of a polymer and enhance surface wettability via the formation of new functional groups on the surface, it is not a permanent modification. Instead, the polymer surface is subject to post-treatment ageing phenomena. These ageing phenomena can be sub-divided into degradative and non-degradative processes. Degradative processes may involve chain scission, crosslinking, and oxidation [23, 24], whereas non-degradative processes may involve hydrophobic recovery that involves chain reorientation and diffusion back towards the bulk of the material. Previous studies have shown that post-treatment ageing is affected by temperature [26], relative humidity [27] and polymer crystallinity [28].

In this study, μPlasma surface modification of HDPE, PA12 and PA6 is explored. These polymeric materials were selected in order to assess the effect of hydrophobicity on the post-treatment ageing process. This study extends previous work via a decoupling of the effects of crystallinity and hydrophilicity on the ageing process. It also develops the characterisation of the ageing process via the application of a stretched exponential function to analyse and characterise the ageing data.

4.2 Materials and Methods

4.2.1 Materials

The materials utilised in this study are listed in Table 4-1. All were supplied in sheet form and were dried in a desiccator for 7 days prior to processing.

Table 4-1. Materials utilised in this study.

Materials	Producer
PA6 sheet	Goodfellow Cambridge Ltd, UK
PA12 sheet	Aldrich, Merck Life Science UK Ltd, UK
HDPE sheet	Aldrich, Merck Life Science UK Ltd, UK

4.2.2 Sample Preparation and Crystallinity Control

The crystallinities of the polymers were varied via a controlled cool from the melt. This was carried out in a heated press (George E. Moore & Sons Ltd, Birmingham, UK).

The polymer samples were placed into a polyethylene terephalate (PET) mould that was composed of three Sections. There was PET spacer of thickness 0.3 mm and either side of this was a sheet of PET that functioned as a release film. This assembly was then placed in the preheated hot press, as shown in Figure 4-1. The polymers were heated for 3 minutes to initiate melting. Then a load of 10 tonnes was applied via the platens for a further 5 minutes causing the polymer melt to flow and then fill the mould. The polymers were then recrystallised by cooling from the melt under different cooling regimes, these are listed in Table 4-2. The melting temperature of the ‘as received’ materials was determined using differential scanning calorimetry (DSC) as described in Section 4.2.3. The melting regions of each material are shown in Figure

4-2 and this informed the selection of the hot-press temperatures which were as follows; HDPE - 160 °C, PA12 - 200 °C and PA6 - 240 °C. The heat of fusion and degree of crystallinity for each recrystallised sample were then determined via DSC (as per section 4.2.3). Samples with comparable crystallinities were then selected for μPlasma treatment, and these are listed in Table 4-3.

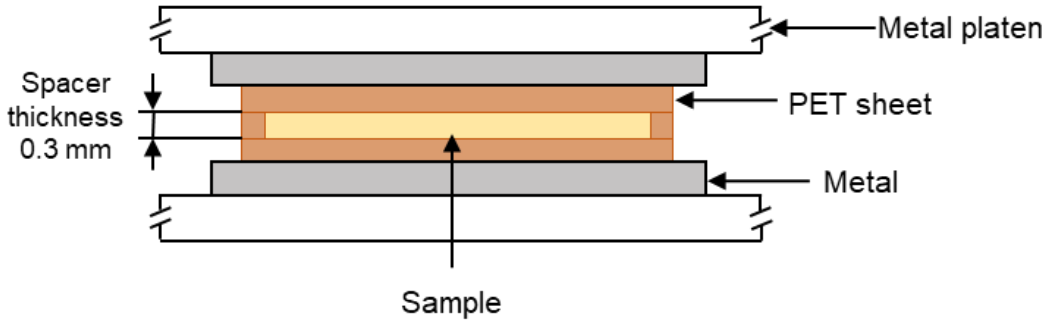

Figure 4-1. Cross-section showing the hot-press arrangement (not to scale).

Table 4-2. Cooling regimes adopted for crystallinity control.

Cooling rate	**Description**
CR1	Rapid extraction from the press and quenching into ice water.
CR2	Cooling in press with a flow of tap water circulating in the platens.
CR3	Removal from the press and cooled in air.
CR4	Cooling in press with open platens.
CR5	Cooling in press with closed platens.

Table 4-3. Degree of crystallinity in HDPE, PA6 and PA12.

Polymers	Crystallinity of the 'as received' material	Cooling regime	Resulting crystallinity post-cooling
HDPE	42.9% (± 1.8)	CR1	34.3% (± 1.7)
PA12	22.6% (± 1.6)	CR5	32.3% (± 2.0)
PA6	25.4% (± 0.8)	CR4	33.8% (± 0.8)

4.2.3 Measurement of Crystallinity Using Differential Scanning Calorimetry (DSC)

A differential scanning calorimeter (PerkinElmer DSC-7, PerkinElmer Inc. Waltham, MA, USA) was used for determining the melting point and degree of crystallinity of the cooled polymers. Disc-shaped samples were placed in aluminium pans and encapsulated with lids (Aluminium 40 µL flat DSC pans and lids, Thermal Instruments Ltd, Lancashire, UK). Sample weight was 5 ± 0.1 mg. The samples were heated at 50 K min^{-1}, and the melting point and heat of fusion were calculated. The resulting degrees of crystallinity were determined from the melting region, according to a method described previously [158]. It is displayed in Figure 4-2 that the T_m values for HDPE, PA12 and PA6 were 143 ˚C, 183 ˚C and 225 ˚C, respectively.

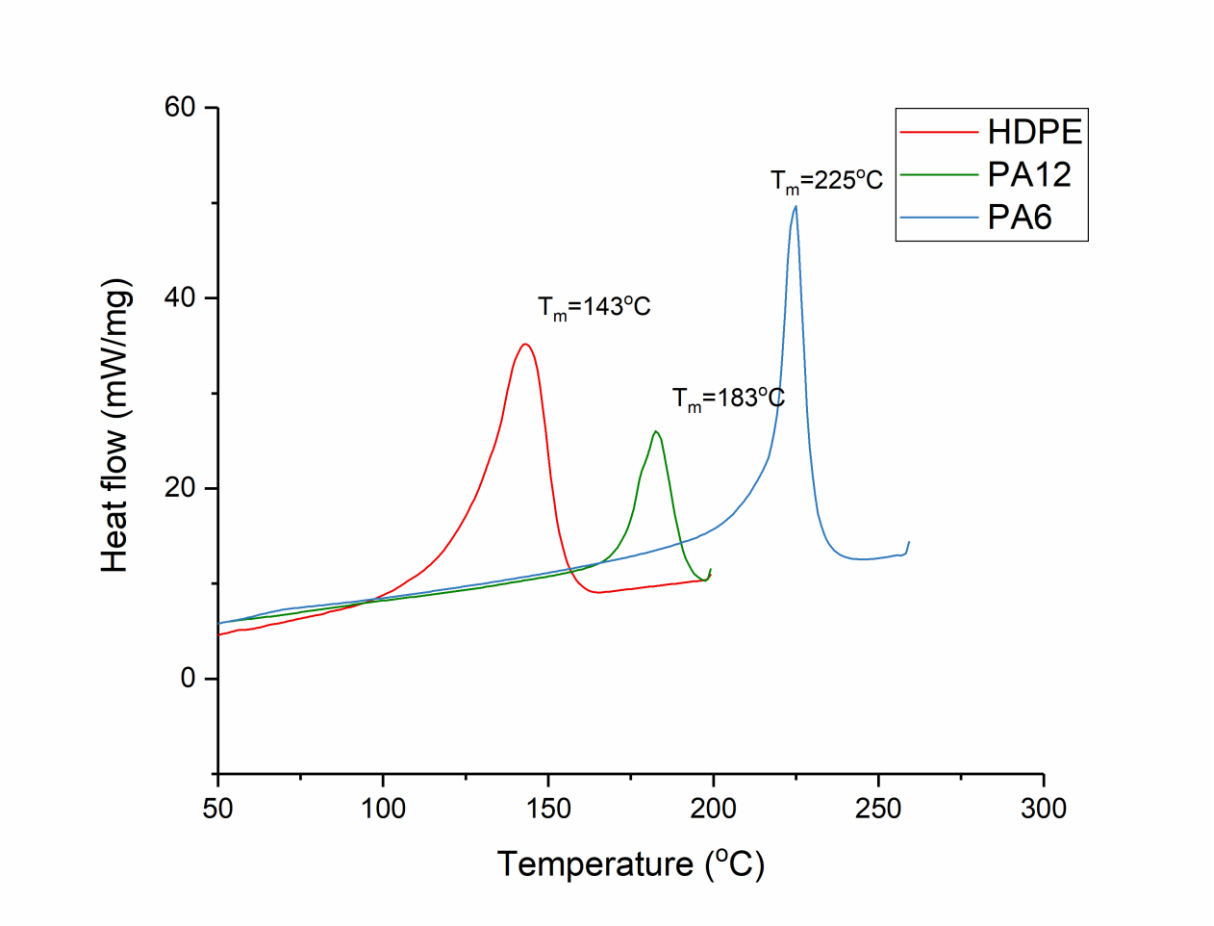

Figure 4-2. The thermal responses of HDPE, PA12 and PA6 recorded using DSC at a heating rate of 50 °C/min.

4.2.4 µPlasma Surface Modification

Both the plaque and film polymer surfaces were cleaned using ethanol before µPlasma modification. The µPlasma modification was carried out using a Roth & Rau Pixdro LP50 plasma inkjet printer (InnoPhysics, Eindhoven, The Netherlands) with an InnoPhysics POD24 print-head. A printing rate of 20 mm/s, a working distance from the sample surface to the tips of the printing needles of 100 µm, and an accelerating voltage of 7 kV were chosen as the µPlasma modification parameters, which had previously been reported to induce the most significant enhancement in wettability [27].

Additionally, in this study, the polymer surfaces were modified using a single treatment scan.

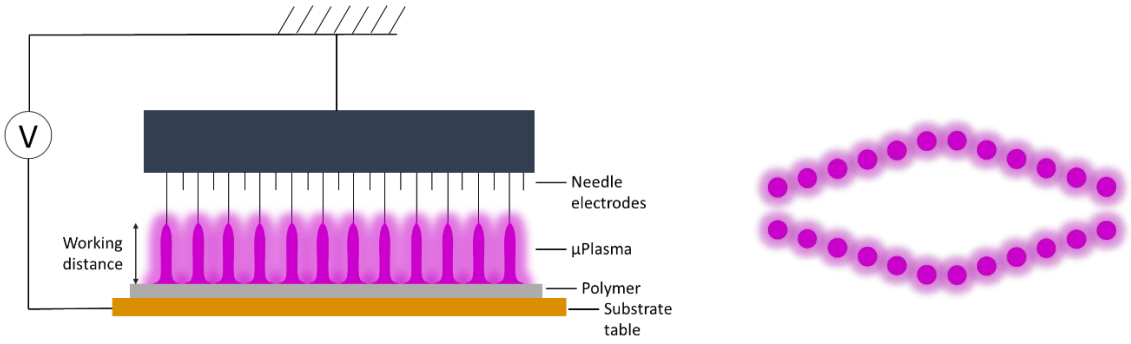

(a) (b)

Figure 4-3. (a) Schematic of µPlasma modification setup, (b) µPlasma discharges pattern generated by 24 needle electrons from top view [27].

Figure 4-4. µPlasma modification pattern [27].

4.2.5 Atomic Force Microscopy (AFM)

Surface morphology was examined using an atomic force microscope (Bruker Multimode AFM) operating with a silicon cantilever (Nanosensors PPP-NCHR, tip radius <10 nm, length 125 µm, resonant frequency 330 kHz) under a “tapping mode”. Before use, the cantilever was cleaned by rinsing with ethanol and exposure in a UV-ozone chamber for 10 minutes. Images were generated across an area of 17 µm x 17 µm, with a minimum 3 different positions recorded for each type of surface. 3D height

profiles, average roughness and root mean square (RMS) roughness data were obtained from the AFM data using an open-sourced image processing tool (Gwyddion, SourceForge, San Diego).

4.2.6 Measurement and Analysis of Contact Angle

The contact angles of the untreated and treated polymer surfaces were measured in accordance with the ISO 19403-2:2020 standard [152] using an experimental apparatus under the sessile drop method. The apparatus was adjusted to allow for samples to be placed in line with the camera and light source to ensure a clear and flat view of the droplet, which therefore enabled comparable measurements between polymers. An optimised measuring technique was utilised from our previous work [27]. 6 µL ionised water droplets were formed on sample surfaces using a calibrated pipette. Averages and standard deviations of contact angle values were obtained using three repeat droplets for each sample type. Both left and right contact angles were measured for each droplet using the Ossila contact angle measurement software (Ossila Ltd, Sheffield, UK).

4.2.7 Phenomenological Modelling the Post-treatment Ageing Process

A stretched exponential function was used as the basis of a phenomenological model of the post-treatment ageing (or relaxation) process. The Kohlrausch–Williams–Watts (KWW) function has been applied to various relaxation phenomena in polymers including dielectric relaxation [159], and in a slightly modified form, to enthalpy relaxation (or physical ageing) [25]. The basic stretched exponential function is shown in Equation (4-1), where the relaxation of the quantity $\emptyset(t)$ is given by,

$$\emptyset(t) = \exp\left[-\left(\frac{t}{\tau}\right)^{\beta}\right] \quad (4\text{-}1)$$

Where t is time, τ is the characteristic relaxation time constant, and β is the stretching exponent with a value between 0 and 1, which determines the shape of the ageing curve. To characterise the post-treatment ageing process, a modified KWW function was employed in which the change in contact angle ($\Delta\theta$) varied with time according to Equation (4-2).

$$\Delta\theta(t) = \Delta\theta_{\infty}\left\{1 - exp\left[-\left(\frac{t}{\tau}\right)^{\beta}\right]\right\} \quad (4\text{-}2)$$

The three unknown parameters τ , θ_{∞} (the contact angle when t approaches ∞) and β were determined using non-linear least square fitting. The modification shown in Equation (4-2) is after that of Cowie and Ferguson [25].

4.2.8 Fourier Transform Infrared Spectroscopy (FTIR)

The infrared (IR) spectra were obtained using a Nicolet MAGNA 860 FTIR spectrometer (Thermo-Scientific, USA) fitted with an attenuated total reflectance (ATR) accessory (Golden Gate ATR, Specac, UK). The samples were µPlasma treated 10 times and then transferred instantly to the ATR (treated surface in contact with the ATR crystal). The spectral range was between 500-4000 cm^{-1}. 100 scans were recorded at a resolution of 2 cm^{-1}.

4.3 Results and Discussion

4.3.1 Characterisation of the Hydrophilicity of PA6, PA12 and HDPE

To measure moisture uptake in the polymer samples listed in Table 4-1, they were dried in a desiccator for a period of one week and then the weight was measured. Samples were then immersed in distilled water for 24 hours and the weight measured once more. It can be seen in Table 4-4 that HDPE exhibited no water absorption (0% gain), revealing the hydrophobic nature of the material. Whereas the weight of PA6 and PA12 increased 6.674% and 3.070%, respectively, indicating higher moisture absorption capability and a higher degree of hydrophilicity in the polyamides.

Table 4-4**.** Moisture absorption of PA6, PA12 and HDPE after immersing in water

Polymers	**Weight (dry)** ±0.001g	**Weight (water immersed for 24h)** ±0.001g	**Percentage increase**
HDPE	0.730g	0.730g	0.000%
PA12	0.0228g	0.0235g	3.070%
PA6	0.0959g	0.1023g	6.674%

To support the above observation, the surface contact angles of three untreated polymer surfaces were measured and the values are listed in Table 4-5. It is notable that HDPE exhibited a contact angle higher than 90 ° (92.9 ± 2.6 °), indicating its hydrophobic surface, whereas the polyamides were found to have hydrophilic surfaces, as their contact angles were both lower than 90 °. PA6 exhibited the lowest angle (75.9 ± 2.2 °), suggesting the highest degree of hydrophilicity. Between HDPE and PA6, the surface contact angle of PA12 was measured to be 82.3 ± 1.8 °, which also indicated a hydrophilic surface.

Table 4-5. Contact angle measurements of untreated PA6, PA12 and HDPE surfaces.

Polymers	Water contact angles	Diiodomethane contact angles
HDPE	92.9 ± 2.6 °	55.1± 2.8 °
PA12	82.3 ± 1.8 °	41.1± 2.4 °
PA6	75.9 ± 2.2 °	30.7± 2.6 °

Using the Fowkes Equation, the surface free energies of the three untreated polymers were determined from the measurement of the contact angles formed with two liquids: deionised water and diiodomethane (shown in Table 4-5). As shown in Table 4-6, HDPE exhibited a total surface free energy of 32.1 mN/m, which was lower than both PA6 (40.6 mN/m) and PA12 (40.4 mN/m). Although the total surface free energies of PA6 and PA12 were found to be similar, the ratio of the polar components to the total surface free energy of PA6 was significantly higher (11%) than that of both PA12 and HDPE (4.7%) and (2.2%). The wetting envelopes shown in Figure 4-5 were determined using these surface free energy values (the associated method is described in detail elsewhere [20]). Complete wetting (where the contact angle = 0 °) can be expected when the values of polar and dispersive components of the liquid surface energy lie within the enclosed area of the wetting envelope. As shown in Figure 4-5, PA6 is clearly the most hydrophilic material in this study, but is interesting to note that a liquid with higher polar surface energy is more likely to completely wet PA6, while a liquid with higher dispersive surface energy is more likely to completely wet PA12.

The moisture absorption capability and the calculated wettability data that is represented by total surface free energy and wetting envelope for the three polymers was in accordance with the water absorption capability. This is because the polyamide

materials are inherently polar owing to the presence of polar amide groups (-C(=O) N=), which enables hydrogen bonding with water. As a result, polyamides exhibit a greater hydrophilicity. Polyethylene, on the other hand, is inherently nonpolar due to the presence of C-H and CH2 groups in the backbone.

Table 4-6. Surface free energies of untreated PA6, PA12 and HDPE.

Polymers	Total(mN / m)	Polar (mN / m)	Dispersive (mN / m)
HDPE	32.1	0.7 (2.2%)	31.4 (97.8%)
PA12	40.4	1.9 (4.7%)	38.5 (95.3%)
PA6	40.6	4.5 (11%)	36.1 (89%)

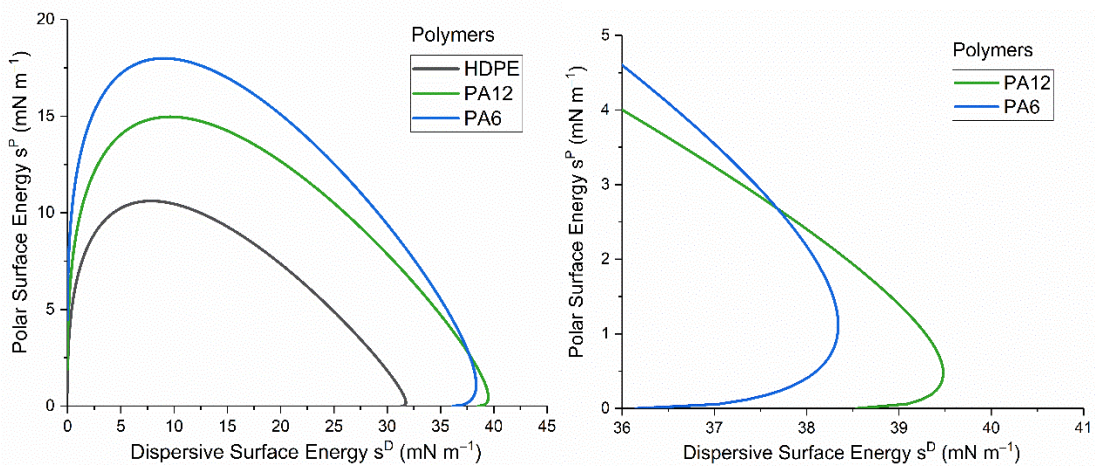

(a) (b)

Figure 4-5. (a) Wetting envelopes for liquids that should completely wet (i.e., 0 ° contact angle) untreated PA6, PA12 and HDPE surfaces, (b) enlarged cross section of PA6 and PA12.

4.3.2 Surface Morphology of µPlasma Modified PA6, PA12 and HDPE.

The surface morphology of untreated and µPlasma treated materials (HDPE, PA12 and PA6) were investigated through the use of AFM, and the topographical images of the three polymer surfaces are displayed in Figure 4-6. It was apparent that following

μPlasma treatment, the surfaces became more textured (more rough). To quantify the effect of μPlasma modification on polymer surface roughness, the root mean square roughness (S_q) of three polymers was calculated, this is illustrated in Figure 4-7. It was observed that the roughness of the HDPE surface increased following one treatment scan, increasing from an S_q of 11.6 nm (untreated) to 12.5 nm (7.8% increase). Similar findings were observed for the polyamides, with S_q increasing of 20.2% (from 9.8 nm to 11.78 nm) and 16.0 % (from 21.2 nm to 24.6 nm) for PA12 and PA6, respectively, following μPlasma modification.

The increase in roughness after μPlasma modification is possibly due to the higher ablation rate of the amorphous phase compared to the crystalline phase on the semicrystalline polymers surfaces [160]. However, the changes were relatively insignificant, withs RMS increases of 7.8% for HDPE, 20.2% for PA12 and 16.0% for PA6. This is attributed to the short duration of the single μPlasma modification, which was insufficient in producing a substantial difference in the roughness of the polymer surface.

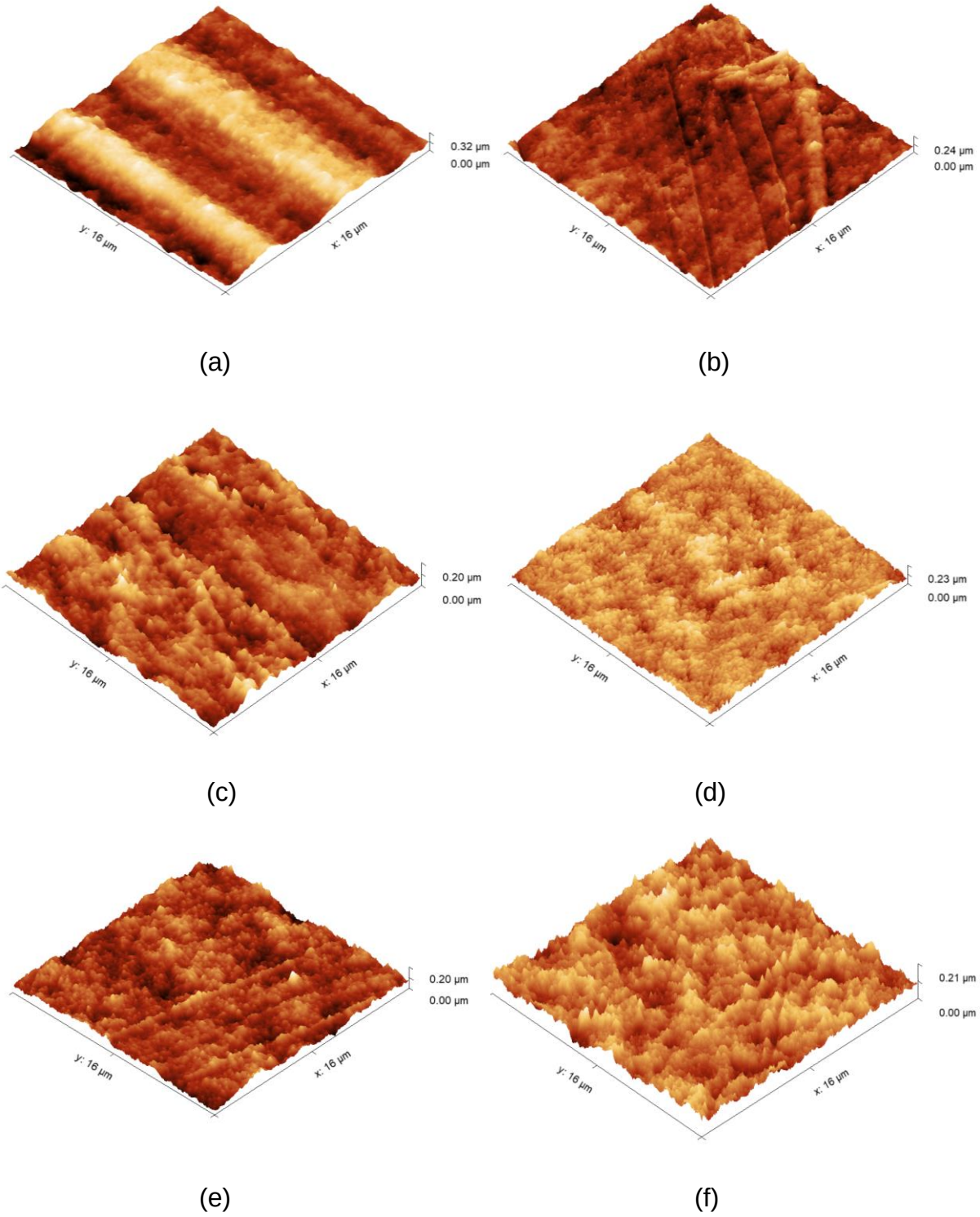

Figure 4-6. AFM 3D-view images of (a and b) untreated and µPlasma treated HDPE, (c and d) untreated and treated PA12, and (e and f) untreated and treated PA6 surface morphologies.

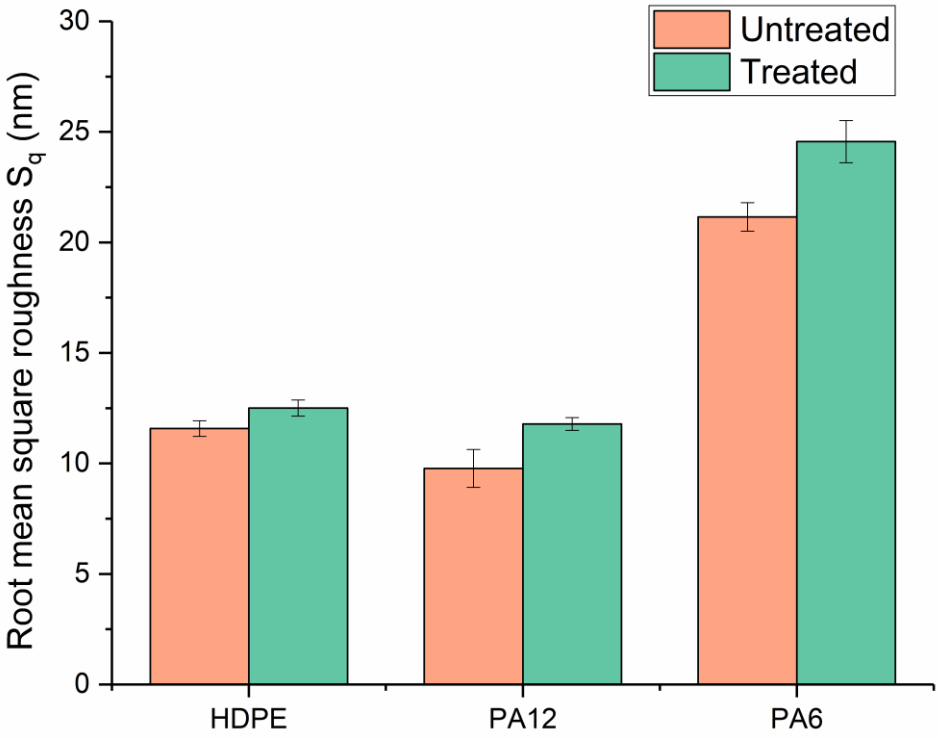

Figure 4-7. Root mean square roughness (Sq) of untreated HDPE, PA12 and PA6 surfaces and µPlasma treated sample surfaces with different treatment scans.

4.3.3 Chemical Analysis of the Polymer Surfaces Using FTIR.

The ATR-FTIR analysis revealed notable changes to the chemical composition of the polymer surfaces following µPlasma modification. Figure 4-8 shows the spectra of untreated HDPE and µPlasma treated HDPE sampled every hour for 5 hours. A broad band in the region of 3200-3500 cm^{-1} corresponding to hydroxyl groups (-OH) appeared following µPlasma modification. Two relatively narrow bands in the region of 1600-1750 cm^{-1}, corresponding to the carbonyl group (C=O), and the region of 1085 - 1225 cm^{-1}, related to the ether group (C-O), were also observed. Moreover, all the new peaks that appeared on the HDPE surface after the µPlasma modification were attributed to oxygen-containing polar groups, indicating that the functional groups on

the HDPE surface reacted with the oxygen in the plasma during the treatment process. These newly formed polar functional groups are known to give higher hydrophilicity to the polymer surface [161]. However, over a period of five hours post-treatment, there was a decrease in intensity of all treatment-associated bands.

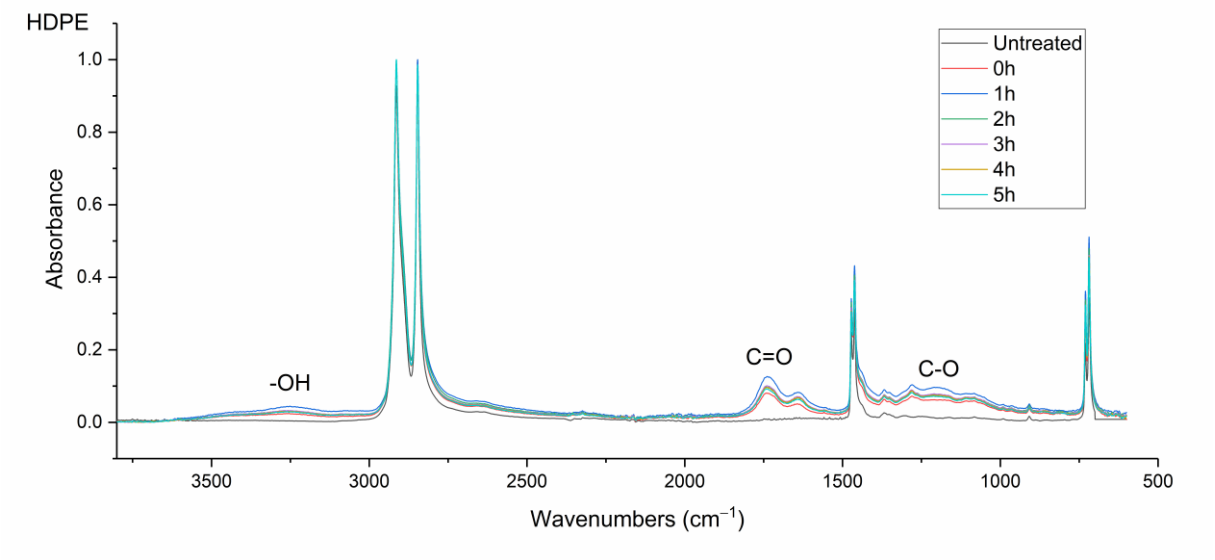

Figure 4-8. FTIR spectra of the untreated and µPlasma treated (0-5h aged) HDPE thin films.

FTIR spectra of untreated and µPlasma treated polyamides aged for 5 hours are presented in Figure 4-9 (a and b) for PA12 and Figure 4-9 (c and d) for PA6. Similar trends to HDPE were found following µPlasma modification, including the formation of a hydroxyl band (-OH) in the region of 3200-3500 cm^{-1} and carbonyl band (C=O) in the region of 1600-1750 cm^{-1}. In addition, there was increased intensity of the amide bands (N-H) in the region between 3000-3400 cm^{-1} and -OH bands in the region between 1330-1440 cm^{-1}. This indicates a higher surface hydrophilicity of the polyamides following µPlasma modification, as all the increased bands are polar groups. The intensity of the peaks decreased over the 5 hours of ageing (but over the

timescale of this experiment, these new bands were retained albeit at reduced intensities for all three materials). However, notably for PA6, the carbonyl (C=O) band increased with ageing time, rather than decreasing like other bands (as shown in Figure 4-9 (d)).

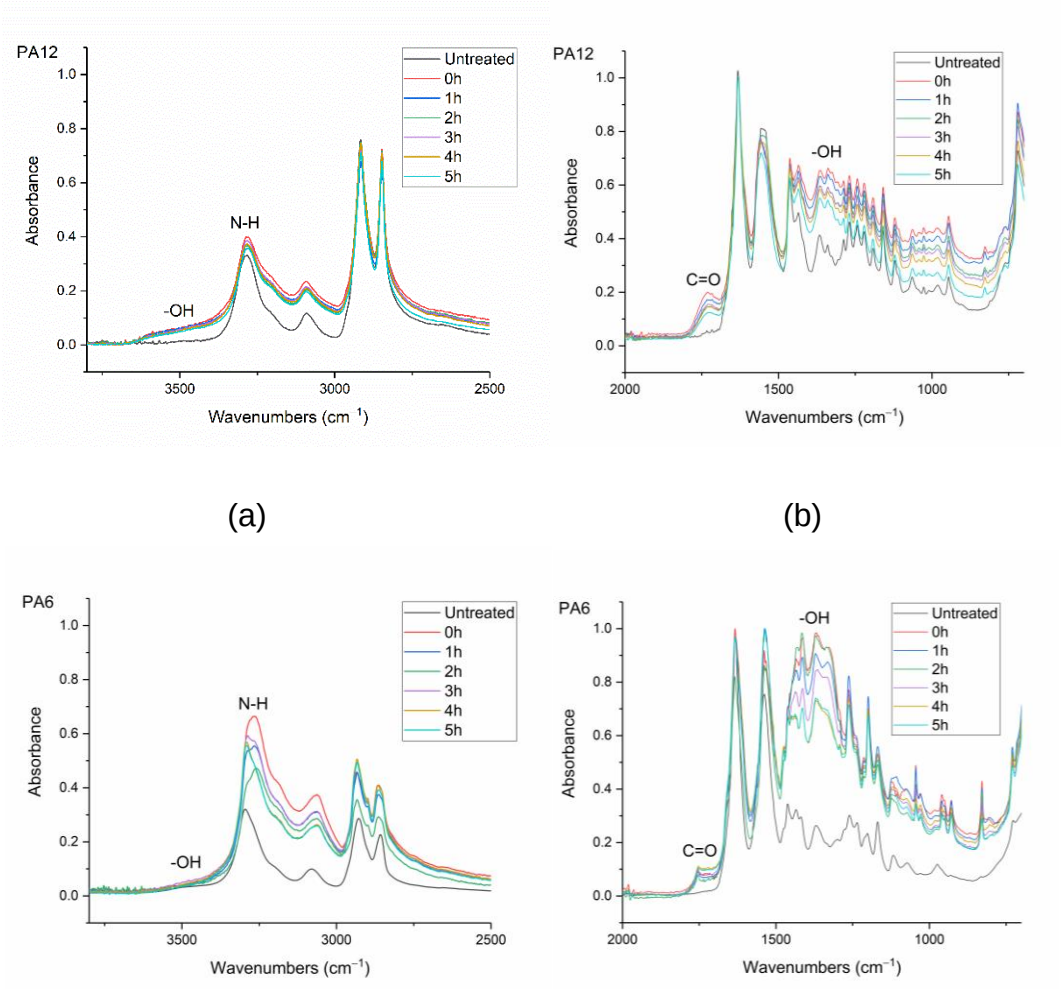

Figure 4-9. FTIR spectra of the untreated and treated 10 µPlasma scans in 0-5h ageing time: (a) PA12 3800-2500 cm^{-1}, (b) PA12 2000-700 cm^{-1}, (c) PA6 3800-2500 cm^{-1}, (d) PA6 2000-700 cm^{-1}.

4.3.4 Variation of Contact Angle with Time Post-treatment

Following a single µPlasma treatment scan, immediately after treatment, the measured contact angle was found to decrease for all three polymers (shown in Table 4-7). A reduction of 47.3° (50.1%), 42.6° (51.8%) and 50.1° (66.0%) for HDPE, PA12 and PA6 was found respectively confirming an immediate enhancement in wettability of the polymers.

Table 4-7. Contact angle measurements of µPlasma modified PA6, PA12 and HDPE surfaces.

Polymers	Contact angles (Untreated)	Contact angles (Treated 0h)
HDPE	92.9 ± 2.6 °	45.6± 1.8 °
PA12	82.3 ± 1.8 °	39.7± 2.5 °
PA6	75.9 ± 2.2 °	25.8± 2.1 °

It was noted in Section 4.3.3 that new polar functional groups were formed and their intensity increased substantially immediately following µPlasma modifications for all three polymers. Conversely, the increase in roughness on the polymer surfaces were limited with only 18.3% for HDPE, 25.9% for PA12, and 2.4% PA6 as mentioned in Section 4.3.2. These findings indicate that the change in roughness is unlikely to be the dominant variable for the enhanced wettability of the polymers. In contrast, the effect of µPlasma on the chemical compositions were clear, especially for PA6. Therefore, it can be concluded that the change in chemical compositions that attributed to the generation of the polar functional groups through µPlasma modifications are likely to play the dominant role for the change in wettability of the polymer surfaces.

However, it was found that the initial improvement in the wettability was not permanent (at least under ambient atmospheric conditions), as the contact angles were found to increase significantly following μPlasma modification of all three materials, indicating a reduction in wettability. The variation of contact angle with time (ageing time) for each material is shown in Figure 4-10. The intensity of the polar groups including hydroxyl -OH, carbonyl C=O, amide bands (N-H), and ether C-O groups all decrease, with ageing time following μPlasma modifications for the three polymers. This also suggests that the decrease in wettability corresponds to the decrease in polar functional groups. The behaviour of all three materials was similar in that after an initial rapid increase, the contact angle tended towards a plateau. Although it is noted that the relaxation/recovery of the contact angle in HDPE was weaker than in either PA12 or PA6. The contact angles eventually reach a plateau when hydrophobic recovery behaviour develops a balanced equilibrium.

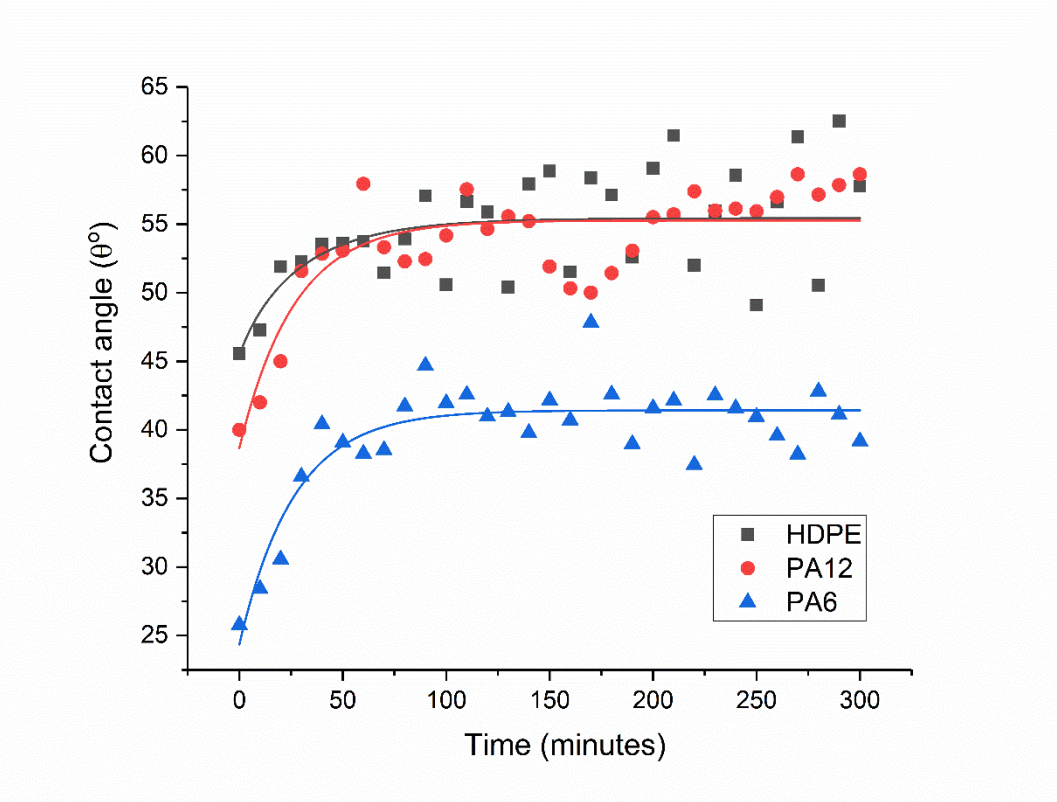

Figure 4-10. Variation of the contact angles of HDPE, PA12 and PA6 with ageing over 5h following μPlasma modification.

To quantify these variations and yield a more accurate determination of the maximum predicted change in contact angle, the contact angle data was fitted using Equation (4-2) and the parameters τ , θ_∞ and β were determined as shown in Table 4-8. It is apparent that the stretched exponential function describes the ageing phenomenon adequately well as evidenced by the R^2 values.

As shown in Table 4-8, the shortest relaxation time τ was observed for PA6, followed by PA12. The longest relaxation time was found for HDPE, which took almost twice as long as PA6. The values of the predicted maximum contact angles θ_∞ are also shown in Table 4-8. Although the polymer surfaces had clearly aged on storage for five hours,

the contact angles were not found to return to the original untreated values, indicating that the modified wettability was at least partially retained on all three polymer surfaces.

Table 4-8. Kinetic parameters describing the relaxation of the contact angle during post-treatment ageing.

Polymers	Contact angles (Untreated)	Contact angles (Treated 0h)	Relaxation time τ	Stretching exponent β	θ_∞	R^2
HDPE	92.9 °	45.6 °	62.7 min	0.54	58.2 °	0.59
PA12	82.3 °	39.7 °	54.9 min	0.33	59.6 °	0.71
PA6	75.9 °	25.8 °	35.4 min	0.48	43.4 °	0.77

It was also found using Equation (4-2) that the maximum contact angle (the region where the curves reach a plateau and tend towards equilibrium values) increased by 27.6% for HDPE, 50.1% for PA12 and 68.2% for PA6 compared to their treated but unaged equivalents. This result strongly suggests that the relaxation time of the polymers is related to their hydrophilicities: the higher the hydrophilicity, the faster the relaxation time after the µPlasma modification. This can be attributed to the increase in chain mobility in the region of the surface caused by hydrogen bonding between water and the newly formed polar groups in this region of the material [46].

Generally, the newly formed polar groups tend to reorientate or diffuse back the bulk material to move away from a non-polar environment such as air, which is known as hydrophobic recovery [117]. The higher hydrophilicity of a material facilitates the process of hydrophobic recovery. This is because the increased hydrophilicity of a material enhances the absorption of water molecules, which increase the free volume of the area in the region of the polymer surface, thereby enhancing the mobility of the chains and functional groups [124]. The increased chain mobility promotes the

migration of these polar groups into the bulk of the sample and thereby results in an increase in the contact angle.

It was also noted that in Section 4.3.3 the carbonyl (C=O) band in PA6 increased rather than decreasing like other polar groups with ageing time (as shown in Figure 4-9 (d)), therefore suggesting oxidation facilitated the ageing process of PA6 [162]. This could be another reason why PA6 experienced a faster ageing than the other polymers.

4.4 Conclusions

Surface contact angle measurements, moisture absorption capability measurements, and calculations of wetting envelopes revealed that the hydrophilicity of the three polymers was in an order of PA6 > PA12 > HDPE, with HDPE being identified as hydrophobic. The wettability of the polymers was improved substantially through μPlasma modification, with increases in surface roughness and the introduction of more polar functional groups. The change in chemical compositions of the polymer surfaces were believed to be the dominant factor for the improvement in wettability. Although the wettability enhancement of the three polymer surfaces following μPlasma modification was significant, it was subjected to an ageing phenomenon. The contact angle increased 27.6% for HDPE, 50.1% for PA12 and 68.2% for PA6 following five-hour ageing, compared to their treated but unaged equivalents. However, the wettability was still partially remained. With the assistance of KWW modelling, it was found that the ageing rate was dependent on the degree of hydrophilicity of the polymers, i.e., the higher the hydrophilicity, the faster the ageing process. This finding was further confirmed by FTIR through the reduction of the polar functional groups including hydroxyl -OH, carbonyl C=O, amide bands (N-H), and ether C-O groups.

5 Enhancing the Bond Strength between Glass Fibre Reinforced Polyamide 6 and Aluminium through µPlasma Surface Modification.

Abstract

Thermoplastic polymers generally exhibit relatively low surface energies and this often results in limited adhesion when bonded to other materials. Plasma surface modification offers the potential to functionalise the polymer surfaces, and thereby enhance the bond strength between dissimilar materials. In this study, glass fibre reinforced polyamide 6 (GFPA6) was modified using a novel µPlasma surface treatment technique and the effectiveness of the adhesive bond with aluminium was evaluated. The treated GFPA6 surfaces were characterised using atomic force microscopy (AFM), Raman spectroscopy, contact angle measurements, surface free energy calculations and wetting envelope analysis. The results show that there was a near exponential growth in root mean square roughness with increasing treatment scans. A significant increase in carbonyl and amide functionality on the polymer surface was observed using Raman spectroscopy. The total surface energy was found to increase from 42.2 mN/m to 67.6 mN/m with only one single treatment scan. Significant increases in the tensile shear strength from 1kN to 2.3kN were observed for 10 treatment scans, but no further increase was observed with additional treatment scans. These observations, coupled with the atmospheric nature of the technique, points to great potential as a rapid, on-line, and effective, polymer surface treatment technique.

Key words: µPlasma; thermoplastic; wettability; bond strength; aluminium; ageing

5.1 Introduction

Reduction in CO_2 emissions from motor vehicles is being achieved through a variety of means, one of which is vehicle light-weighting which enhances fuel efficiency through the replacement of structural metallic components in the vehicle with parts made from long fibre glass reinforced polymer matrix composites [163]. The polymer matrix can be a thermoset (e.g. an epoxy system) or thermoplastic (e.g. polyamide) [164]. While both these matrices offer a route to a reduction in weight, thermoplastic matrices offer significant advantages over thermosets in that they can be recycled and the part production time is significantly reduced [2, 165]. In the context of the automotive (and aerospace) industry, an important thermoplastic composite is glass fibre reinforced polyamide 6 (GFRPA6), which exhibits good thermal stability and high tensile strength [3, 4].

Often there is a need for thermoplastic composites to be joined with metals [5]. These hybrid structures facilitate the design of parts that not only exhibit increased strength, stiffness, and resistance to crack-induced physical damage, but yield a weight reduction [6]. Numerous approaches have been developed for the joining of polymers and metals, with mechanical fastening being the most traditional method [7]. However, problems can arise because of the use of mechanical fastening methods, for example, the drilling process concentrates stresses at the location of rivets or screws, which are then prone to cracking when high loads are applied [166]. In addition, the presence of bolts can increase the weight of the structure and compromise weather-sealing.

Adhesive bonding provides an alternative approach to the joining of materials and offers the potential for achieving better seals and defect-free connection between

dissimilar materials. In addition, it eliminates the needs for mechanical components such as rivets and screws, thereby reducing both the stress concentrations in the joints and the weight in the hybrid structures [6]. To achieve a good structural bond, epoxy-based adhesives are often employed, but prior treatment such as surface modification of the thermoplastic surface are normally required to improve their surface adhesive properties before the adhesive bonding of the materials. This is necessary because thermoplastic surfaces typically have low surface free energies, which makes them difficult to wet, and therefore, they demonstrate poor adhesive properties [10]. A range of studies have confirmed that plasma treatments can improve the wettability, and therefore, adhesive properties of polymer surfaces [11-14]. In addition, it has been reported that plasma treated surfaces can improve the bonding strength between polymers and metals [15, 16]. Unlike conventional plasma treatment systems, which require vacuum systems to operate, new µPlasma treatments can be performed under atmospheric pressure. As a result, the need for vacuum systems is eliminated, leading to increased treatment scalability, reduced treatment durations, and lower costs. µPlasma surface modification also allows for the local treatment of polymers and the design of surface patterns [167], which increases energy efficiency, as only the desired regions are treated. However, it has been reported previously that as for other plasma treatments the effects of µPlasma treatment are non-permanent. A post-treatment ageing process occurs that results in a significant decrease of surface wettability of the treated surface within the first 80 minutes after µPlasma treatment [27].

To the best of the authors knowledge, to date no previous studies have reported on the effect of plasma surface treatment on the adhesive bonding between glass fibre reinforced polyamide 6 (GFPA6) and aluminium. Therefore, the aim of this study is to

characterise the effect of μPlasma surface modification of GFPA6 on the bond strength of epoxy-adhered GFPA6-aluminium joints. A tensile lap-shear test was selected for the mechanical characterisation and the influence of treatment repetitions (1, 10 and 20 μPlasma treatment scans) on the bond strength was assessed. A range of microscopy-based techniques were deployed in order to characterise the polymer surfaces and the changes in surface wettability of GFPA6 were determined via contact angle measurements, surface free energy calculations and wetting envelope analysis. Moreover, the study seeks to explore the significance of the post-treatment ageing process that has been reported previously [27] and understand its implications for the joining procedure.

5.2 Materials and Methods

5.2.1 Materials

The glass fibre reinforced polyamide-6 (GFRPA6) used in this study was a Celstran@CFR-TP PA6 GF60-03 tape (GFPA6, Celanese Corporation, Dallas, TX, USA). The GFPA6 is composed of 60 wt.% uniaxial long glass fibre reinforced and 40 wt.% polyamide 6 and has a tensile strength of 240MPa. A AA6082-T6 aluminium alloy (London, Smiths Metal Centres Ltd, UK), with a yield tensile strength of 270MPa, was used as the other dissimilar material for joining. The alloying composition of the AA6082-T6 was 0.7-1.3 wt% Si, 0.6-1.2 wt% Mg, 0.4-1.0 wt% Mn, 0-0.5 wt% Fe, 0-0.25 wt% Cr, 0-0.2 wt% Zn, 0-0.1 wt% Ti, 0-0.1 wt% Cu. The two materials were joined together using MG Chemical 9200 FR Liquid Epoxy Adhesive (Corby, RS Components Ltd, UK). This adhesive system is reported to exhibit a tensile shear strength of 10

N/mm² (with aluminium). The protocol associated with the joining method is described in detail in section 5.2.5.

5.2.2 µPlasma Treatment

The GFPA6 surfaces were cleaned using ethanol and dried in air. After cleaning, µPlasma modification was performed using a Roth & Rau Pixdro LP50 plasma inkjet printer (InnoPhysics, Eindhoven, The Netherlands). The print-head (InnoPhysics POD24) within the device was connected to an alternative current power supply with 24 needles, as shown in Figure 5-1 . Previously published treatment settings for the surface modification of GFPA6 surface were used within this study [27]. For convenience, the optimal parameters were found to be as follows; an accelerating voltage of 7 kV, a printing rate of 20 mm/s, and a working distance from the sample surface to the tips of the printing needles of 100 µm.

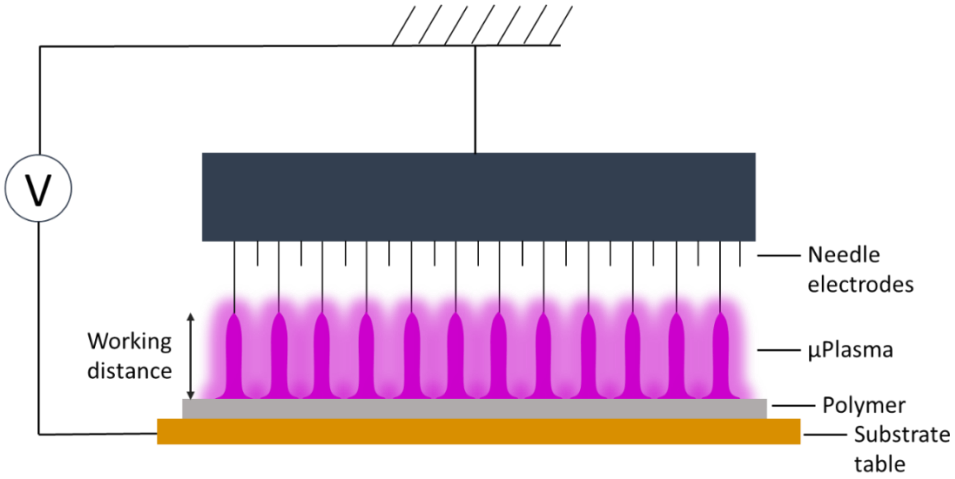

Figure 5-1. An illustration of the µPlasma printing head with 24 needle electrodes.

5.2.3 Atomic Force Microscopy (AFM)

Atomic force microscope (AFM; Dimension 3100, Bruker, Billerica, USA) was used for surface morphology examination of the materials. The AFM was operated with a silicon nitride cantilevers (PPP-NCHR, tip radius <10 nm, length 125 um, resonant frequency 330 kHz, Nanosensor, Apex Probes Ltd, UK) under a tapping mode. The cantilevers were cleaned using an ethanol rinse and exposure to UV-zone for 10 mins before each scan. The scans were acquired on three different locations on each sample surface with a scan area of 17 μm x 17 μm. 3D height profiles and root mean square (RMS) roughness measurements were obtained using the (Gwyddion, SourceForge, San Diego).

5.2.4 Contact Angle Measurements

The contact angles of GFPA6 surfaces were measured using the sessile drop method. An experimental apparatus conforming to the ISO 19403-2:2020 standard [152] was utilised, where a camera connected to a monitor, a height (*z*-axis) adjustable sample stage, and an adjustable light source were aligned in a straight line to ensure measured contact angles were always obtained at the same angle. The measurements were performed under the ambient conditions using deionised water as the test liquid. Water droplets with a volume of 6 μL were carefully deposited onto the sample surfaces using a calibrated pipette. Ten repeat measurements were carried out on each sample, with both left and right contact angles being used to ensure an accurate average contact angle measurement. The contact angle images were analysed using the Ossila contact angle measurement software (Ossila Ltd, Sheffield, UK).

5.2.5 Joining Method

The GFPA6 and AA6082 samples were cut into 100×25 mm pieces. Prior to joining, the AA6082 plates were roughened using #120 grit SiC paper. To ensure uniform roughness on all samples, surfaces were ground horizontally and vertically, 15 times each. The ground AA6082 materials were then ultrasonically cleaned in acetone for 5 minutes to remove loose debris. The GFPA6 material surfaces were treated using μPlasma before the joining. In this study, the two materials (GFPA6 and AA6082) were joined together using an epoxy adhesive that was made of two components (resin and hardener). The two parts were well mixed in a 1:1 ratio, with a mass of 0.1 ± 0.001 g for each part.

The joining procedure is illustrated in Figure 5-2. The mixed adhesive was evenly applied on the GFPA6 material surface immediately after μPlasma treatment, before joining with the AA6082, with joining area (plasma treated) of 12.5 mm × 25 mm. The joined materials were then cured in air at room temperature for 24 hours before tensile testing was carried out. Expediting the joining process was deemed to be of significant importance because it has been previously reported that the effects of plasma surface treatment are not permanent in that a post-treatment ageing process takes place in the hours that follow the treatment [27].

5.2.6 Tensile Lap-shear Test

Uni-axial tensile lap-shear tests were conducted using an Instron 3367 tensile testing system (Instron, Massachusetts, US) with a load cell of 30 kN. The testing specimen are shown in Figure 5-2 (a), which follows the EN ISO 4587 tensile lap-shear test

standard. A tab was applied on each side to ensure parallel tensile testing was performed. The tests were carried out using a crosshead speed of 0.2 mm/min and tests were repeated 6 times for each variable (untreated and µPlasma treated one, 10 and 20 treatment scans).

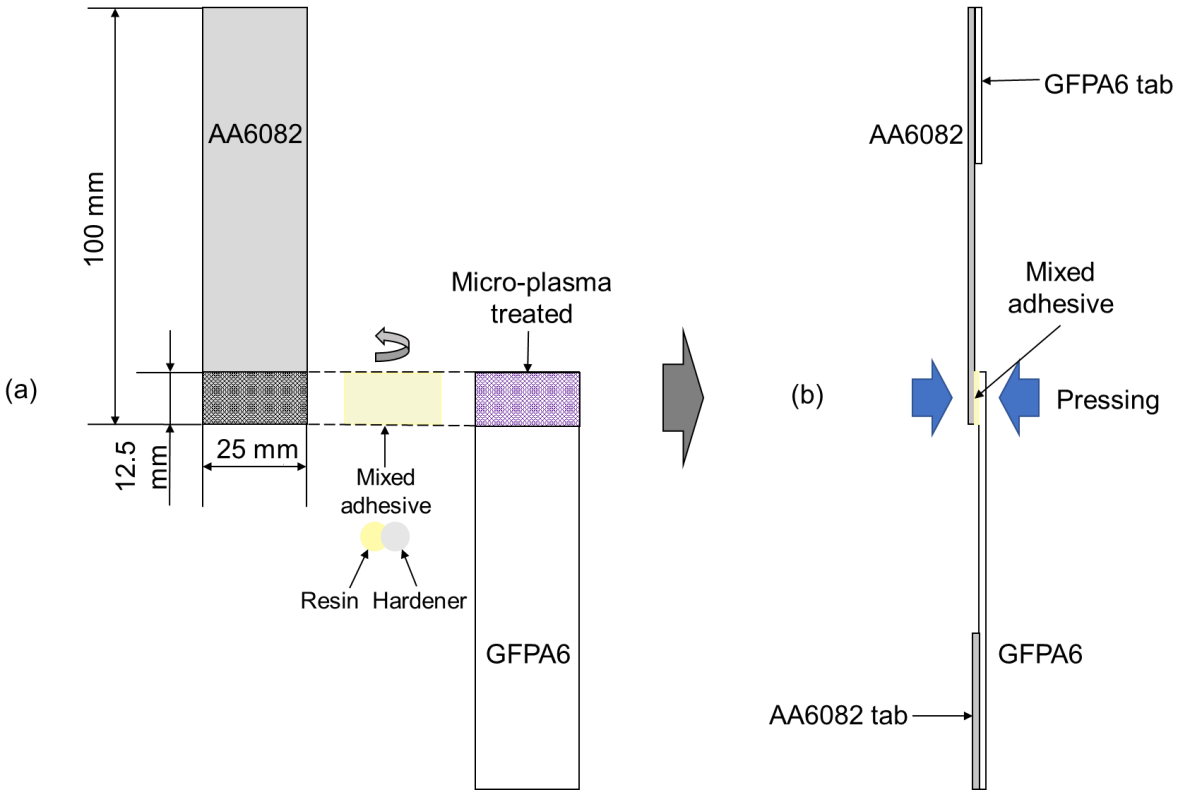

Figure 5-2. A schematic illustration of (a) the joining method and sample size, and (b)the specimen for tensile lap-shear test after joining.

5.2.7 Image Segmentation

The coverage of the adhesive on broken GFPA6 surfaces after failure was analysed using the TWS (trainable Weka segmentation) plugin for Image J (Version 1.54c, Bethesda, Maryland, USA). Prior to the image segmentation, the adhesive area and polymer surface area were distinguished as two different classes by training classifier. This was done by drawing freehand lines on the adhesive area and set as class 1,

while the polymer surface area was as class 2. The percentage of total area was then calculated using Image J.

5.2.8 Scanning Electron Microscopy (SEM)

A TM3030 SEM (Hitachi High-Technologies Corporation, Tokyo, Japan) was used to observe surface morphology of samples after tensile testing. Prior to SEM imaging, the sample surfaces were gold sputter coated using an EMITECH K550 Sputter Coater (EMITECH, Kent, UK) at 25 mA for three minutes.

5.2.9 Raman Spectroscopy

Raman spectra were obtained using a Raman Microscope (InVia Raman Microscope, Renishaw plc., Wotton-under-edge, UK) with a laser wavelength of λ = 488 nm and an excitation power of ~2 mW. A confocal microscope with ×50 objective was used to focus the laser beam onto the samples with a spot-diameter of about 865 nm. A Raman data set consisting of 289 spectrums were collected using Raman mapping (each spot with a size of 150 × 150 μm) in a grid pattern over an area of 2550 × 2550 μm on the sample surface. The spectra were then deconvoluted and analysed using Casa XPS, where the average of the 289 spectra was summarised.

5.3 Results

5.3.1 Effect of μPlasma Modification on the Surface Morphology of GFPA6

The 3D surface morphology of untreated and μPlasma treated GFPA6 was examined using AFM. As shown in Figure 5-3, the surface morphology of the untreated GFRP6 appeared relatively smooth, and with a single μPlasma treatment, the resulting surface

was not discernibly different. However, the surface roughness of GFPA6 increased significantly after 10 and 20 µPlasma treatment scans. It is notable that the material surface after 20 µPlasma treatment scans exhibited an uneven surface with distinctly raised fibres and pronounced grooves.

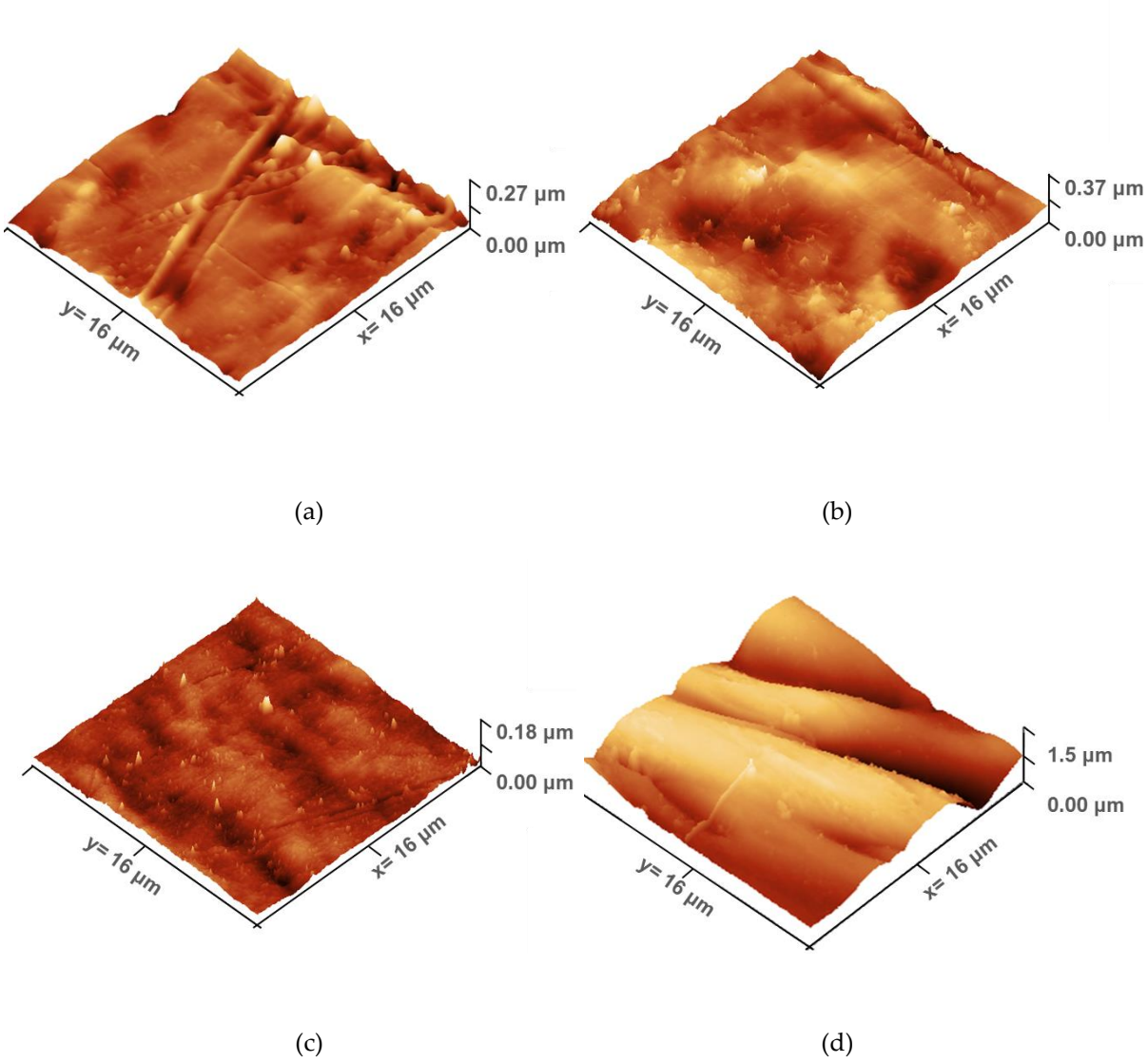

Figure 5-3. 3D AFM images of surface morphology of (a) untreated, and µPlasma treated different times: (b) 1, (c) 10 and (d) 20.

To quantify the observations in relation to surface roughness, the root mean square (RMS) roughness (S_q) was calculated and the variations are illustrated in Figure 5-4. Although no obvious roughness change can be observed in Figure 5-3b, the value of S_q was revealed to increase with the increasing number of µPlasma treatment scans. The value of S_q initially increased from 65.0 nm to 72.8 nm following one µPlasma treatment scan, indicating a modest increase in surface roughness. More substantial increases were observed for 10 µPlasma treatment scans, with the value of S_q increased to 140.9 nm following 10 µPlasma treatment scans. The most significant increase in RMS roughness of the GFPA6 surfaces was observed for 20 µPlasma treatment scans with the value of S_q increased to 369.7 nm, which corresponds to an approximately 5 times greater roughness as the untreated surface. In summary, this demonstrated that the surface roughness of GFPA6 can be significantly increased following µPlasma modification, with the magnitude of the effect rose with the number of µPlasma treatments. Significant increase of S_q was observed following 20 µPlasma treatment scans.

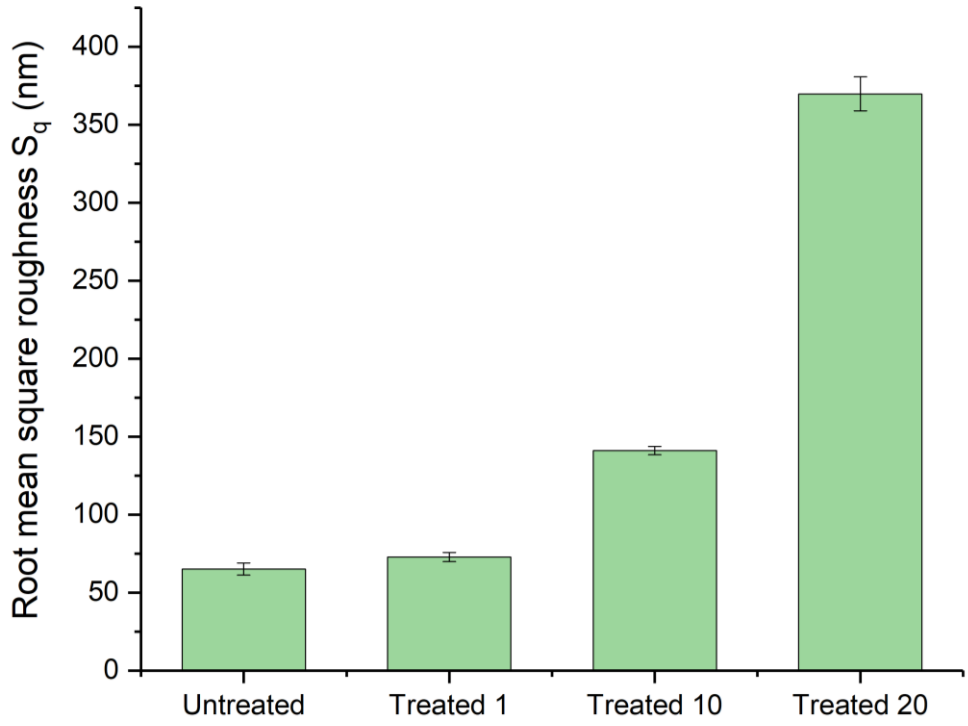

Figure 5-4. Root mean square (RMS) roughness of untreated GFPA6, µPlasma treated once, 10 and 20 times.

5.3.2 Surface Wettability

Substantial enhancement in surface wettability was found following one µPlasma treatment, as evidenced by a 61.5% reduction in contact angle (decreasing from 78.8 ° to 30.3 °) as observed in Figure 5-5. Following 10 and 20 µPlasma treatment scans, the contact angles decreased by 64.6% and 71.1% (going from 78.8 ° to 27.9 ° and 22.8 °) respectively, in comparison with the untreated surface. The results demonstrated that, beyond a single treatment scan, further µPlasma treatment scans did not significantly improve the surface wettability (despite an increase in roughness). To gain a better understanding of the surface wettability, the surface free energy was calculated using the contact angle results from tests with deionised water and diiodomethane. As shown in Figure 5-6, the total surface free energy increased from

42.2 mN/m to 67.6 mN/m following a single μPlasma treatment, with increased contribution from polar surface energy components and decrease of dispersive components. The total surface free energy increased to 69.6 mN/m for 10 treatment scans, which suggests that the surface free energy change was limited beyond a single treatment scan.

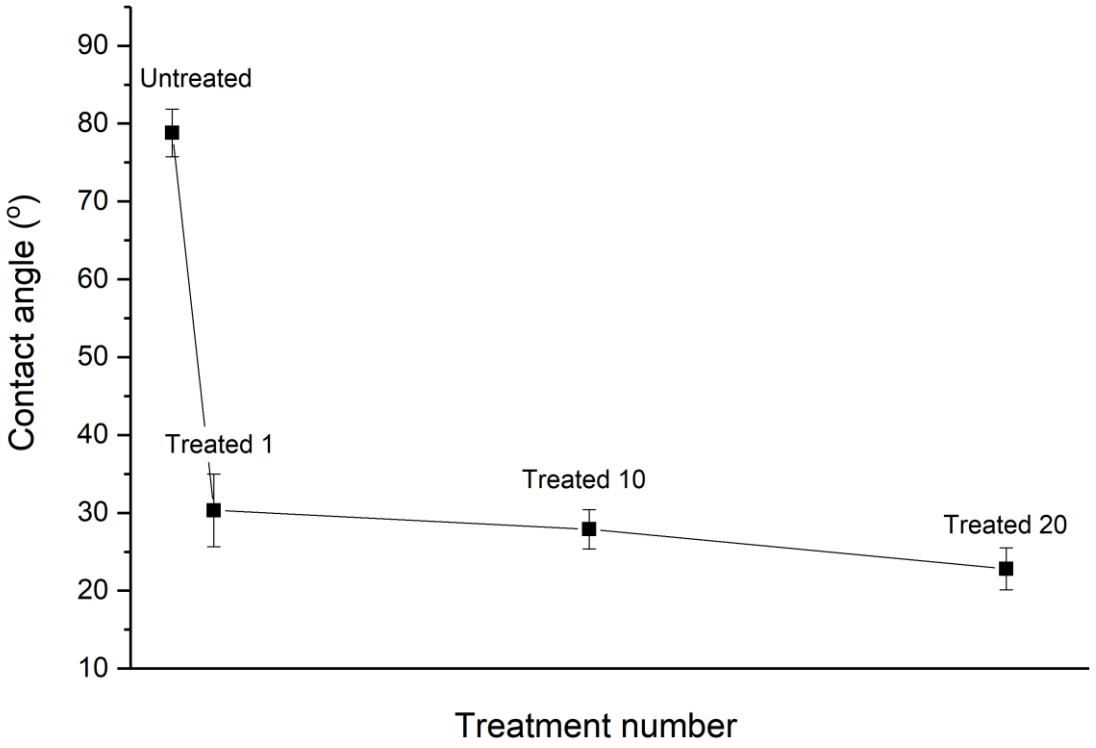

Figure 5-5. Variation of the contact angle of the GFPA6 surface with the number of μPlasma treatment scans.

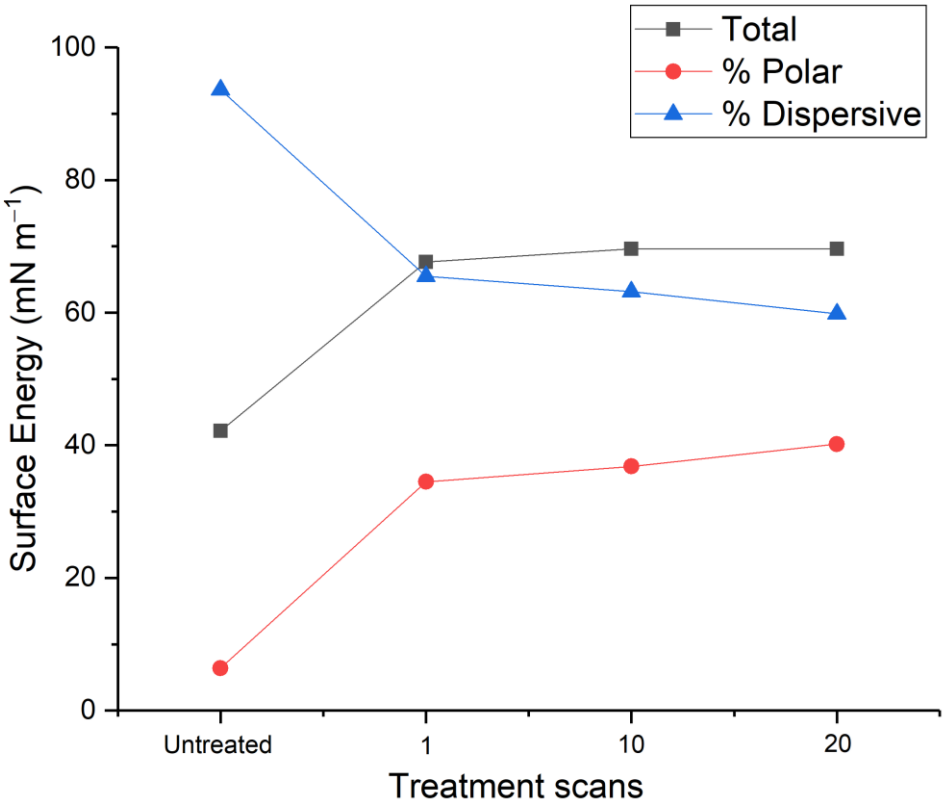

Figure 5-6. Surface energy (total, polar and dispersive) of untreated GFPA6 and µPlasma treated GFPA6 with different treatment scans.

Similar trends were observed for the wetting envelopes of the different samples (as shown in Figure 5-7). The wetting envelope, which can be used for predicting the wettability of the materials surface, was calculated through the surface energy of the solid material using the Fowkes Equation. The method employed is reported in detail elsewhere [27]. When the liquid with surface dispersive σ^D and polar σ^s components are within the values enclosed by the wetting envelope, the liquid is hypothesised to be able to completely wet the surface (i.e., contact angle of 0 °). Therefore, larger wetting envelopes indicate better wettability of a sample surface. Figure 5-7 revealed that the enclosed area of the wetting envelope increased substantially following a single µPlasma treatment scan. However, only limited increases were found with further increases of the number of µPlasma treatment scans. So clearly, the surface

wettability was significantly improved following one µPlasma treatment scan (as demonstrated by the contact angle, surface free energy and wetting envelope data); however, although not detrimental, the influence of further (10 or 20) treatment repetitions did not significantly improve the surface wettability of the GFPA6.

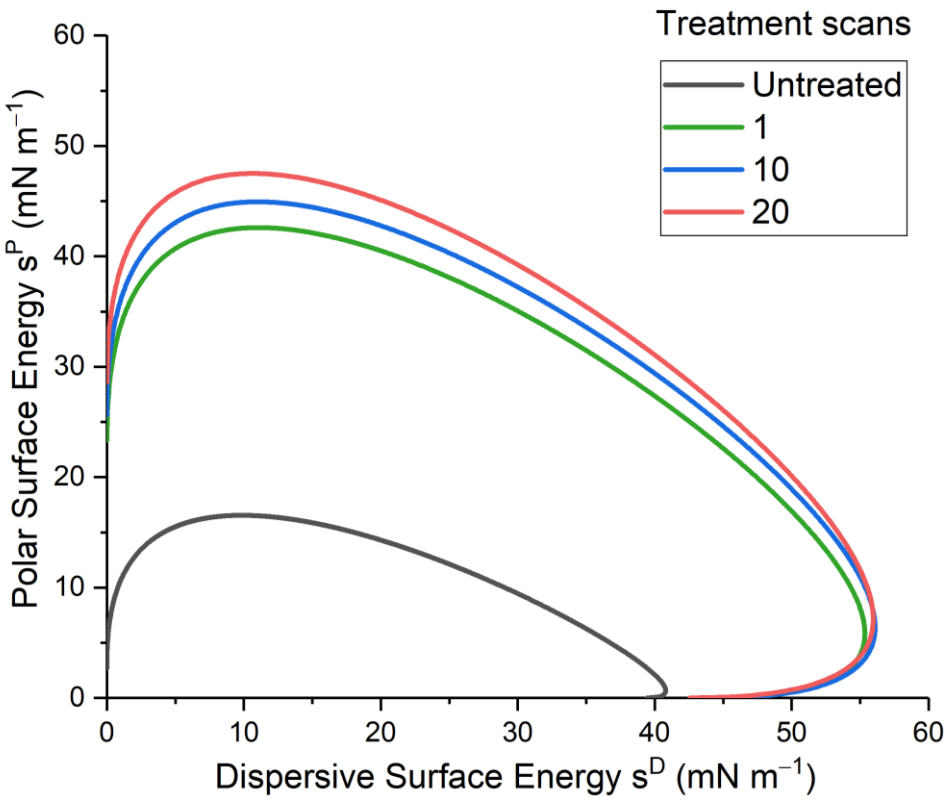

Figure 5-7. Wetting envelope of untreated and µPlasma treated GFPA6 surface with different treatment scans.

5.3.3 Raman Spectroscopy

Analysis of the chemical composition of untreated and µPlasma treated GFPA6 was conducted using Raman spectroscopy, as illustrated in Figure 5-8. Three intense peaks were observed in the untreated material between the Raman shifts of 2800 to 3000 cm^{-1}, which were assigned to symmetric and asymmetric vibrations of CH_2 moieties of the polymer. The band centred at 1093 cm^{-1} was attributed to C-C

stretching, while the bands at 1450 and 1646 were attributed to CH_2 bending and C=O stretching in amide groups, respectively. N-H stretching of the amides was also observed at a Raman shift of 3307 cm^{-1}. A list of the Raman shifts of the major peaks and their assigned chemical vibrations are reported in Table 5-1.

Profound increases of the major bands were observed after µPlasma treatment, which indicated that the chemical composition on the surface of the GFPA6 was altered by the µPlasma treatment. A significant increase of the intensity of the symmetric and asymmetric CH_2 peaks were observed with increasing numbers of µPlasma treatment scans. The effect of the treatment on the polar amide group is shown in Figure 5-9, where again, a pronounced increase with treatment number was apparent.

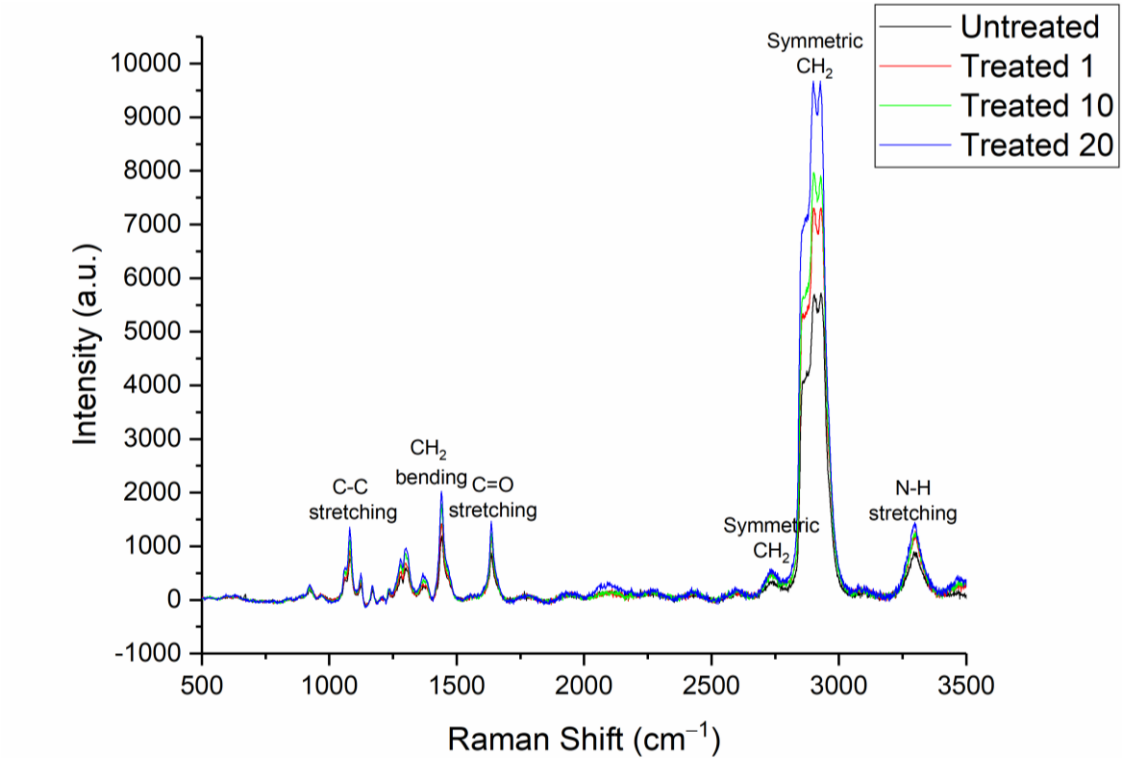

Figure 5-8. Raman spectra of untreated GFPA6 and µPlasma treated GFPA6 with different (1, 10, 20) treatment scans.

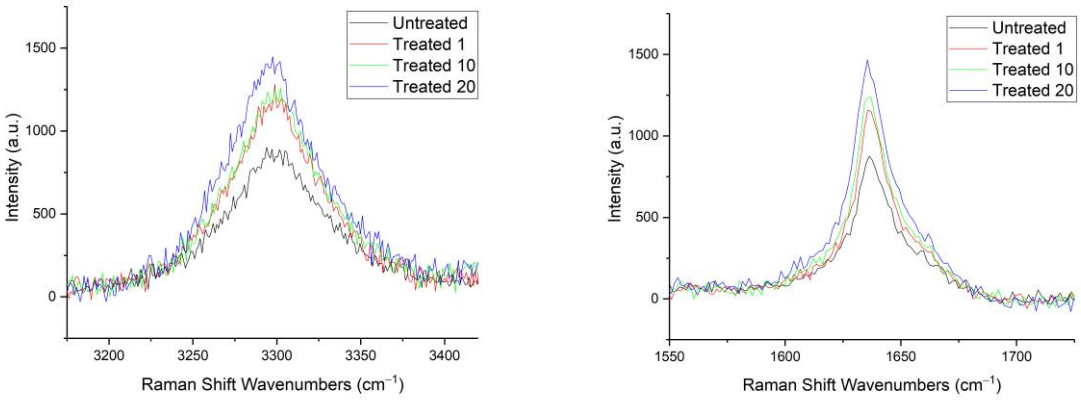

(a) (b)

Figure 5-9. Raman spectra of GFPA6 in (a) wavenumber 3307 cm^{-1} (N-H stretching), and wavenumber 1646 cm^{-1} (C=O stretching) untreated and µPlasma treated GFPA6 with different (1, 10, 20) treatment scans.

Table 5-1. The observed assignments of major Raman peaks of GFPA6 in different wavenumbers [168, 169].

Wavenumber (cm^{-1})	Assignments
1060-1129	C-C stretching
1450	CH_2 bending
1646	C=O stretching
2865	Symmetric CH_2
2912	Symmetric CH_2
2936	Asymmetric CH_2
3307	N-H stretching

The average intensity of the amide bands increases with the number of the µPlasma treatment scans. The most significant intensity increase is found following the first µPlasma treatment scan, with more subtle increases for 10 and 20 treatment scans.

Raman mapping was used to reveal the distribution of the amide band across a 2550 × 2550 μm^2 area of the surface of each sample group. Colour heat maps in Figure 5-10

and quantitative data (of the averaged intensities and ranges of each map) in Table 5-2 are used to convey and analyse the mapping data. Despite the low average intensity under Raman mapping, homogenous coverage of the polar amide groups was revealed on the surface of the untreated GFPA6. As shown in Table 5-2, the average intensity increased by 56.6% for C=O stretching and 35.6% for N-H stretching following one μPlasma treatment scan. Considering the magnitude of the increase in the number of scans, the change in average intensity produced after 10 scans was less pronounced compared to one, especially for the N-H stretching (which only increased from 35.6% to 37.1%). The peak intensity range was observed to widen following one μPlasma treatment scan (Figure 5-10), going from 4201.6 to 7607.6 for C=O stretching and from 30746.4 to 51509.6 for N-H stretching, which indicate heterogeneous distribution bands across the surface. However, when the number of scans was increased to 10, the amide bands appeared to become homogeneous across the majority of the surface, as the range of intensity decreased to 6342.4 for C=O stretching and 43809.2 for N-H stretching. A significant segregation of the two bands was then found after 20 μPlasma treatment scans, as evidenced by the significant increased intensity range to 9552.6 for C=O stretching and 76493.4 for N-H stretching.

Table 5-2. Average intensity and range of intensity across the area.

Bands	Treatment scans	Change in average intensity (%)	Average intensity (a.u.)	Standard deviation (±)	Range of intensity
C=O stretching	0	0	5639.5	973.2	4201.6
	1	56.6	8829.8	2204.9	7607.6
	10	73.5	9787.3	1645.7	6342.4
	20	99.3	11239.0	2724.2	9552.6
N-H stretching	0	0	55906.0	7839.4	30746.4
	1	35.6	75829.0	12560.8	51509.6
	10	37.1	76636.9	12274.0	43809.2
	20	54.5	86386.1	21030.1	76493.4

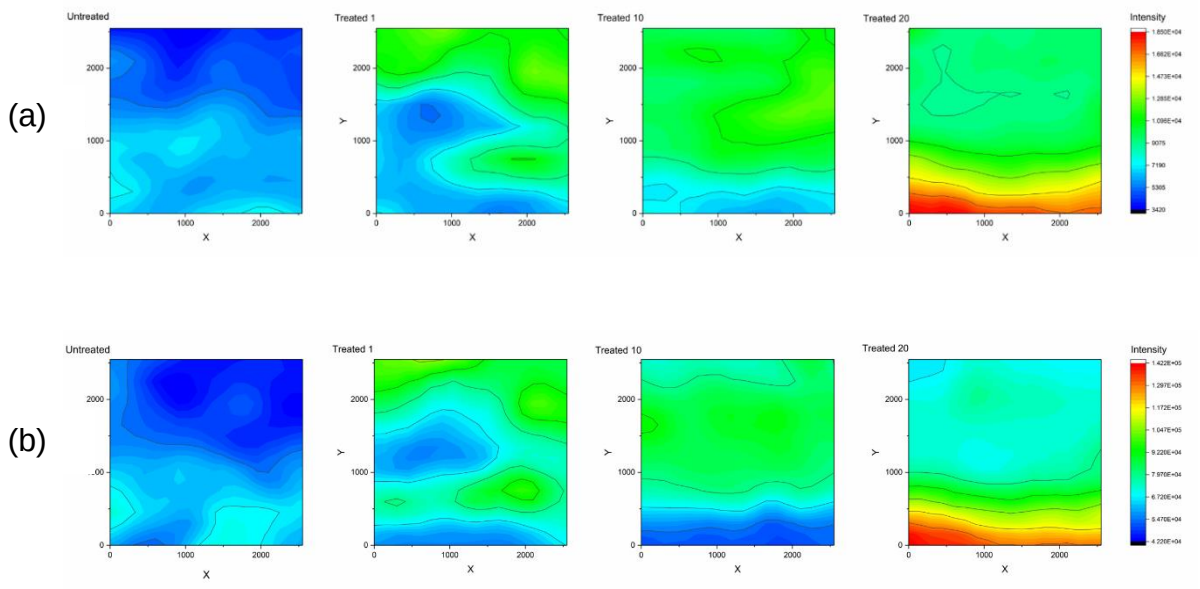

Figure 5-10. Distribution of the (a) C=O stretching in the wavenumber of 1646 cm^{-1}, and (b) N-H stretching in wavenumber of 3307 cm^{-1} on the untreated and μPlasma treated sample surfaces (with 1, 10 20 treatment scans) with size of 2550 × 2550 μm represented by heat colour mapping.

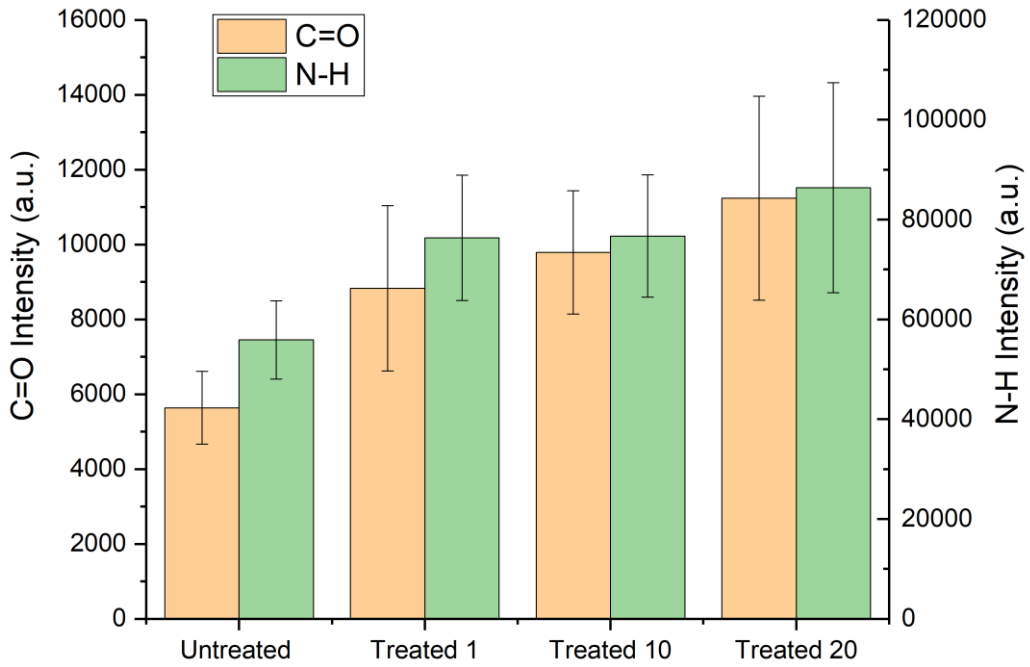

Figure 5-11. Average intensity and standard deviation of the amide band on the untreated and μPlasma treated (with 1,10 and 20 treatment scans) on the sample surface.

5.3.4 Adhesive Bonding of GFPA6

Figure 5-12 shows a comparison of the tensile shear strength of untreated and μPlasma treated GFPA6. Following a single μPlasma treatment scan, a substantial increase in tensile shear strength from 1003.2 N to 1788.1 N was observed. The tensile shear strength was found to further increase to 2268.1 following 10 μPlasma scans (almost double the tensile shear strength of the untreated GFPA6). However, further increases of the number of μPlasma scans did not result in further improvement of the tensile shear strength, with the strength increasing by only 25.4 N (as compared with 10 scans), which is in contrast to the effect of μPlasma treatments on the surface

roughness, where the roughness increased substantially when increasing μPlasma treatment scans to 20.

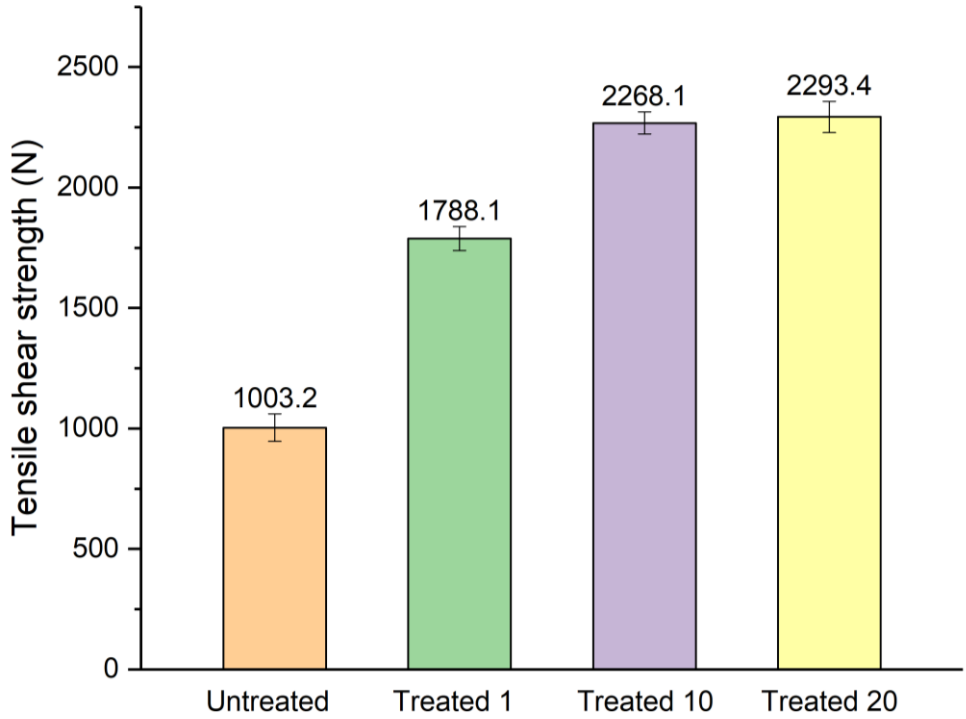

Figure 5-12. The tensile shear strength of the bond between GFPA6 and aluminium in different conditions (untreated and μPlasma treated with 1, 10 and 20 treatment scans) and AA-6082 using epoxy adhesive.

Illustrative fracture surfaces are shown in Figure 5-13. In the untreated samples, due to the weak bonding of the adhesive to the polymer surface, the coverage of the adhesive residue on the polymer surface was very limited, but with increased treatment scans, more adhesive was retained on the polymer surface. Analysis of the surfaces revealed that following a single μPlasma treatment scan, the percentage coverage of the residual adhesive on the polymer surface increased from 12.2% (untreated) to 29.8% (shown in Table 5-3). Whole (or bulk) regions of adhesive were found to peel away from the aluminium sheet, therefore indicating that the adhesive bonding between the

GFPA6 surface and epoxy adhesives had improved after μPlasma treatment. When 10 μPlasma treatment scans were performed on the sample surface, the amount of adhesive residue increased significantly, covering the majority of the previously joined surface (83.9%). The amount of the adhesive residue was similar (81.2%) when 20 μPlasma treatment scans were applied.

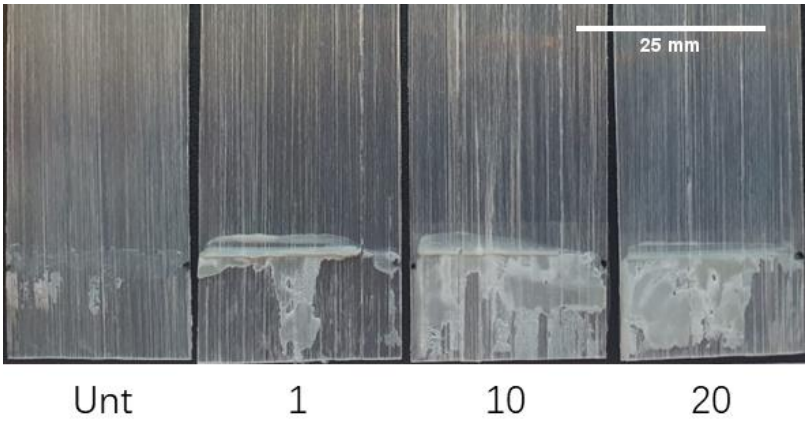

Figure 5-13. Image of distribution of adhesive residue on the Untreated GFPA6 and μPlasma treated 1, 10 and 20 scans after tensile lap-shear test failure and (f) different failure modes distributed on GFPA6 surface after fracture.

Table 5-3. Area covered by the residual adhesive on the sample surface.

Treatment	Area%
Untreated	12.2
Treated 1	29.8
Treated 10	83.9
Treated 20	81.2

Figure 5-14 shows the fracture surfaces as recorded by SEM. In the untreated samples, there is little evidence of adhesion of the epoxy to the polymer surface (consistent with adhesive failure), however, there is some limited evidence of thin striations of adhesive residue on the fibres (suggesting highly localised thin-layer cohesive failure).

However, following a single µPlasma treatment scan of the GFPA6 surface, damage of the surface became apparent coupled with some residual adhesive on the surface (Figure 5-14 b). This surface damage was attributed to the pull force that generated by the improved bonding between the sample surface and the epoxy adhesive during the tensile failure, suggesting a higher bonding strength.

When the number of treatment scans increased to 10 and then 20 (as shown in Figure 5-14 c and d), more extensive adhesive residue coverage was observed. Damaged adhesive layers were observed on both 10 and 20 µPlasma scanned surface. These layers presented with coarse structures and round pits, likely developed from air bubbles formed when the resin and hardener were mixed. In addition, deformation was revealed of the GFPA6 material surface as a result of strong pull forces, which indicate that this part of bonding failure was due to substrate failure.

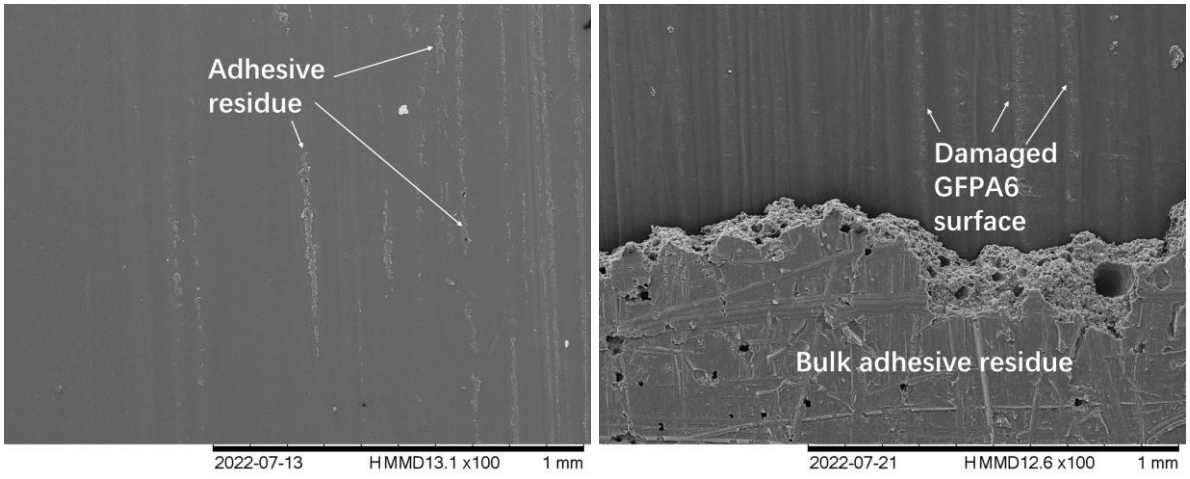

(a) (b)

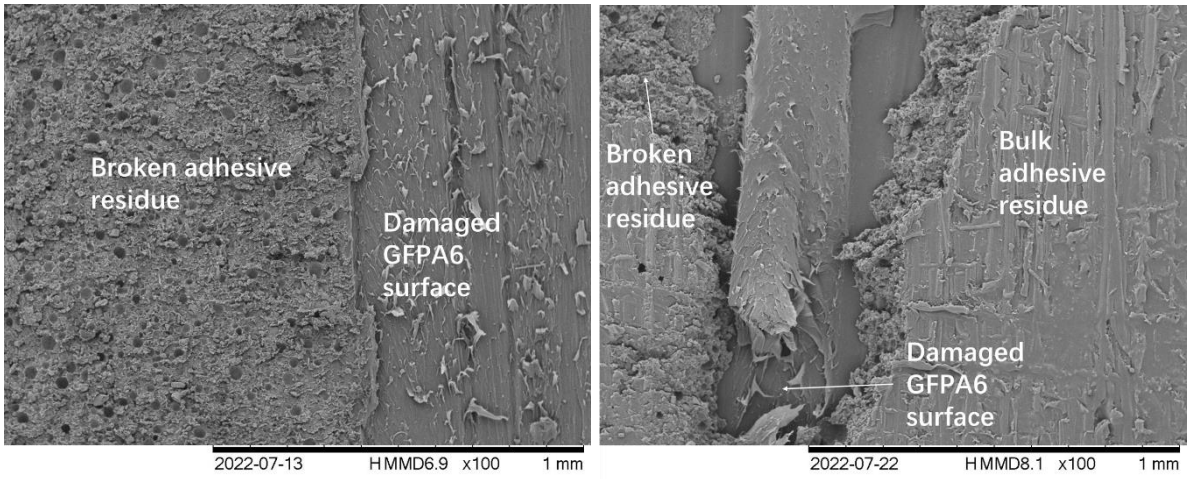

(c) (d)

Figure 5-14. SEM images of tensile fracture GFPA6 surfaces of (a) untreated, and µPlasma treated different scans: (b) 1 scan, (c) 10 scans and (d) 20 scans.

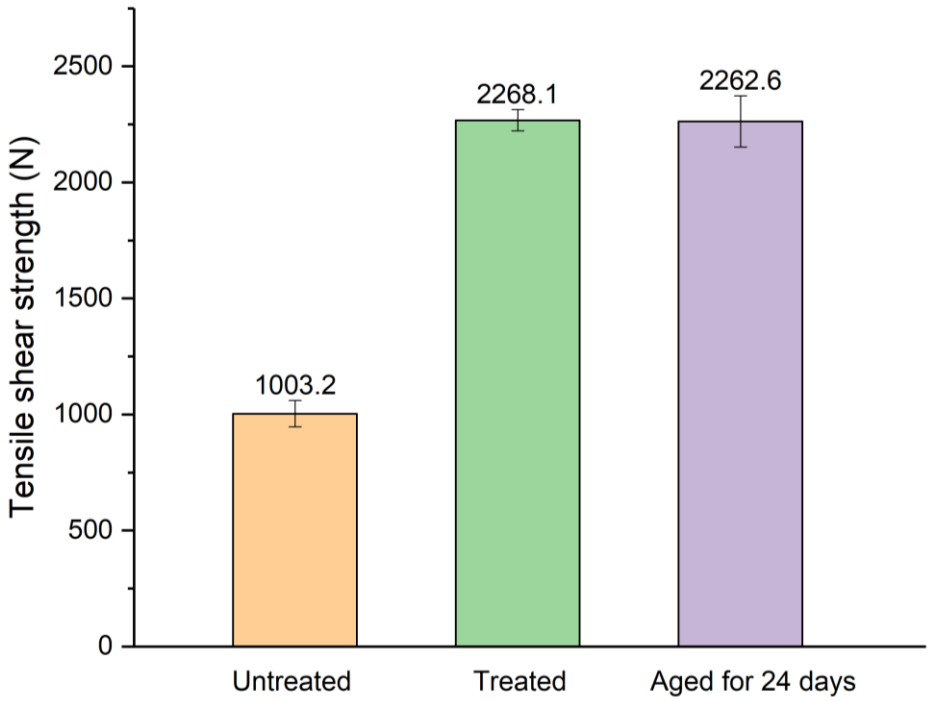

Figure 5-15. Comparison of untreated GFPA6-epoxy-AA6082, 10 scans of µPlasma treated GFPA6-epoxy-AA6082, and 10 scans of µPlasma treated GFPA6-epoxy-AA6082 aged in the air for 24 days.

As noted above, the effects of μPlasma surface treatment have been found to be non-permanent and post-treatment ageing occurs. Therefore, in this study, adhesive bonding was expedited to ensure that little or no ageing had occurred prior to joining the surfaces. However, to determine whether the ageing process could still occur in the joined samples, joined GFPA6-epoxy-AA6082 samples were stored under ambient conditions for 24 days prior to mechanical testing. Compared to the unaged GFPA6-epoxy-AA6082 (whereby the tensile lap-shear test was carried out immediately after joining and curing), the tensile shear strength was found to decrease by only 6.6 N out of 2268.1 N. This presents a smaller decrease in tensile shear strength than the deviation of the strength data (45.3 N and 110.4 N for the unaged and aged samples respectively). This demonstrates that the 24-day ageing behaviour had negligible effect on the performance of the joined GFPA6-epoxy-AA6082 and that from mechanical test perspective, the ageing process in joined materials is effectively eliminated.

5.4 Discussion

The μPlasma treatment has been demonstrated to be able to both physically and chemically modify the polymer surface, as indicated by the measurement of roughness and surface wettability. The increase in roughness can be attributed to the process of ablation in which polymeric material is lost from the surface [170]. While increasing the number of treatment scans clearly increased the roughness, the effect was relatively limited for a single treatment scan (a 15.6% increase in RMS roughness). Studies have shown that a change in roughness on a sample surface plays an important role in determining its wettability [171, 172]. However, in this study, it was found the change in wettability of the GFPA6 surface (using contact

angle, surface free energy and wetting envelope measurements) did not increase in proportion to the change in surface roughness (as shown in Figure 5-16). Although the contact angles were found to substantially reduce (61.5%) following one μPlasma treatment scan, further decreases in the measured contact angle was limited for 10 and 20 μPlasma treatment scans. Similar trends were observed in surface free energy and wetting envelope. μPlasma treatment resulted in an increase in the peak intensities corresponding to the polar groups, for example the C=O stretching at 1646 cm^{-1}. One treatment brought the largest change of the intensity increase in C=O group compared to 10 and 20, which is corresponding to the results of wettability. Therefore, given the above observations it is apparent that in this instance, wettability is controlled primarily by the presence of polar functional groups on the surface and not the surface roughness.

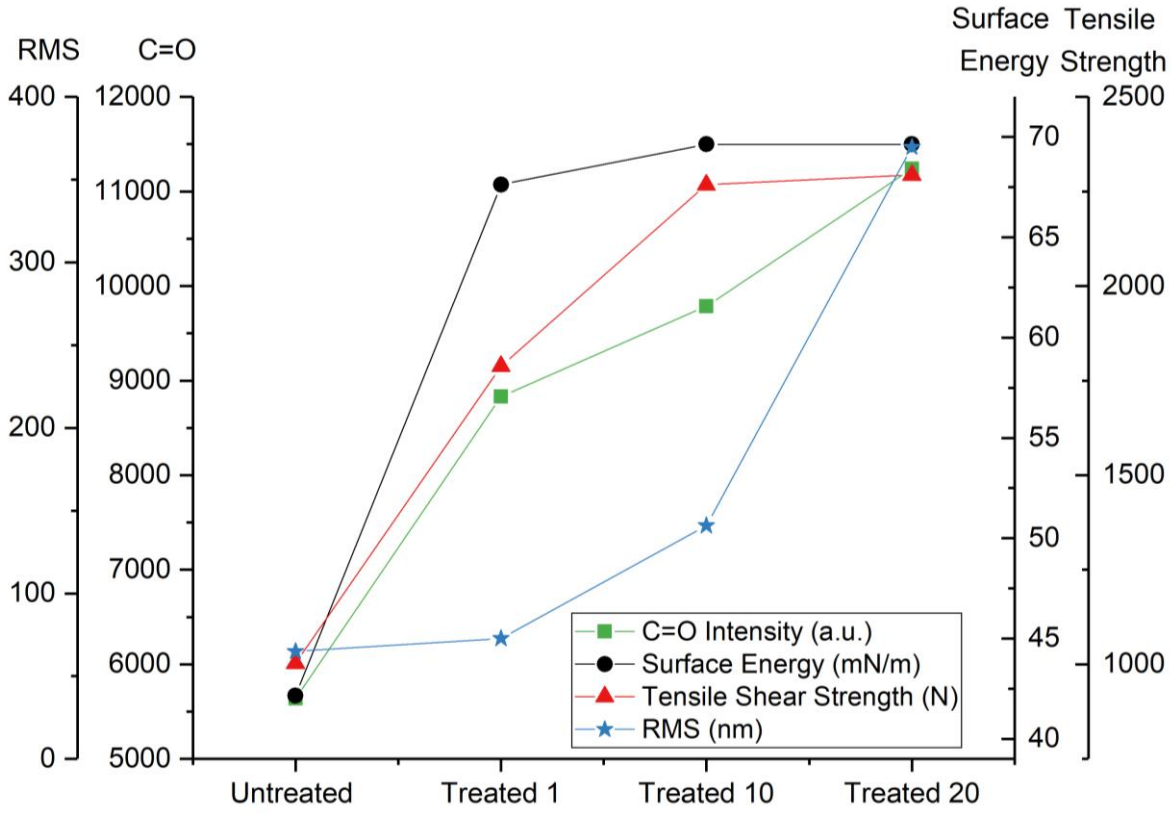

Figure 5-16. Comparison of the change in C=O intensity, surface energy, tensile shear strength and RMS of untreated and µPlasma treated (with 1, 10 and 20 scans) GFPA6.

The results from the tensile lap-shear tests indicated that the bonding strength of GFPA6-epoxy-AA6082 increased significantly following µPlasma treatment of the GFPA6 surface. This finding correlated with the improved wettability after µPlasma treatment (as shown in Figure 5-16), and indicates that the bonding strength is largely determined by the material surface wettability rather than the surface roughness. However, no discernible improvement in bonding strength was found when increasing the number of treatments to 20. Similar findings were reported by Ku et al. [15], who investigated the peel and shear strength between polypropylene and aluminium after atmospheric plasma treatment of polypropylene, and reported that, 8 out of 2, 4, 6, 8

and 10 treatment scans produced the strongest adhesion. However, there may be over etching of the surface as the number of treatment scans exceeds 10, as evidenced by the exposure of the fibres on the surface and the formation of distinct grooves between them, as shown in Figure 5-3. During the joining process, the relatively high viscosity of the epoxy adhesive could hinder flow into the sharp valleys of the grooves. Therefore, this may have limited the overall interface area between the epoxy adhesive and the GFPA6 surface giving rise to weaker overall bonding. However, the increase in the proportion of surface functional groups, which enable stronger localised bonding, may have compensated for this leading to a bond strength that is comparable to that recorded for 10 µPlasma treatments.

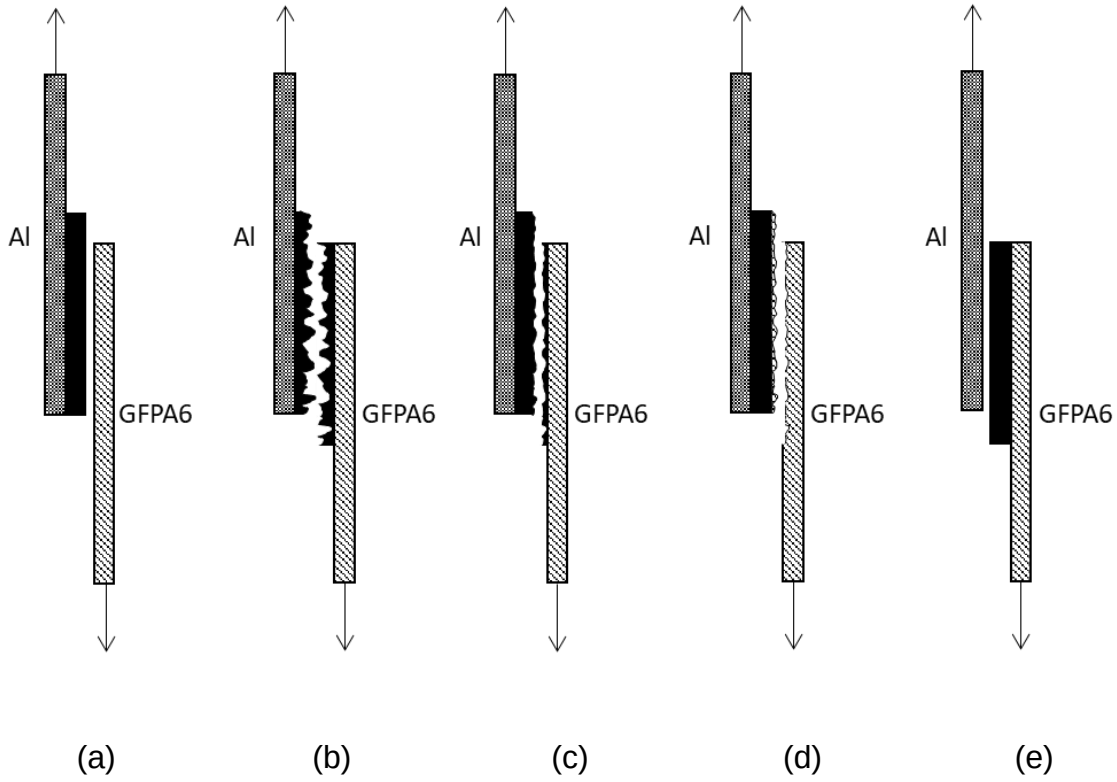

Figure 5-17. Illustration of failure mode that happened when broken: (a) adhesive failure of GFPA6, (b) cohesive failure, (c) thin-layer cohesive failure, (d) light-tear failure and(e) adhesive failure of Al.

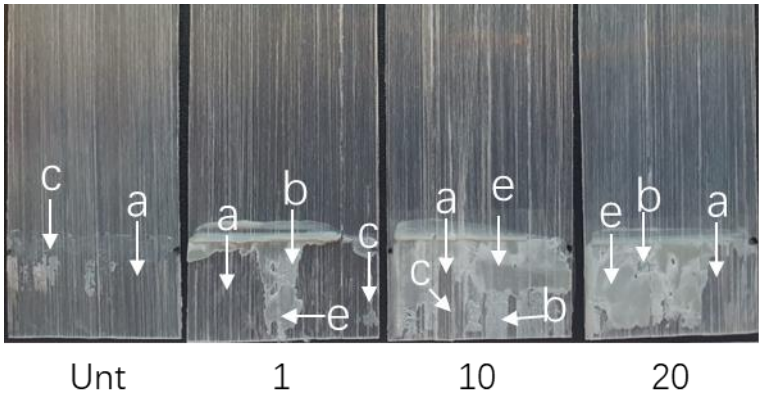

Figure 5-18. Illustration of failure mode that happened when broken: (a) adhesive failure of GFPA6, (b) cohesive failure, (c) thin-layer cohesive failure, (d) light-tear failure and (e) adhesive failure of Al.

The analysis of the surface morphology of GFPA6 after fracture confirms that μPlasma treatments can enhance the surface bonding of GFPA6-epoxy-AA6082, as can be seen the failure modes illustrated in Figure 5-17and the surface morphology observed in Figure 5-14. It was shown on the untreated GFPA6 surface that the majority of the adhesive had been completely removed following the tensile lap-shear test, which is consistent with adhesive failure and some (limited) cohesive failure mode, and suggests poor bonding. The degree of adhesive remaining on the material surface increased substantially with increasing numbers of μPlasma scans. As shown in Figure 5-18, a mix of light-tear, adhesion and thin-layer cohesion failure modes were observed after single μPlasma treatments of the GFPA6 surface, which suggested stronger bonding with the epoxy resin. Moreover, the portions of the surface which were composed of intact adhesive with a smooth surface indicated the initiation of adhesive failure between the epoxy surface and the aluminium surface. After 10 and 20 μPlasma treatment scans, broken adhesives and stretching of the GFPA6 substrate was observed, accompanied with a more complex mixtures of failure modes, including adhesive, cohesive, thin-layer cohesive, light-tear and adhesive failure of Al failure

modes, which also imply substantial enhancement of the bonding strength. Additionally, significantly greater amount of smooth intact epoxy resin could be observed on the 10 and 20 scanned surfaces, which also indicate that the load at failure of the tensile lap-shear test was more strongly related to the strength and quality of adhesion between the aluminium surface and the epoxy-resin. This shift in failing surface supports the measured enhancement of surface functionality and wettability. The residual adhesive coverage on the sample surface and failure modes following different treatment scans were summarised in Table 5-4.

Table 5-4. Summary of residual adhesive coverage on the sample surface and failure modes following different treatment scans.

Treatment	Residual adhesive coverage area%	Failure modes
Untreated	12.2	(a) adhesive failure of GFPA6 (c) thin-layer cohesive failure
Treated 1	29.8	(a) adhesive failure of GFPA6 (b) cohesive failure (c) thin-layer cohesive failure (e) adhesive failure of Al
Treated 10	83.9	(a) adhesive failure of GFPA6 (b) cohesive failure (c) thin-layer cohesive failure (d) light-tear failure (e) adhesive failure of Al
Treated 20	81.2	(a) adhesive failure of GFPA6 (b) cohesive failure (c) thin-layer cohesive failure (d) light-tear failure (e) adhesive failure of Al

Interestingly, as the number of μPlasma treatment scans increased from 10 to 20, no significant change in the tensile shear strength could be measured and the fracture surface morphology was not significantly altered, which are both consistent with the observed changes in wettability. The 10 μPlasma treated surface reveals largely homogeneous coverage of the epoxy resin on the GFPA6 surface, which implies that the bonding between the GFPA6 and the epoxy resin did not contribute to the dominating failure modes of the GFPA6-epoxy-AA6082 joint. Instead, the most prominent failure modes appear to be adhesive failure with the aluminium surface (smooth intact epoxy resin) and cohesive failure within the resin (fractured and rough epoxy surface). Interestingly, the 20 μPlasma treated surface does not present with significant increase in the adhesive failure from the aluminium surface, but instead presents with the return of adhesive failure on the GFPA6 surface. This can be explained by the heterogeneous surface modification (as shown by Raman mapping) and increase surface roughness (as shown by AFM imaging and the exposure of the glass fibre) of the 20 μPlasma treated surface. The combined action of these can act to both reduce the usable surface area for adhesion (by creating narrow crevices) and create disproportionate loading of the bonding interface by creating regions of significantly stronger bonding that transfer the load towards the less strongly adhered surfaces, thereby subjecting those regions to larger forces (and subsequently more failure). This indicates that the homogeneity of the polar groups on the surface is more essential than higher intensity of the peaks for enhancing the bonding strength of GFPA6-epoxy-AA6082, which supports that the bonding strength correlates closely with the water wettability (that measured polar functional groups).

Once adhered, a storage period of 24 hours did not appear to significantly influence the bonding strength of the of GFPA6-epoxy-AA6082 sample. This suggests that the epoxy adhesive can form permanent bonds with the functional groups introduced on the surface after μPlasma treatment, thereby preventing the reorientation or diffusion of polar moieties back to into the bulk of the GFRPA6 sample (hydrophobic recovery [173, 174]).

5.5 Conclusion

This study has shown that μPlasma surface treatment of glass fibre reinforced polyamide 6 is highly beneficial in terms of the effectiveness of the adhesive bond with aluminium. Bond strength was found to increase with the number of treatment scans, but no more than ten scans was found to be the optimum. The increase in bond strength was attributed to increases in the following material characteristics; surface energy, polarity and roughness, but the dominant factor that affected the bond strength was deemed to be the increased polarity of the polymer surface. Of key importance in this study was the immediate fabrication of the test sample post-treatment. This approach ensured the effects of post-treatment ageing were minimised and that the maximum benefit available from the surface treatment was realised. From a commercial perspective, the study has shown that μPlasma surface treatment is sufficiently effective when a relatively low number of treatment scans are employed. This, coupled with the atmospheric nature of the technique, points to great potential as a low-cost, on-line, polymer surface treatment technique.

6 Conclusion and Future Work

6.1 Conclusion

This study investigated the effect of µPlasma surface modification on the surfaces of thermoplastics including polyamide 6 (PA6), polyamide 12 (PA12) and high-density polyethylene (HDPE), especially glass fibre reinforced polyamide 6 (GFPA6). This research has improved the bonding strength of the epoxy-adhered GFPA6-aluminium joints. The joint can be used to replace the metal structural components of vehicles to reduce weight, improve the fuel efficiency, and thereby reduce CO_2 emissions from motor vehicles.

In the first part of this study, it was found that the accuracy of contact angle on GFPA6 was influenced by various factors such as the alignment of the fibres on the polymer, the liquid droplet size, orientations of the contact angles, types of test liquids, and most interestingly, the dryness of the polymer. It was revealed that the ageing of the samples following the µPlasma surface modification is slower when the samples were pre-dried before the treatment. The treated samples were then stored in the environment with different humidity, it was also discovered that the ageing rate was massively affected by the humidity in the environment. The ageing rate was reduced by approximately 50% when storing the samples in the vacuum (0% humidity) than in the air (50–60% humidity). This means that the ageing process of post-treated polymers can be influenced by the exist of water.

Therefore, in the second part of the study, three polymers with different degrees of hydrophilicity were investigated to discover whether the hydrophilicity of the materials

themselves would have an influence on the ageing process. Building on the wettability measurement on the sample surface using contact angle treatment, this part extended the testing of surface morphology and chemical compositions before and after the μPlasma surface modification.

Additionally, to quantify the ageing process in the first 5 hours and produce a more accurate determination of the maximum predicted change in contact angle, the contact angle data was modelled using a modified stretched exponential Kohlrausch–Williams–Watts (KWW) model. It was confirmed that the degree of the hydrophilicity of a polymer was directly related to the ageing rate. The greater the hydrophilicity of the polymer, the faster the observed ageing rate.

The third part of the study gives practical significance to the first two parts. The μPlasma surface treated GFPA6 was bonded to Aluminium (AA6082-T6) using epoxy adhesives. The bonding strength was improved by 2.3 times compared to the untreated one. Based on the surface wettability represented by the contact angle, surface free energy and wetting envelope data in the first part, study of the change in surface morphology and chemical compositions were carried out on GFPA6 in the third part. The relationship between the surface morphology, surface chemical composition and the increase in surface wettability on the sample surface before and after the μPlasma surface modification were concluded in this part. Although the parameters used were based on the first part of the study, however, unlike the first part of this study where one single μPlasma treatment scan was sufficient to reduce the contact angle of the GFPA6 surface, it was revealed that 10 μPlasma treatment scans improved the bonding strength of GFPA6-epoxy-aluminium adhered joints more than 1 and 20 scans.

As rapid ageing behaviour was observed for all materials including GFPA6, HDPE, PA12 and PA6 in the first and second parts of the study, the impact of ageing behaviour on the bonding strength of the GFPA6-epoxy-aluminium adherent joints was also investigated. It was found that the bonding strength of plasma functionalised surfaces did not deteriorate after 24 days of ageing, which suggests that, although the µPlasma treated GFPA6 surfaces experienced rapid initial ageing, GFPA6-epoxy-aluminium adherent joints were not subject to significant ageing when µPlasma treated GFPA6 surfaces were dried and immediately joined with aluminium adhered surfaces.

6.2 Future Work

6.2.1 Further Improvement of the Bonding Strength of GFPA6-epoxy-aluminium Adhered Joints

The bonding strength of GFPA6-epoxy-aluminium adhered joints was significantly increased with the µPlasma modification of GFPA6 in the present study. The highest bonding strength was achieved when 10 µPlasma treatment scans were applied on the surface of GFPA6, an improvement over the single scan experiment. Therefore, it is still worth investigating whether a higher bonding strength can be achieved between 1 and 10 µPlasma treatment scans. To determine the optimal number of µPlasma treatment scans required to achieve the highest bonding strength, the GFPA6 will be treated for 2-9 scans before joining, and the bonding strength will be evaluated through the tensile lap shear test.

Additionally, while GFPA6 was µPlasma treated before joining, the AA6082 was only ground using roughened #120 grit SiC paper to increase the roughness on the surface.

To further improve the bonding strength of the GFPA6-epoxy-aluminium adhered joints, the aluminium can also be plasma treated before joining to GFPA6 using epoxy adhesive. The μPlasma treated GFPA6 with the highest bond strength can then be joined with μPlasma treated AA6082. If μPlasma treated AA6082 can further enhance the bonding strength of GFPA6-epoxy-aluminium adhered joints, the number of treatment scans of μPlasma on AA6082 will also be optimised, following the same procedure used for μPlasma treated GFPA6. To characterise the physical and chemical changes following μPlasma surface modification of the AA6082 surface, Atomic Force Microscopy (AFM) and Raman spectroscopy will be performed.

In summary, this future work aims to optimise the number of the μPlasma treatment scans required to achieve the highest bonding strength of GFPA6-epoxy-aluminium adhered joints, and to explore the potential of μPlasma treatment on the surface of AA6082 to further improve the bonding strength.

6.2.2 μPlasma Patterning

μPlasma treatment enables the localised treatment of polymers and the design of surface patterns, which increases energy efficiency. However, the present work has applied the μPlasma treatment to the entire polymer surface. Therefore, in future work, designing a μPlasma treatment pattern to modify the polymer surfaces to fully exploit the pattern design function of the μPlasma device. In this regard, the pattern will be designed as a cobweb. This is inspired by nature as the cobweb catch more small bugs, therefore, μPlasma treated cobweb might improve the adhesive properties even better).

The physical and chemical changes of GFPA6 following μPlasma surface modification will be characterised using Atomic Force Microscopy (AFM) and Raman Spectroscopy. The wettability of the treated and untreated GFPA6 surface will be determined through contact angle tests, accompanied by the calculation of surface energy and wetting envelope. The bonding strength of GFPA6-epoxy-aluminium adhered joints (with GFPA6 treated with a cobweb pattern μPlasma) will be evaluated by tensile lap-shear test. The results will be compared with those from the μPlasma modification of the whole polymer surface to determine whether the patterned treatment enhances wetting properties more effectively.

Overall, this future work aims to investigate the effectiveness of a patterned μPlasma modification in enhancing the surface wettability of GFPA6, and the bonding strength of GFPA6-epoxy-aluminium adhered joints.

7 References

[1] P. Kiss, J. Schoefer, W. Stadlbauer, C. Burgstaller, and V.-M. Archodoulaki, "An experimental study of glass fibre roving sizings and yarn finishes in high-performance GF-PA6 and GF-PPS composite laminates," *Composites Part B: Engineering,* vol. 204, p. 108487, 2021.

[2] M. Biron, *Thermoplastics and thermoplastic composites*. William Andrew, 2018.

[3] D. Vlasveld, P. Parlevliet, H. Bersee, and S. Picken, "Fibre–matrix adhesion in glass-fibre reinforced polyamide-6 silicate nanocomposites," *Composites Part A: Applied Science and Manufacturing,* vol. 36, no. 1, pp. 1-11, 2005.

[4] X.-F. Wei, K. J. Kallio, S. Bruder, M. Bellander, R. T. Olsson, and M. S. Hedenqvist, "High-performance glass-fibre reinforced biobased aromatic polyamide in automotive biofuel supply systems," *Journal of Cleaner Production,* vol. 263, p. 121453, 2020.

[5] R. Naik, S. Panda, and V. Racherla, "A new method for joining metal and polymer sheets in sandwich panels for highly improved interface strength," *Composite Structures,* vol. 251, p. 112661, 2020.

[6] A. Pramanik *et al.*, "Joining of carbon fibre reinforced polymer (CFRP) composites and aluminium alloys–A review," *Composites Part A: Applied Science and Manufacturing,* vol. 101, pp. 1-29, 2017.

[7] A. Galińska and C. Galiński, "Mechanical joining of fibre reinforced polymer composites to metals—a review. Part II: riveting, clinching, non-adhesive form-locked joints, pin and loop joining," *Polymers,* vol. 12, no. 8, p. 1681, 2020.

[8] S. T. Amancio Filho and L.-A. Blaga, *Joining of polymer-metal hybrid structures: principles and applications*. John Wiley & Sons, 2018.

[9] S. Amancio‐Filho and J. Dos Santos, "Joining of polymers and polymer–metal hybrid structures: recent developments and trends," *Polymer engineering & science,* vol. 49, no. 8, pp. 1461-1476, 2009.

[10] C. Fuentes *et al.*, "Effect of physical adhesion on mechanical behaviour of bamboo fibre reinforced thermoplastic composites," *Colloids and surfaces A: physicochemical and engineering aspects,* vol. 418, pp. 7-15, 2013.

[11] G. Wade and W. Cantwell, "Adhesive bonding and wettability of plasma treated, glass fiber-reinforced nylon-6, 6 composites," *Journal of materials science letters,* vol. 19, no. 20, pp. 1829-1832, 2000.

[12] K. S. Kim, C. M. Ryu, C. S. Park, G. S. Sur, and C. E. Park, "Investigation of crystallinity effects on the surface of oxygen plasma treated low density polyethylene using X-ray photoelectron spectroscopy," *Polymer,* vol. 44, no. 20, pp. 6287-6295, 2003.

[13] T. Desmet, R. Morent, N. De Geyter, C. Leys, E. Schacht, and P. Dubruel, "Nonthermal plasma technology as a versatile strategy for polymeric biomaterials surface modification: a review," *Biomacromolecules,* vol. 10, no. 9, pp. 2351-2378, 2009.

[14] Z. Gao, J. Sun, S. Peng, L. Yao, and Y. Qiu, "Surface modification of a polyamide 6 film by He/CF4 plasma using atmospheric pressure plasma jet," *Applied Surface Science,* vol. 256, no. 5, pp. 1496-1501, 2009.

[15] J. Ku, I. Jung, K. Rhee, and S. Park, "Atmospheric pressure plasma treatment of polypropylene to improve the bonding strength of polypropylene/aluminum composites," *Composites Part B: Engineering,* vol. 45, no. 1, pp. 1282-1287, 2013.

[16] A. Carradò, O. Sokolova, B. Donnio, and H. Palkowski, "Influence of corona treatment on adhesion and mechanical properties in metal/polymer/metal systems," *Journal of Applied Polymer Science,* vol. 120, no. 6, pp. 3709-3715, 2011.

[17] M. Nakamura, T. Ohno, N. Konishi, K. Miyata, and N. Kamezawa, "Characterization of hydrogenation and dehydrogenation of post-plasma treated low-pressure chemical-vapor-deposited amorphous silicon films," *Journal of applied physics,* vol. 62, no. 9, pp. 3740-3746, 1987.
[18] I. Novák, M. Števiar, and I. Chodák, "Surface energy and adhesive properties of polyamide 12 modified by barrier and radio-frequency discharge plasma," *Monatshefte für Chemie/Chemical Monthly,* vol. 137, no. 7, pp. 943-952, 2006.
[19] S. Periyasamy, R. ASM, and P. G. Patil, "Submicron surface roughening of aliphatic polyamide 6, 6 fabric through low temperature plasma and its effect on interfacial bonding in rubber composite," *Journal of Industrial Textiles,* vol. 47, no. 8, pp. 2029-2049, 2018.
[20] C. Mandolfino, E. Lertora, and C. Gambaro, "Influence of cold plasma treatment parameters on the mechanical properties of polyamide homogeneous bonded joints," *Surface and Coatings Technology,* vol. 313, pp. 222-229, 2017.
[21] F. R. Oliveira, A. Zille, and A. P. Souto, "Dyeing mechanism and optimization of polyamide 6, 6 functionalized with double barrier discharge (DBD) plasma in air," *Applied Surface Science,* vol. 293, pp. 177-186, 2014.
[22] Z. Gao, "Modification of surface properties of polyamide 6 films with atmospheric pressure plasma," *Applied Surface Science,* vol. 257, no. 14, pp. 6068-6072, 2011.
[23] D. C. Bastos, A. E. Santos, M. L. da Silva, and R. A. Simão, "Hydrophobic corn starch thermoplastic films produced by plasma treatment," *Ultramicroscopy,* vol. 109, no. 8, pp. 1089-1093, 2009.
[24] S. Roy, C. Yue, Y. Lam, Z. Wang, and H. Hu, "Surface analysis, hydrophilic enhancement, ageing behavior and flow in plasma modified cyclic olefin copolymer (COC)-based microfluidic devices," *Sensors and Actuators B: Chemical,* vol. 150, no. 2, pp. 537-549, 2010.
[25] J. M. Cowie and R. Ferguson, "Physical aging studies in poly (vinylmethyl ether). I. Enthalpy relaxation as a function of aging temperature," *Macromolecules,* vol. 22, no. 5, pp. 2307-2312, 1989.
[26] C. Della Volpe, L. Fambri, R. Fenner, C. Migliaresi, and A. Pegoretti, "Air-plasma treated polyethylene fibres: effect of time and temperature ageing on fibre surface properties and on fibre-matrix adhesion," *Journal of materials science,* vol. 29, no. 15, pp. 3919-3925, 1994.
[27] C. Che, B. Dashtbozorg, X. Li, H. Dong, and M. Jenkins, "Effect of µPlasma Modification on the Wettability and the Ageing Behaviour of Glass Fibre Reinforced Polyamide 6 (GFPA6)," *Materials,* vol. 14, no. 24, p. 7721, 2021.
[28] Y. I. Yun *et al.*, "Aging behavior of oxygen plasma-treated polypropylene with different crystallinities," *Journal of adhesion science and technology,* vol. 18, no. 11, pp. 1279-1291, 2004.
[29] D. J. Skrovanek, S. E. Howe, P. C. Painter, and M. M. Coleman, "Hydrogen bonding in polymers: infrared temperature studies of an amorphous polyamide," *Macromolecules,* vol. 18, no. 9, pp. 1676-1683, 1985.
[30] A. Shrivastava, *Introduction to Plastics Engineering*. William Andrew, 2018.
[31] A. Rudin and P. Choi, "Chapter 4-Mechanical properties of polymer solids and liquids," *The Elements of Polymer Science & Engineering,* pp. 149-229, 2013.
[32] L. W. McKeen, *Permeability properties of plastics and elastomers*. William Andrew, 2016.
[33] B. Obi, *Polymeric Foams Structure-Property-Performance: A Design Guide*. William Andrew, 2017.
[34] C. Vasile, *Handbook of polyolefins*. CRC Press, 2000.
[35] L. Li, C.-M. Chan, J.-X. Li, K.-M. Ng, K.-L. Yeung, and L.-T. Weng, "A direct observation of the formation of nuclei and the development of lamellae in polymer spherulites," *Macromolecules,* vol. 32, no. 24, pp. 8240-8242, 1999.

[36] A. Wang, C. Chen, L. Liao, J. Qian, F.-G. Yuan, and N. Zhang, "Enhanced β-phase in direct ink writing PVDF thin films by intercalation of graphene," *Journal of Inorganic and Organometallic Polymers and Materials,* vol. 30, pp. 1497-1502, 2020.
[37] D. J. Kemmish, *Practical guide to high performance engineering plastics*. Smithers Rapra, 2011.
[38] J. Chacón, M. Caminero, P. Núñez, E. García-Plaza, I. García-Moreno, and J. Reverte, "Additive manufacturing of continuous fibre reinforced thermoplastic composites using fused deposition modelling: Effect of process parameters on mechanical properties," *Composites science and technology,* vol. 181, p. 107688, 2019.
[39] A. Kausar, "Advances in carbon fiber reinforced polyamide-based composite materials," *Advances in Materials Science,* vol. 19, no. 4, pp. 67-82, 2019.
[40] R. Deshmukh and A. Shetty, "Surface characterization of polyethylene films modified by gaseous plasma," *Journal of applied polymer science,* vol. 104, no. 1, pp. 449-457, 2007.
[41] H. Zhang *et al.*, "Roll-to-roll DBD plasma pretreated polyethylene web for enhancement of Al coating adhesion and barrier property," *Applied Surface Science,* vol. 388, pp. 539-545, 2016.
[42] I. Novák *et al.*, "High-density polyethylene functionalized by cold plasma and silanes," *Vacuum,* vol. 86, no. 12, pp. 2089-2094, 2012.
[43] A. Emblem, "Plastics properties for packaging materials," in *Packaging Technology*: Elsevier, 2012, pp. 287-309.
[44] R. David, S. Tambe, S. Singh, V. Raja, and D. Kumar, "Thermally sprayable grafted LDPE/nanoclay composite coating for corrosion protection," *Surface and Coatings Technology,* vol. 205, no. 23-24, pp. 5470-5477, 2011.
[45] E. Kuram, E. Tasci, A. I. Altan, M. M. Medar, F. Yilmaz, and B. Ozcelik, "Investigating the effects of recycling number and injection parameters on the mechanical properties of glass-fibre reinforced nylon 6 using Taguchi method," *Materials & Design,* vol. 49, pp. 139-150, 2013.
[46] V. Venoor, J. H. Park, D. O. Kazmer, and M. J. Sobkowicz, "Understanding the effect of water in polyamides: a review," *Polymer Reviews,* vol. 61, no. 3, pp. 598-645, 2021.
[47] L. Tušek, M. Nitschke, C. Werner, K. Stana-Kleinschek, and V. Ribitsch, "Surface characterisation of NH3 plasma treated polyamide 6 foils," *Colloids and Surfaces A: Physicochemical and Engineering Aspects,* vol. 195, no. 1-3, pp. 81-95, 2001.
[48] G. Borcia, N. Dumitrascu, and G. Popa, "Influence of dielectric barrier discharge treatments on the surface properties of polyamide-6 films," *J. Optoelectron. Adv. Mater,* vol. 7, no. 5, pp. 2535-2538, 2005.
[49] J. Hnilica, L. Potočňáková, M. Stupavská, and V. Kudrle, "Rapid surface treatment of polyamide 12 by microwave plasma jet," *Applied surface science,* vol. 288, pp. 251-257, 2014.
[50] S. Roy *et al.*, "Triggering compatibility and dispersion by selective plasma functionalized carbon nanotubes to fabricate tough and enhanced Nylon 12 composites," *Polymer,* vol. 58, pp. 153-161, 2015.
[51] C. Hui, C. Qingyu, W. Jing, X. Xiaohong, L. Hongbo, and L. Zhanjun, "Interfacial enhancement of carbon fiber/nylon 12 composites by grafting nylon 6 to the surface of carbon fiber," *Applied Surface Science,* vol. 441, pp. 538-545, 2018.
[52] Y. Ding *et al.*, "Properties and morphology of supertoughened polyamide 6 hybrid composites," *Journal of Applied Polymer Science,* vol. 126, no. 1, pp. 194-204, 2012.
[53] D. Holmes, C. Bunn, and D. Smith, "The crystal structure of polycaproamide: Nylon 6," *Journal of Polymer Science,* vol. 17, no. 84, pp. 159-177, 1955.
[54] D. Laura, H. Keskkula, J. Barlow, and D. Paul, "Effect of glass fiber surface chemistry on the mechanical properties of glass fiber reinforced, rubber-toughened nylon 6," *Polymer,* vol. 43, no. 17, pp. 4673-4687, 2002.
[55] J. Thomason, "The influence of fibre length, diameter and concentration on the impact performance of long glass-fibre reinforced polyamide 6, 6," *Composites Part A: Applied Science and Manufacturing,* vol. 40, no. 2, pp. 114-124, 2009.

[56] M. He, Z. Wang, R. Wang, L. Zhang, and Q. Jia, "Preparation of bio-based polyamide elastomer by using green plasticizers," *Polymers,* vol. 8, no. 7, p. 257, 2016.
[57] V. Miri, O. Persyn, J.-M. Lefebvre, and R. Seguela, "Effect of water absorption on the plastic deformation behavior of nylon 6," *European Polymer Journal,* vol. 45, no. 3, pp. 757-762, 2009.
[58] R. Kumar and H. Münstedt, "Polyamide/silver antimicrobials: effect of crystallinity on the silver ion release," *Polymer International,* vol. 54, no. 8, pp. 1180-1186, 2005.
[59] V. M. Litvinov and J. P. Penning, "Phase composition and molecular mobility in nylon 6 fibers as studied by proton NMR transverse magnetization relaxation," *Macromolecular Chemistry and Physics,* vol. 205, no. 13, pp. 1721-1734, 2004.
[60] A. Akbari, R. Yegani, and B. Pourabbas, "Synthesis of high dispersible hydrophilic poly (ethylene glycol)/vinyl silane grafted silica nanoparticles to fabricate protein repellent polyethylene nanocomposite," *European Polymer Journal,* vol. 81, pp. 86-97, 2016.
[61] D. Ahmad, I. Van Den Boogaert, J. Miller, R. Presswell, and H. Jouhara, "Hydrophilic and hydrophobic materials and their applications," *Energy Sources, Part A: Recovery, Utilization, and Environmental Effects,* vol. 40, no. 22, pp. 2686-2725, 2018.
[62] R. A. Jones and R. W. Richards, *Polymers at surfaces and interfaces*. 1999.
[63] K. Kawashima, R. Inoue, T. Kanaya, G. Matsuba, K. Nishida, and M. Hino, "Distribution of glass transition temperature Tg in a polymer thin film by neutron reflectivity," in *Journal of Physics: Conference Series*, 2009, vol. 184, no. 1: IOP Publishing, p. 012004.
[64] J. Forrest, K. Dalnoki-Veress, J. Stevens, and J. Dutcher, "Effect of free surfaces on the glass transition temperature of thin polymer films," *Physical review letters,* vol. 77, no. 10, p. 2002, 1996.
[65] J. Friedrich, *The plasma chemistry of polymer surfaces: advanced techniques for surface design*. John Wiley & Sons, 2012.
[66] L. Sabbatini and P. G. Zambonin, *Surface characterization of advanced polymers*. Wiley-VCH, 1993.
[67] T. Kajiyama, K. Tanaka, and A. Takahara, "Surface molecular motion of the monodisperse polystyrene films," *Macromolecules,* vol. 30, no. 2, pp. 280-285, 1997.
[68] M. Morra, E. Occhiello, L. Gila, and F. Garbassi, "Surface dynamics vs. adhesion in oxygen plasma treated polyolefins," *The Journal of Adhesion,* vol. 33, no. 1-2, pp. 77-88, 1990.
[69] J.-H. Wang, P. Claesson, J. Parker, and H. Yasuda, "Dynamic contact angles and contact angle hysteresis of plasma polymers," *Langmuir,* vol. 10, no. 10, pp. 3887-3897, 1994.
[70] F. M. Fowkes, "Attractive forces at interfaces," *Industrial & Engineering Chemistry,* vol. 56, no. 12, pp. 40-52, 1964.
[71] F. Völkermeyer, P. Jaeschke, U. Stute, and D. Kracht, "Laser-based modification of wettablility for carbon fiber reinforced plastics," *Applied Physics A,* vol. 112, pp. 179-183, 2013.
[72] E. Liston, L. Martinu, and M. Wertheimer, "Plasma surface modification of polymers for improved adhesion: a critical review," *Journal of adhesion science and technology,* vol. 7, no. 10, pp. 1091-1127, 1993.
[73] S. K. Nemani *et al.*, "Surface modification of polymers: methods and applications," *Advanced Materials Interfaces,* vol. 5, no. 24, p. 1801247, 2018.
[74] S. Regis, M. Jassal, N. Mukherjee, Y. Bayon, N. Scarborough, and S. Bhowmick, "Altering surface characteristics of polypropylene mesh via sodium hydroxide treatment," *Journal of Biomedical Materials Research Part A,* vol. 100, no. 5, pp. 1160-1167, 2012.
[75] J. Marchand-Brynaert, M. Deldime, I. Dupont, J.-L. Dewez, and Y.-J. Schneider, "Surface functionalization of poly (ethylene terephthalate) film and membrane by controlled wet chemistry: chemical characterization of carboxylated surfaces," *Journal of colloid and interface science,* vol. 173, no. 1, pp. 236-244, 1995.

[76] N. Encinas, M. Pantoja, J. Abenojar, and M. Martínez, "Control of wettability of polymers by surface roughness modification," *Journal of Adhesion Science and Technology,* vol. 24, no. 11-12, pp. 1869-1883, 2010.
[77] H. Moghadamzadeh, H. Rahimi, M. Asadollahzadeh, and A. Hemmati, "Surface treatment of wood polymer composites for adhesive bonding," *International Journal of Adhesion and Adhesives,* vol. 31, no. 8, pp. 816-821, 2011.
[78] J. Breuer, S. Metev, and G. Sepold, "Photolytic surface modification of polymers with UV-laser radiation," *Journal of adhesion science and technology,* vol. 9, no. 3, pp. 351-363, 1995.
[79] S. Eve and J. Mohr, "Study of the surface modification of the PMMA by UV-radiation," *Procedia Engineering,* vol. 1, no. 1, pp. 237-240, 2009.
[80] H. Kaczmarek, J. Kowalonek, A. Szalla, and A. Sionkowska, "Surface modification of thin polymeric films by air-plasma or UV-irradiation," *Surface Science,* vol. 507, pp. 883-888, 2002.
[81] X. Fu, R. L. Sammons, I. Bertóti, M. J. Jenkins, and H. Dong, "Active screen plasma surface modification of polycaprolactone to improve cell attachment," *Journal of Biomedical Materials Research Part B: Applied Biomaterials,* vol. 100, no. 2, pp. 314-320, 2012.
[82] J. Friedrich, "The plasma chemistry of polymer surfaces: advanced techniques for surface design, 2012," ed: Weinheim: Wiley-VCH.
[83] B. Dashtbozorg, X. Tao, and H. Dong, "Active-screen plasma surface multi-functionalisation of biopolymers and carbon-based materials–An overview," *Surface and Coatings Technology,* p. 128188, 2022.
[84] G. Kaklamani, J. Bowen, N. Mehrban, H. Dong, L. M. Grover, and A. Stamboulis, "Active screen plasma nitriding enhances cell attachment to polymer surfaces," *Applied surface science,* vol. 273, pp. 787-798, 2013.
[85] U. Kogelschatz, "Dielectric-barrier discharges: their history, discharge physics, and industrial applications," *Plasma chemistry and plasma processing,* vol. 23, no. 1, pp. 1-46, 2003.
[86] X. Zhang, Y. Cui, C.-M. J. Tay, and B. Khoo, "Ultrasound generated by alternating current dielectric barrier discharge plasma in quiescent air," *Plasma Sources Science and Technology,* vol. 29, no. 1, p. 015017, 2020.
[87] V. I. Gibalov and G. J. Pietsch, "The development of dielectric barrier discharges in gas gaps and on surfaces," *Journal of Physics D: Applied Physics,* vol. 33, no. 20, p. 2618, 2000.
[88] K. Kostov, Y. Hamia, R. Mota, A. Dos Santos, and P. Nascente, "Treatment of polycarbonate by dielectric barrier discharge (DBD) at atmospheric pressure," in *Journal of Physics: Conference Series*, 2014, vol. 511, no. 1: IOP Publishing, p. 012075.
[89] A. Nastuta, G. Rusu, I. Topala, A. Chiper, and G. Popa, "Surface modifications of polymer induced by atmospheric DBD plasma in different configurations," *J. Optoelectron. Adv. Mater,* vol. 10, no. 8, pp. 2038-2042, 2008.
[90] S. A. Al-Bataineh *et al.*, "Fabrication and operation of a microcavity plasma array device for microscale surface modification," vol. 9, no. 7, pp. 638-646, 2012.
[91] E. J. Szili *et al.*, "Microplasma array patterning of reactive oxygen and nitrogen species onto polystyrene," vol. 5, p. 1, 2017.
[92] J. Schalken, M. Creatore, P. Verhoeven, and A. Stevens, "μPlasma Printing Deposition of Amine-Containing Organo-Silane Polymers by Means of 3-Aminopropyl Trimethoxysilane," *Nanoscience and Nanotechnology Letters,* vol. 7, no. 1, pp. 62-66, 2015.
[93] M. Mozetič, "Surface modification to improve properties of materials," ed: Multidisciplinary Digital Publishing Institute, 2019.
[94] M. Iqbal, D. K. Dinh, Q. Abbas, M. Imran, H. Sattar, and A. Ul Ahmad, "Controlled surface wettability by plasma polymer surface modification," *Surfaces,* vol. 2, no. 2, pp. 349-371, 2019.
[95] W. Brennan, W. Feast, H. Munro, and S. Walker, "Investigation of the ageing of plasma oxidized PEEK," *Polymer,* vol. 32, no. 8, pp. 1527-1530, 1991.

[96] L. Carrino, W. Polini, and L. Sorrentino, "Ageing time of wettability on polypropylene surfaces processed by cold plasma," *Journal of Materials Processing Technology,* vol. 153, pp. 519-525, 2004.
[97] J. Cowie and R. Ferguson, "Physical ageing of poly (methyl methacrylate) from enthalpy relaxation measurements," *Polymer,* vol. 34, no. 10, pp. 2135-2141, 1993.
[98] C. Jama, O. Dessaux, P. Goudmand, L. Gengembre, and J. Grimblot, "Treatment of poly (ether ether ketone)(PEEK) surfaces by remote plasma discharge. XPS investigation of the ageing of plasma-treated PEEK," *Surface and interface analysis,* vol. 18, no. 11, pp. 751-756, 1992.
[99] R. Verkuijlen, M. Van Dongen, A. Stevens, J. Van Geldrop, and J. Bernards, "Surface modification of polycarbonate and polyethylene naphtalate foils by UV-ozone treatment and µPlasma printing," *Applied Surface Science,* vol. 290, pp. 381-387, 2014.
[100] Q. Wei, "Surface characterization of plasma-treated polypropylene fibers," *Materials Characterization,* vol. 52, no. 3, pp. 231-235, 2004.
[101] B. Bae, B.-H. Chun, and D. Kim, "Surface characterization of microporous polypropylene membranes modified by plasma treatment," *Polymer,* vol. 42, no. 18, pp. 7879-7885, 2001.
[102] A. Oravcova and I. Hudec, "The influence of atmospheric pressure plasma treatment on surface properties of polypropylene films," *Acta Chim. Slovaca,* vol. 3, pp. 57-62, 2010.
[103] N. Gomathi and S. Neogi, "Surface modification of polypropylene using argon plasma: Statistical optimization of the process variables," *Applied Surface Science,* vol. 255, no. 17, pp. 7590-7600, 2009.
[104] F. Du Toit and R. Sanderson, "Surface Fluorination of polypropylene: 1. Characterisation of surface properties," *Journal of fluorine chemistry,* vol. 98, no. 2, pp. 107-114, 1999.
[105] L. Sorrentino, L. Carrino, and G. Napolitano, "Oxygen cold plasma treatment on polypropylene: influence of process parameters on surface wettability," *Surface Engineering,* vol. 23, no. 4, pp. 247-252, 2007.
[106] H. Guezenoc, Y. Segui, S. Thery, and K. Asfardjani, "Adhesion characteristics of plasma-treated polypropylene to mild steel," *Journal of adhesion science and technology,* vol. 7, no. 9, pp. 953-965, 1993.
[107] R. Nisticò *et al.*, "Effect of atmospheric oxidative plasma treatments on polypropylenic fibers surface: Characterization and reaction mechanisms," *Applied Surface Science,* vol. 279, pp. 285-292, 2013.
[108] B. Blackman, A. Kinloch, and J. Watts, "The plasma treatment of thermoplastic fibre composites for adhesive bonding," *Composites,* vol. 25, no. 5, pp. 332-341, 1994.
[109] J. Schäfer, T. Hofmann, J. Holtmannspötter, M. Frauenhofer, J. von Czarnecki, and H.-J. Gudladt, "Atmospheric-pressure plasma treatment of polyamide 6 composites for bonding with polyurethane," *Journal of Adhesion Science and Technology,* vol. 29, no. 17, pp. 1807-1819, 2015.
[110] H. Lee, I. Ohsawa, and J. Takahashi, "Effect of plasma surface treatment of recycled carbon fiber on carbon fiber-reinforced plastics (CFRP) interfacial properties," *Applied Surface Science,* vol. 328, pp. 241-246, 2015.
[111] J. Li, "The research on the interfacial compatibility of polypropylene composite filled with surface treated carbon fiber," *Applied Surface Science,* vol. 255, no. 20, pp. 8682-8684, 2009.
[112] S. Tiwari and J. Bijwe, "Surface treatment of carbon fibers-a review," *Procedia Technology,* vol. 14, pp. 505-512, 2014.
[113] M. Smith, "Surface modification of high-strength reinforcing fibers by plasma treatment," Allied-Signal Aerospace Co., Kansas City, MO (United States). Kansas City Div., 1991.
[114] S. Pal, S. Ghatak, S. De, and S. DasGupta, "Evaluation of surface roughness of a plasma treated polymeric membrane by wavelet analysis and quantification of its enhanced performance," *Applied Surface Science,* vol. 255, no. 5, pp. 2504-2511, 2008.

[115] D. E. Packham, "Surface energy, surface topography and adhesion," *International journal of adhesion and adhesives,* vol. 23, no. 6, pp. 437-448, 2003.
[116] H. Yousefi, M. Ghoranneviss, A. Tehrani, and S. Khamseh, "Investigation of glow discharge plasma for surface modification of polypropylene," *Surface and Interface Analysis: An International Journal devoted to the development and application of techniques for the analysis of surfaces, interfaces and thin films,* vol. 35, no. 12, pp. 1015-1017, 2003.
[117] J. Friedrich, "Interaction between Plasma and Polymers," *The Plasma Chemistry of Polymer Surfaces,* pp. 11-33, 2012.
[118] D. Clark and A. Dilks, "An investigation of the vacuum UV spectra of inductivity coupled RF plasmas excited in inert gases as a function of some of the operating parameters," *Journal of Polymer Science: Polymer Chemistry Edition,* vol. 18, no. 4, pp. 1233-1246, 1980.
[119] F. Garbassi, M. Morra, E. Occhiello, and F. Garbassi, *Polymer surfaces: from physics to technology*. Wiley Chichester, 1998.
[120] C. Borcia, I. Punga, and G. Borcia, "Surface properties and hydrophobic recovery of polymers treated by atmospheric-pressure plasma," *Applied surface science,* vol. 317, pp. 103-110, 2014.
[121] J. Hyun, "A new approach to characterize crystallinity by observing the mobility of plasma treated polymer surfaces," *Polymer,* vol. 42, no. 15, pp. 6473-6477, 2001.
[122] I. Junkar, U. Cvelbar, A. Vesel, N. Hauptman, and M. Mozetič, "The role of crystallinity on polymer interaction with oxygen plasma," *Plasma Processes and Polymers,* vol. 6, no. 10, pp. 667-675, 2009.
[123] E. Occhiello, M. Morra, G. Morini, F. Garbassi, and P. Humphrey, "Oxygen-plasma-treated polypropylene interfaces with air, water, and epoxy resins: Part I. Air and water," *Journal of Applied Polymer Science,* vol. 42, no. 2, pp. 551-559, 1991.
[124] N. De Geyter, R. Morent, and C. Leys, "Influence of ambient conditions on the ageing behaviour of plasma-treated PET surfaces," *Nuclear Instruments and Methods in Physics Research Section B: Beam Interactions with Materials and Atoms,* vol. 266, no. 12-13, pp. 3086-3090, 2008.
[125] M. Mortazavi and M. Nosonovsky, "A model for diffusion-driven hydrophobic recovery in plasma treated polymers," *Applied Surface Science,* vol. 258, no. 18, pp. 6876-6883, 2012.
[126] *ASTM D5573 - 99(2019)*, United States, 2019.
[127] S. M. Hasheminia, B. C. Park, H.-J. Chun, J.-C. Park, and H. S. Chang, "Failure mechanism of bonded joints with similar and dissimilar material," *Composites Part B: Engineering,* vol. 161, pp. 702-709, 2019.
[128] H. C. Cartledge, C. Baillie, and Y.-W. Mai, "Friction and wear mechanisms of a thermoplastic composite GF/PA6 subjected to different thermal histories," *Wear,* vol. 194, no. 1-2, pp. 178-184, 1996.
[129] J. Thomason, "The influence of fibre length, diameter and concentration on the modulus of glass fibre reinforced polyamide 6, 6," *Composites Part A: Applied Science and Manufacturing,* vol. 39, no. 11, pp. 1732-1738, 2008.
[130] B. Wang and H. Gao, "Fibre Reinforced Polymer Composites," in *Advances in Machining of Composite Materials*: Springer, 2021, pp. 15-43.
[131] B. Mouhmid, A. Imad, N. Benseddiq, S. Benmedakhène, and A. Maazouz, "A study of the mechanical behaviour of a glass fibre reinforced polyamide 6, 6: Experimental investigation," *Polymer testing,* vol. 25, no. 4, pp. 544-552, 2006.
[132] J. Thomason, "The influence of fibre properties of the performance of glass-fibre-reinforced polyamide 6, 6," *Composites science and technology,* vol. 59, no. 16, pp. 2315-2328, 1999.
[133] Y. Xiao *et al.*, "A novel phosphorous-containing polymeric compatibilizer: effective reinforcement and flame retardancy in glass fiber reinforced polyamide 6 composites," *Composites Part B: Engineering,* vol. 205, p. 108536, 2021.

[134] N. Myshkin and A. Kovalev, "Adhesion and surface forces in polymer tribology—A review," *Friction,* vol. 6, no. 2, pp. 143-155, 2018.
[135] C. Canal, R. Molina, E. Bertran, and P. Erra, "Wettability, ageing and recovery process of plasma-treated polyamide 6," *Journal of Adhesion Science and Technology,* vol. 18, no. 9, pp. 1077-1089, 2004.
[136] B. Dashtbozorg *et al.*, "Development of surfaces with antibacterial durability through combined S phase plasma hardening and athermal femtosecond laser texturing," *Applied Surface Science,* vol. 565, p. 150594, 2021.
[137] H. R. Erfani Gahrooei, M. H. Ghazanfari, and F. Karimi Malekabadi, "Wettability alteration of reservoir rocks to gas wetting condition: A comparative study," *The Canadian Journal of Chemical Engineering,* vol. 96, no. 4, pp. 997-1004, 2018.
[138] J. W. Kim, S. H. Yoo, Y. B. Kong, S. O. Cho, and E. J. Lee, "Hydrophilicity Improvement of Polymer Surfaces Induced by Simultaneous Nuclear Transmutation and Oxidation Effects Using High-Energy and Low-Fluence Helium Ion Beam Irradiation," *Polymers,* vol. 12, no. 12, p. 2770, 2020.
[139] X. Chen, X. Yin, and J. Jin, "A Study on the Wettability of Ion-Implanted Stainless and Bearing Steels," *Metals,* vol. 9, no. 2, p. 208, 2019.
[140] F. Abbasi, H. Mirzadeh, and A. A. Katbab, "Modification of polysiloxane polymers for biomedical applications: a review," *Polymer International,* vol. 50, no. 12, pp. 1279-1287, 2001.
[141] H. Dong and T. Bell, "State-of-the-art overview: ion beam surface modification of polymers towards improving tribological properties," *Surface and Coatings Technology,* vol. 111, no. 1, pp. 29-40, 1999.
[142] M. Ito, J. S. Oh, T. Ohta, M. Shiratani, and M. Hori, "Current status and future prospects of agricultural applications using atmospheric‐pressure plasma technologies," *Plasma Processes and Polymers,* vol. 15, no. 2, p. 1700073, 2018.
[143] K. D. Weltmann *et al.*, "The future for plasma science and technology," *Plasma Processes and Polymers,* vol. 16, no. 1, p. 1800118, 2019.
[144] N. Lucas, R. Franke, A. Hinze, C. P. Klages, R. Frank, and S. Büttgenbach, "Microplasma Stamps for Area‐Selective Modification of Polymer Surfaces," *Plasma Processes and Polymers,* vol. 6, no. S1, pp. S370-S374, 2009.
[145] T. Murakami, S.-i. Kuroda, and Z. Osawa, "Dynamics of polymeric solid surfaces treated with oxygen plasma: Effect of aging media after plasma treatment," *Journal of colloid and interface science,* vol. 202, no. 1, pp. 37-44, 1998.
[146] I. R. Marques *et al.*, "Simple approach for the plasma treatment of polymeric membranes and investigation of the aging effect," *Journal of Applied Polymer Science,* vol. 138, no. 24, p. 50558, 2021.
[147] J. Nakamatsu, L. F. Delgado-Aparicio, R. Da Silva, and F. Soberon, "Ageing of plasma-treated poly (tetrafluoroethylene) surfaces," *Journal of adhesion science and technology,* vol. 13, no. 7, pp. 753-761, 1999.
[148] R. Thompson, D. Austin, C. Wang, A. Neville, and L. Lin, "Low-frequency plasma activation of nylon 6," *Applied Surface Science,* vol. 544, p. 148929, 2021.
[149] D. Pappas *et al.*, "Surface modification of polyamide fibers and films using atmospheric plasmas," *Surface and Coatings Technology,* vol. 201, no. 7, pp. 4384-4388, 2006.
[150] Y. Baek, J. Kang, P. Theato, and J. Yoon, "Measuring hydrophilicity of RO membranes by contact angles via sessile drop and captive bubble method: A comparative study," *Desalination,* vol. 303, pp. 23-28, 2012.
[151] Q. Li *et al.*, "Understanding the dependence of contact angles of commercially RO membranes on external conditions and surface features," *Desalination,* vol. 309, pp. 38-45, 2013.
[152] *Paints and varnishes — Wettability*, British Standard, 2020.

[153] Z. Károly, G. Kalácska, L. Zsidai, M. Mohai, and S. Klébert, "Improvement of adhesion properties of polyamide 6 and polyoxymethylene-copolymer by atmospheric cold plasma treatment," *Polymers,* vol. 10, no. 12, p. 1380, 2018.
[154] Y. Ma *et al.*, "Effect of hot water on the mechanical performance of unidirectional carbon fiber-reinforced nylon 6 composites," *Composites Science and Technology,* vol. 200, p. 108426, 2020.
[155] B. S. Gupta, I. Reiniati, and M.-P. G. Laborie, "Surface properties and adhesion of wood fiber reinforced thermoplastic composites," *Colloids and Surfaces A: Physicochemical and Engineering Aspects,* vol. 302, no. 1-3, pp. 388-395, 2007.
[156] I. Levchenko, S. Xu, O. Baranov, O. Bazaka, E. P. Ivanova, and K. Bazaka, "Plasma and polymers: recent progress and trends," *Molecules,* vol. 26, no. 13, p. 4091, 2021.
[157] L. Bárdos and H. Baránková, "Cold atmospheric plasma: Sources, processes, and applications," *Thin solid films,* vol. 518, no. 23, pp. 6705-6713, 2010.
[158] Y. Kong and J. Hay, "The measurement of the crystallinity of polymers by DSC," *Polymer,* vol. 43, no. 14, pp. 3873-3878, 2002.
[159] G. Williams and D. C. Watts, "Non-symmetrical dielectric relaxation behaviour arising from a simple empirical decay function," *Transactions of the Faraday society,* vol. 66, pp. 80-85, 1970.
[160] N. S. Kasálková, P. Slepička, Z. Kolská, P. Hodačová, Š. Kučková, and V. Švorčík, "Grafting of bovine serum albumin proteins on plasma-modified polymers for potential application in tissue engineering," *Nanoscale Research Letters,* vol. 9, no. 1, pp. 1-7, 2014.
[161] C. Ma *et al.*, "Atmospheric-pressure plasma assisted engineering of polymer surfaces: From high hydrophobicity to superhydrophilicity," *Applied Surface Science,* vol. 535, p. 147032, 2021.
[162] J. Rani *et al.*, "Epoxy to carbonyl group conversion in graphene oxide thin films: effect on structural and luminescent characteristics," *The Journal of Physical Chemistry C,* vol. 116, no. 35, pp. 19010-19017, 2012.
[163] W. Zhang and J. Xu, "Advanced lightweight materials for Automobiles: A review," *Materials & Design,* p. 110994, 2022.
[164] P. Mallick, "Thermoplastics and thermoplastic–matrix composites for lightweight automotive structures," in *Materials, design and manufacturing for lightweight vehicles*: Elsevier, 2021, pp. 187-228.
[165] R. Bernatas, S. Dagréou, A. Despax-Ferreres, and A. Barasinski, "Recycling of fiber reinforced composites with a focus on thermoplastic composites," *Cleaner Engineering and Technology,* vol. 5, p. 100272, 2021.
[166] R. W. Messler, *Joining of materials and structures: from pragmatic process to enabling technology*. Butterworth-Heinemann, 2004.
[167] A. Mameli *et al.*, "Area-selective atomic layer deposition of In2O3: H using a μ-plasma printer for local area activation," *Chemistry of Materials,* vol. 29, no. 3, pp. 921-925, 2017.
[168] H. Uematsu *et al.*, "Relationship between crystalline structure of polyamide 6 within carbon fibers and their mechanical properties studied using Micro-Raman Spectroscopy," *Polymer,* vol. 223, p. 123711, 2021.
[169] W. Maddams and I. Royaud, "The application of Fourier transform Raman spectroscopy to the identification and characterisation of polyamides—II. Double-number nylons," *Spectrochimica Acta Part A: Molecular Spectroscopy,* vol. 47, no. 9-10, pp. 1327-1333, 1991.
[170] E. Baburaj, D. Starikov, J. Evans, G. Shafeev, and A. Bensaoula, "Enhancement of adhesive joint strength by laser surface modification," *International journal of adhesion and adhesives,* vol. 27, no. 4, pp. 268-276, 2007.
[171] H. B. Baniya, R. P. Guragain, B. Baniya, and D. P. Subedi, "Cold atmospheric pressure plasma jet for the improvement of wettability of polypropylene," *International Journal of Polymer Science,* vol. 2020, 2020.

[172] F. Rupp, L. Scheideler, D. Rehbein, D. Axmann, and J. Geis-Gerstorfer, "Roughness induced dynamic changes of wettability of acid etched titanium implant modifications," *Biomaterials,* vol. 25, no. 7-8, pp. 1429-1438, 2004.

[173] V. Jokinen, P. Suvanto, and S. Franssila, "Oxygen and nitrogen plasma hydrophilization and hydrophobic recovery of polymers," *Biomicrofluidics,* vol. 6, no. 1, p. 016501, 2012.

[174] E. Bormashenko, G. Chaniel, and R. Grynyov, "Towards understanding hydrophobic recovery of plasma treated polymers: Storing in high polarity liquids suppresses hydrophobic recovery," *Applied Surface Science,* vol. 273, pp. 549-553, 2013.